SMIP13

SMIP13 SEMINAR ON
UTILIZATION OF STRONG-MOTION DATA

Los Angeles, California
October 10, 2013

PROCEEDINGS

Sponsored by

California Strong Motion Instrumentation Program
California Geological Survey
California Department of Conservation

Co-Sponsors

California Seismic Safety Commission
California Governor's Office of Emergency Services
California Department of Transportation
Office of Statewide Health Planning and Development

The California Strong Motion Instrumentation Program (CSMIP), a program within the California Geological Survey (CGS) of the California Department of Conservation, records the strong shaking of the ground and structures during earthquakes for analysis and utilization by the engineering and seismology communities through a statewide network of strong motion instruments (www.conservation.ca.gov/CGS/smip). CSMIP is advised by the Strong Motion Instrumentation Advisory Committee (SMIAC), a committee of the California Seismic Safety Commission. Major program funding is provided by an assessment on construction costs for building permits issued by cities and counties in California, with additional funding from the California Governor's Office of Emergency Services (Cal OES), the California Department of Transportation (Caltrans) and the Office of Statewide Health Planning and Development (OSHPD).

In July 2001, the California Governor's Office of Emergency Services (Cal OES) began funding for the California Integrated Seismic Network (CISN), a newly formed consortium of institutions engaged in statewide earthquake monitoring that grew out of TriNet, funded by FEMA, and includes CGS, USGS, Caltech and UC Berkeley. The goals are to record and rapidly communicate ground shaking information in California, and to analyze the data for the improvement of seismic codes and standards (www.cisn.org). CISN produces ShakeMaps of ground shaking, based on shaking recorded by stations in the network, within minutes following an earthquake. The ShakeMap identifies areas of greatest ground shaking for use by OES and other emergency response agencies in the event of a damaging earthquake.

The Center for Engineering Strong Motion Data (CESMD) is operated by the CSMIP Program of the CGS in cooperation with the National Strong-Motion Project (NSMP) and the Advanced National Seismic System (ANSS) of the U.S. Geological Survey (USGS). The CESMD builds on and incorporates the CISN Engineering Data Center and will continue to serve the California region while expanding to serve other ANSS regions. The Data Center provides strong-motion data rapidly after a significant earthquake in the United States. Users also have direct access to data from previous earthquakes and detailed information about the instrumented structures and sites. The Data Center is co-hosted by CGS and USGS at www.strongmotioncenter.org

DISCLAIMER

SMIP13

SMIP13 SEMINAR ON
UTILIZATION OF STRONG-MOTION DATA

Los Angeles, California
October 10, 2013

PROCEEDINGS

Edited by

Moh Huang

Sponsored by

California Strong Motion Instrumentation Program
California Geological Survey
California Department of Conservation

Co-Sponsors

California Seismic Safety Commission
California Governor's Emergency Services
California Department of Transportation
Office of Statewide Health Planning and Development

PREFACE

The California Strong Motion Instrumentation Program (CSMIP) in the California Geological Survey of the California Department of Conservation established a Data Interpretation Project in 1989. Each year CSMIP Program funds several data interpretation contracts for the analysis and utilization of strong-motion data. The primary objectives of the Data Interpretation Project are to further the understanding of strong ground shaking and the response of structures, and to increase the utilization of strong-motion data in improving post-earthquake response, seismic code provisions and design practices.

As part of the Data Interpretation Project, CSMIP holds annual seminars to transfer recent research findings on strong-motion data to practicing seismic design professionals, earth scientists and post-earthquake response personnel. The purpose of the annual seminar is to provide information that will be useful immediately in seismic design practice and post-earthquake response, and in the longer term, useful in the improvement of seismic design codes and practices. Proceedings and individual papers for each of the previous annual seminars are available in PDF format at http://www.consrv.ca.gov/CGS/smip/proceedings.htm Due to the State budget restraints, CSMIP did not fund as many projects as in other years and did not hold an annual seminar in 2010 or 2011. The SMIP13 Seminar is the twenty-second in this series of annual seminars.

The SMIP13 Seminar is divided into two sessions in the morning and two sessions in the afternoon. The sessions in the morning include four invited presentations. They are lessons learned on ground motions from large subduction earthquakes by Professor Stewart of UCLA, significant building records from the 2011 Tohoku earthquake by Professor Kasai of Tokyo Institute of Technology, observations from recent earthquake in China by Dr. Lew of AMEC, and earthquake early warning system by Dr. Given of USGS. The first afternoon session starts with a presentation of some preliminary results from the CSMIP-funded project on port structures by Dr. Dickenson of New Albion Geotechnical, followed by an invited presentation on analyses of records from instrumented bridges by Dr. Shamsabadi of Caltrans. The last session includes an invited presentation by Dr. Naeim of John A. Martin and Associates on instrumentation requirements for tall buildings in Los Angeles, followed by presentations by Dr. Shakal on recent developments at CSMIP, and by Dr. Haddadi on the updates of the Center for Engineering Strong Motion Data. Individual papers and the proceedings are available to the SMIP13 participants in an USB flash drive.

Moh Huang
CSMIP Data Interpretation Project Manager

Appreciation to Members of the Strong Motion Instrumentation Advisory Committee

Main Committee

Chris Poland, Chair, Degenkolb Engineers
Norman Abrahamson, Pacific Gas & Electric Company
Anil Chopra, UC Berkeley
Bruce Clark, Leighton & Associates
Martin Eskijian, California State Lands Commission (retired)
Wilfred Iwan, California Institute of Technology
Tom Ostrom, Caltrans
Farzad Naeim, John A. Martin & Associates
Marshall Lew, AMEC
Bret Lizundia, Rutherford & Chekene
Robert Anderson (ex-officio), Seismic Safety Commission

Ground Response Subcommittee

Marshall Lew, Chair, AMEC
Abbas Abghari, Caltrans
Brian Chiou, Caltrans
Geoffrey Martin, Univ. of Southern California
Ben Tsai, Pacific Gas & Electric Company (retired)

Buildings Subcommittee

Farzad Naeim, Chair, John A. Martin & Associates
Lucie Fougner, Degenkolb Engineers
Donald Jephcott, Structural Engineer
David Leung, City of San Francisco
Bret Lizundia, Rutherford & Chekene
Eduardo Miranda, Stanford University
John Robb, Structural Engineer
Chris Tokas, Office of Statewide Health Planning and Development
Chia-Ming Uang, UC San Diego

Lifelines Subcommittee

Martin Eskijian, Chair, California State Lands Commission (retired)
Craig Davis, Los Angeles Dept. of Water and Power
David Gutierrez, DWR Division of Safety of Dams
Marsha McLaren, Pacific Gas & Electric Company
Tom Ostrom, Caltrans

Data Utilization Subcommittee

Wilfred Iwan, Chair, California Institute of Technology
Representatives from each Subcommittee

TABLE OF CONTENTS

SMIP13 SEMINAR ON UTILIZATION OF STRONG-MOTION DATA

October 10, 2013

Fifth Floor Conference Facilities
Federal Reserve Bank of Los Angeles
950 South Grand Avenue, Los Angeles, California

PROGRAM

8:15 am **REGISTRATION**

9:15 am **WELCOMING REMARKS**
Chris Poland, Strong Motion Instrumentation Advisory Committee (SMIAC)
John Parrish, State Geologist, California Geological Survey

INTRODUCTION
Anthony Shakal, Manager, California Strong Motion Instrumentation Program
Moh Huang, California Strong Motion Instrumentation Program

Session I

Moderator: *Marshall Lew*, AMEC and SMIAC

9:30 am **Lessons Learned on Ground Motions from Large Interface Subduction Zone Earthquakes from 2010 M 8.8 Maule, Chile and 2011 M9.0 Tohoku, Japan Events**
Jonathan Stewart, UCLA

10:00 am **Significant Building Response Records from the 2011 Tohoku Earthquake and the Implications for Seismic Designs and Analyses**
Kazuhiko Kasai and *Kazuhiro Matsuda*, Tokyo Institute of Technology.

10:30 am Break

Session II

Moderator: *Farzad Naeim*, John A. Martin & Assoc. and SMIAC

11:00 am **Observations from the April 20, 2013 Lushan County, Ya'an City, Sichuan Province, China Earthquake**
Marshall Lew, AMEC

11:30 pm **ShakeAlert, an Early Warning System for California and the West Coast**
Douglas Given, USGS, Pasadena

12:00 pm **Lunch**
Lunch will be provided

Session III

Moderator: *Martin Eskijian,* California State Lands Commission (retired) and SMIAC

1:00 pm **Use of Strong Motion Records to Validate Dynamic Soil-Foundation-Structure Interaction Models for Pile Supported Wharves**
Stephen Dickenson, Songtao Yang, Doug Schwarm and *Matt Rees,*
New Albion Geotechnical

1:30 pm **Three Dimensional Global Nonlinear Time History Analysis of Instrumented Bridges to Validate Current Bridge Seismic Design**
Anoosh Shamsabadi, Tom Ostrom, Caltrans, and *Ertugrul Taciroglu,* UCLA

2:00 pm Break

Session IV

Moderator: *Wilfred Iwan,* Caltech and SMIAC

2:30 pm **Instrumentation Requirements for Tall Buildings per the Los Angeles Tall Buildings Structural Design Council 2011 Alternative Analysis and Design Procedure**
Farzad Naeim, John A. Martin & Associates

3:00 pm **Recent Developments and Status of the California Strong Motion Instrumentation Program**
Anthony Shakal, and *Moh Huang,* CGS/CSMIP

Update on Data and Features of the Center for Engineering Strong Motion Data (CESMD)
Hamid Haddadi, CGS/CSMIP and *Christopher Stephens,* USGS/NSMP

3:30 pm **Adjourn**

LESSONS LEARNED ON GROUND MOTIONS FROM LARGE INTERFACE SUBDUCTION ZONE EARTHQUAKES FROM 2010 M 8.8 MAULE, CHILE AND 2011 M9.0 TOHOKU, JAPAN EVENTS

Jonathan P. Stewart

Department of Civil & Environmental Engineering
University of California, Los Angeles

Extended Abstract

In this presentation, I will review the results of analyses of ground motions recorded during the large interface subduction zone earthquakes in Maule Chile (**M** 8.8, 2010) and Tohoku Japan (**M** 9.0, 2011). I will also describe how these analyses influenced the selection of ground motion prediction equations (GMPEs) for subduction zone regions in the Global Earthquake Model (GEM) project organized through the Pacific Earthquake Engineering Research Center (PEER). The work discussed in this presentation is largely presented in prior publications by Boroschek et al. (2012), Stewart et al. (2013a), and Stewart et al. (2013b).

The **M** 8.8 Maule Chile earthquake produced 31 usable strong motion records over a rupture distance range of 30 to 700 km. Site conditions range from firm rock to soft soil but are most often competent soil (NEHRP Category C or C/D). Most of the data were recorded on analogue instruments, which was digitized and processed with low- and high-cut filters designed to maximize the usable frequency range of the signals. The stations closest to the fault plane do not exhibit evidence of ground motion polarization from rupture directivity. Response spectra of nearby recordings on firm ground and soft soil indicate pronounced site effects, including several cases of resonance at site periods. The Atkinson and Boore (2003) GMPE for interface subduction events captures well the distance scaling and dispersion of the data, but under-predicts the overall ground motion level, perhaps due to too-weak magnitude scaling.

The **M** 9.0 Tohoku-oki Japan earthquake produced approximately 2000 ground motion recordings. Stewart et al. (2013a) considered 1238 three-component accelerograms corrected with component-specific low-cut filters. The recordings have rupture distances between 44 and 1000 km, time-averaged shear wave velocities of V_{s30} = 90 to 1900 m/s, and usable response spectral periods of 0.01 to >10 sec. The Tohoku and Maule data support the notion that the increase of ground motions with magnitude saturates at large magnitudes. High frequency ground motions demonstrate faster attenuation with distance in backarc than in forearc regions, which is only captured by one of the four considered ground motion prediction equations for subduction earthquakes (Abrahamson et al., 201s). Event terms evaluated from recordings within 100 km of the fault are generally positive (indicating model under-prediction) at short periods and zero or negative (over-prediction) at long periods. Site amplification scales minimally with V_{s30} at high frequencies, in contrast with other active tectonic regions, but scales strongly with V_{s30} at low frequencies.

The features of the ground motion trends with magnitude and distance observed from the Maule Chile and Tohoku Japan events had a substantial impact on the selection of GMPEs for subduction zones in the GEM-PEER project. I will describe the GMPE selection procedure developed in that project. I will also indicate the GMPEs that were selected and the rationale for doing so.

References

Abrahamson, NA, N Gregor, and K Addo, 2012. BCHydro ground motion prediction equations for subduction earthquakes, *Earthquake Spectra*, submitted.

Atkinson, GM and DM Boore, 2003. Empirical ground-motion relations for subduction-zone earthquakes and their application to Cascadia and other regions, *Bull. Seism. Soc. Am.* **93**, 1703 – 1729.

Boroschek, R, V Contreras , DY Kwak, and JP Stewart, 2012. Strong ground motion attributes of the 2010 Mw 8.8 Maule Chile, Earthquake, *Earthquake Spectra*, **28**, S19-38.

Stewart, JP, S Midorikawa, RW Graves, K Khodaverdi, H Miura, Y Bozorgnia, and KW Campbell, 2013a. Implications of Mw 9.0 Tohoku-oki Japan earthquake for ground motion scaling with source, path, and site parameters, *Earthquake Spectra*, **29**, S1-21.

Stewart, JP, J Douglas, M Javanbarg, Y Bozorgnia, NA Abrahamson, DM Boore, KW Campbell, E Delavaud, M Erdik, and PJ Stafford, 2013b. Selection of ground motion prediction equations for the Global Earthquake Model, *Earthquake Spectra*, DOI: http://dx.doi.org/10.1193/013013EQS017M

SIGNIFICANT BUILDING RESPONSE RECORDS FROM THE 2011 TOHOKU EARTHQUAKE AND THE IMPLICATIONS FOR SEISMIC DESIGNS AND ANALYSES

Kazuhiko Kasai and Kazuhiro Matsuda

Structural Engineering Research Center
Tokyo Institute of Technology, Yokohama, JAPAN

Abstract

Many tall buildings in Tokyo metropolitan area were strongly shaken during the Tohoku Earthquake, March 11, 2011. Most of them are less than 40 years old, and experienced the shaking of such a strong level for the first time, although they suffered little damage. The buildings are conventional seismically-resistant buildings, and those constructed after the 1995 Kobe Earthquake are typically supplementally-damped buildings or base-isolated buildings for seismic damage reduction. Some of the tall buildings are instrumented with sensors and their motions recorded during the event. This paper discusses recorded responses of such tall buildings in Tokyo employing the three distinct structural systems. By estimating contributions of multiple vibration modes, various shaking phenomena observed in the tall building are clarified. Characteristics of the distinct systems and their effects on building contents are contrasted based on mode-based analyses.

Introduction

The Tohoku Earthquake

At 14:46 on March 11, 2011, the East Japan Earthquake of magnitude 9.0 occurred off Sanriku coast of Japan. It caused tremendous tsunami hazard in the pacific coast of eastern Japan, killing more than 15,000 people, destroying and washing away cities. The epicenter was 129km from Sendai, the largest city in the northeast of Japan. The depth of the hypocenter was 24 km. The recorded magnitude places the earthquake as the fourth largest in the world since 1900, following 1960 Chile Earthquake M9.5, 1964 Alaska Earthquake M9.2, 2004 Sumatra Earthquake M9.2, and it is the largest in Japan since modern instrumental recording began 130 years ago. The earthquake has recorded the seismic intensity 7, highest in the Japan Meteorological Agency scale, in the north of Miyagi prefecture.

There were many strong earthquake observation networks in operation under the management of research institutes, universities and companies. A large amount of data was well recorded during the earthquake. Figure 1 shows the distribution of peak ground acceleration (PGA) and velocity (PGV) recorded during the earthquake. K-NET Tsukidate, located in Kurihara city, Miyagi prefecture, is the only station that recorded Intensity 7 during the main shock. A maximum acceleration in the N-S direction reached almost 2699 cm/s^2, representing that the main shock caused excessively severe earthquake motions. Strong motions with PGA

larger than 200 cm/s^2 were observed over a very wide area from Ibaraki to South Iwate. Tokyo is located 300 km away from the epicenter (Figure 1), and its stations recorded PGA of 50 to 150 cm/s^2. The records from stations close to epicenter, such as Sendai, show two wave groups with a time interval of about 50 seconds, and those from southern station such as Ibaraki and Tokyo areas show one large wave group. Such phenomenon occurred due to difference of focal rupture process and the wave propagation to recording stations in the northern and southern portions of the fault area of 500 km long.

As explained elsewhere (Kasai et al. 2012, 2013), many of the ground motion records in Tokyo showed the spectral velocity almost uniform for the vibration periods from 0.5s and 20s, and its magnitude exceeded even the largest spectral value due to the 2004 Niigata Chuetsu Earthquake that concentrated at the period about 7s. Thus, unlike the responses during the 2004 Niigata Chuetsu Earthquake, the responses of the tall buildings in Tokyo were dominated by not only the shorter period motions but also the long period motion.

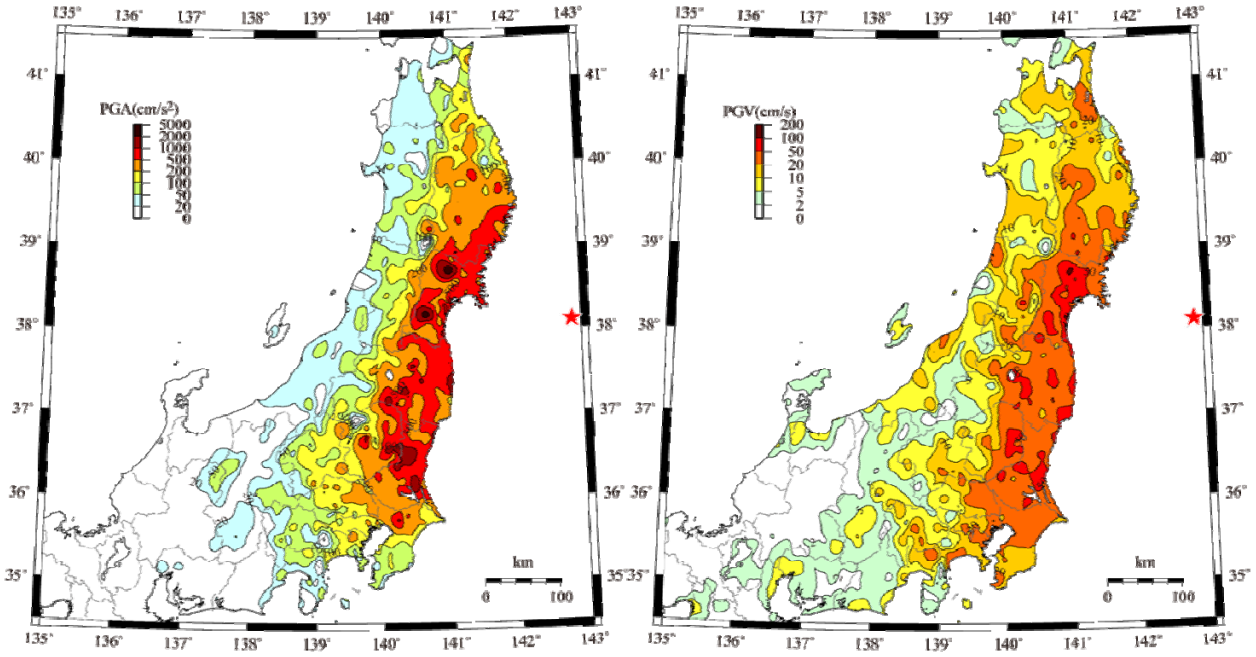

Figure 1. Peak ground accelerations and peak ground velocity recorded in eastern Japan during the 2011 Great East Japan Earthquake (From Dr. Kashima, Building Research Institute, http://www.serc.titech.ac.jp/info/seminar/15WCEE_SS.html)

Objectives and Scopes

Where ground acceleration was large, except for some areas of soft ground, the response spectrum indicated short dominant period, which was probably the main reason for relatively small seismic damage. On the other hand, Tokyo relatively far from the epicenter was subjected to the ground motion of short to long period components. Many tall buildings have been constructed for the last 40 years in Tokyo, and the shaking they experienced is much stronger

than those in the past. Therefore, the response observed are believed to be the precursors for the performance of the tall buildings against the stronger shaking that will definitely occur in future.

Since some tall buildings were instrumented with accelerometers, acceleration records obtained during the earthquake would be one of the best resources to study the building responses (Kasai, 2011a). Pursuant to these, the objective of the present paper is to clarify behavior of tall buildings in Tokyo, based on the responses recorded during the 2011 Tohoku Earthquake. The paper will analyze acceleration records of a typical seismically-resistant building with a low damping ratio, and supplementally-damped and base-isolated buildings whose damping ratios are increased by the new technology using various types of dampers. Virtually, most Japanese tall buildings constructed after the 1995 Kobe Earthquake are either supplementally-damped or base-isolated in order to protect not only the human lives but also the structural components, nonstructural components, and building functions. Therefore, effectiveness of the new technology in achieving the above-mentioned performance will be discussed.

Buildings Considered and Data Analysis Schemes

Buildings Considered

As the important reconnaissance effort of Japan Society of Seismic Isolation (JSSI), three investigation committees were established to examine performance of the buildings with three distinct systems (JSSI, 2012). Since little damage was found from most of such buildings, and available acceleration records of the buildings were studied and compared. This paper explains only a portion of the group of buildings studied by JSSI. The paper considers 29-story conventional seismic-resistant building, 21, 37, 38, 41, and 54-story supplementally-damped buildings, all located in Tokyo, and the 20-story base-isolated building in Yokohama.

Figure 2 shows the response spectra of the base acceleration records in both x- and y-directions and damping ratio 5% for nine buildings located in Tokyo. The response spectra have small coefficient of variation of about 0.2 at the middle to long period range. In view of the strong randomness of earthquake motions, the intensity and characteristics of these input earthquake motions may be considered as similar ones. Consequently, it is reasonable to use the average to represent the input earthquake level in this area. In one sense, it could be considered that all the nine buildings were subjected to a common ground shaking characterized by the average spectral plots.

The ratio of accelerations of top to base will be named as “acceleration magnification ratio (AMR)”. In Figure 3, its value is shown with respect to each building height. In addition to the nine buildings considered in Figure 2, twelve buildings (Kasai, 2011a) are added for comparison over wide range. As noted above, the response spectra for the buildings are similar, and the vibration period of the building is well correlated to its height. However, AMR in Figure 3 does not follow the trend of acceleration spectra in Figure 2a: It is very high for taller buildings, in contrast to low spectral accelerations in Fig. 2a (Kasai, 2011a,b). This is due to significant contribution of higher modes as well as low damping ratio in case of seismic-resistant buildings, as will be discussed.

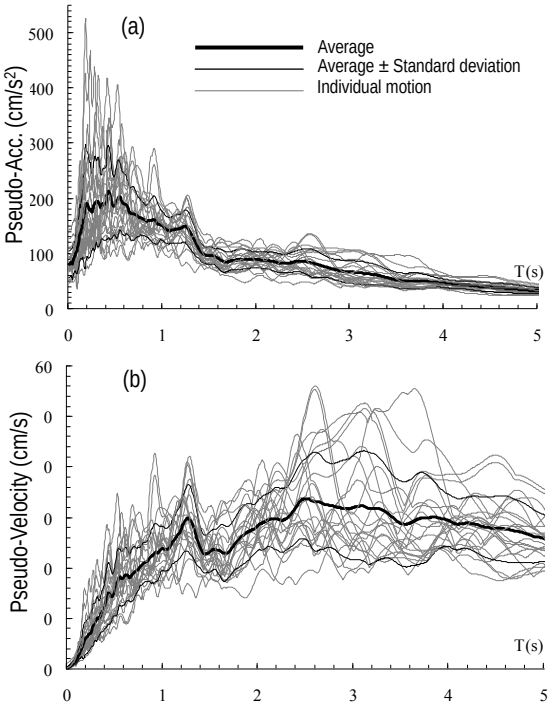

Figure 2. Response spectra ((a) to (c)) generated from the base motions of nine buildings (damping ratio 5%)

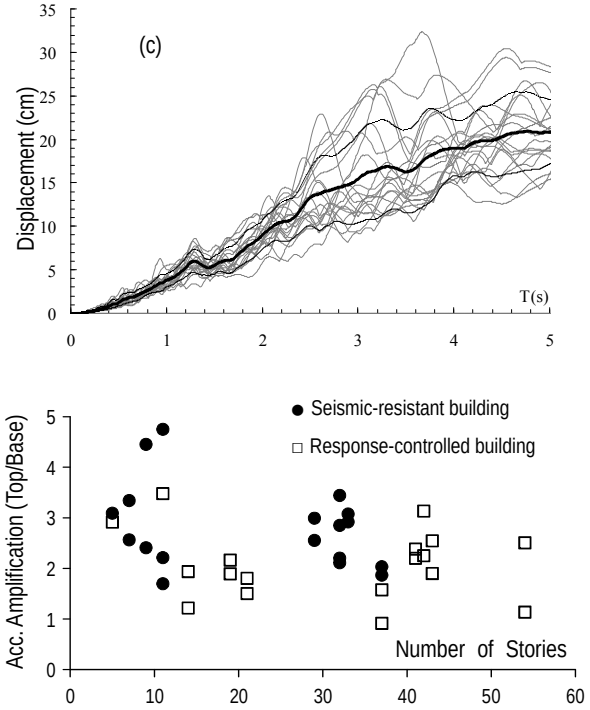

Figure 3. Acceleration magnification ratio (AMR) vs. number of stories of buildings

Data Analysis by Standard Modal Approach

Displacements of the structure are calculated from the recorded accelerations by using two methods. The results are compared with each other in order to confirm their reliability (Kasai, 2013). Method 1 performs double integration together with hi-pass filtering in frequency domain. The cut-off frequency is typically 0.05 or 0.1Hz. Method 2 first obtains modal properties such as vibration period, damping ratio, and participation vector, by applying the basic system identification technique of fitting theoretical transfer function to the curve representing the spectral ratio of recorded accelerations. Using such modal properties and the base acceleration records, mode-superposition time history analysis is performed for the story where the sensor is located to obtain acceleration and displacement. The displacements are compared between methods 1 and 2, and accelerations from method 2 are compared with the recorded accelerations, and good match between them. Thus, calculated modal properties would be adequate and the buildings must also have behaved almost linearly.

Note that method 2 is based on the assumption of linear response, proportional damping, and real number mode. The agreement between the two methods suggests that the buildings had linear or slightly nonlinear behavior during the earthquake as well as moderate amount of damping.

Seismically-Resistant Building

Response Trends in Kanto Area

Six seismically resistant buildings investigated by JSSI and located in Kanto area were 8- to 37-story. The peak accelerations at the building base ranged from 49 to 210 cm/s^2, and those at top of the building ranged from 150 to 427 cm/s^2. The average story drift angle (ratio of peak displacement of top to its height) varied from 0.00061 to 0.00331 rad. In most tall buildings of steel construction, the damping ratios estimated were approximately in the range between 1% and 2%. This is believed to be a main reason for higher AMR shown in Figure 3. Excessive accelerations have been found to cause large economic loss due to the damage on non-structural components and facilities. Thus, acceleration magnification should be taken in structural design more seriously. By this reason, the following discussion will refer to both displacement and acceleration.

29-Story Building

The building is a seismically-resistant 29-story steel building constructed in 1989 (Hisada et al. 2011, 2012, Kasai et al. 2012). It is a school building of Kogakuin University, located in Shinjuku ward of central Tokyo. The building height is 143 m, structural framing height 127.8 m, and floor plan dimension is 38.4 and 25.6 m in EW and NS (x- and y-) directions, respectively (Hisada et al. 2011, 2012, Kasai et al. 2012).

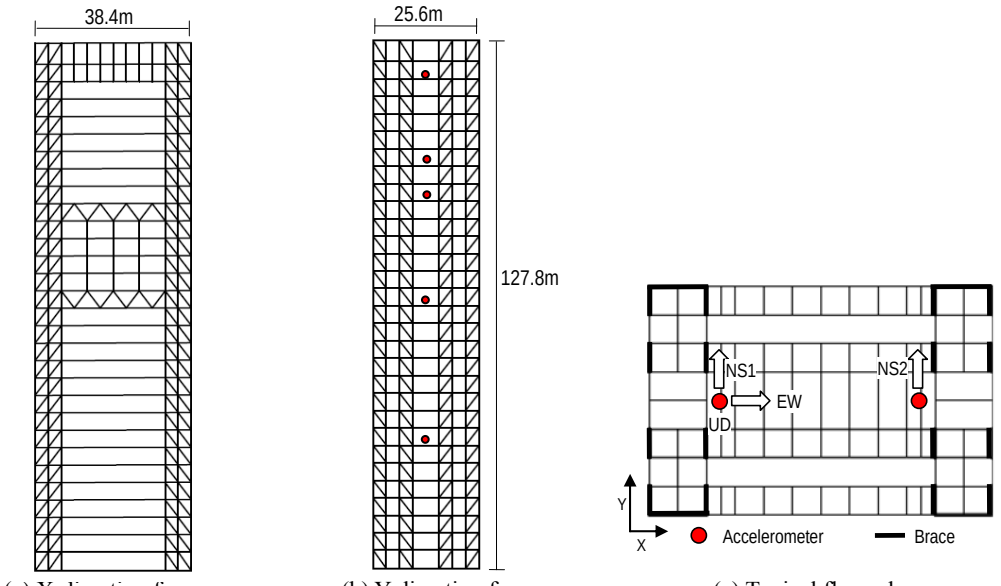

(a) X-direction frame (b) Y-direction frame (c) Typical floor plan

Figure 4. Seismically-resistant 29-story building

The peak accelerations in x- and y-directions were 91 and 89 cm/s^2 at the base, and 235 and 316 cm/s^2 at the top floor, respectively. The average drift angle is 0.029 rad., and the structure remained elastic. The vibration periods for the first three modes are 2.96s, 1.00s, and 0.52s for x-direction, and 3.10s, 0.94s, and 0.47s for y-direction, respectively. Likewise, damping ratios are 0.017, 0.018, and 0.034 for x-direction, and 0.021, 0.016, and 0.034 for y-direction,

respectively. Damping ratio 0.01 was estimated from small amplitude vibration tests before 2011 (Hisada 2011).

Figure 5a shows y-direction pseudo-acceleration response spectra S_{pa} of recorded building base accelerations (solid line) and that of recorded building top floor accelerations (broken line), respectively. Damping ratios are set to 2% and 3%, considering responses of building and non-structural component such as ceiling (Kasai 2011b), respectively. Similarly, Figure 5b shows displacement spectra S_d's of the acceleration records, respectively. The two vertical axes on two sides of each figure are in reference to responses of the building and the component at the top floor, respectively.

S_{pa}'s of recorded base acceleration are large at the building 2nd (0.94s) and 3rd (0.47s) mode periods, suggesting excitation of building's higher modes by ground shaking. S_{pa}'s of recorded top floor acceleration are extremely large at the 1st (3.09s) and 2nd (0.94s) modes of the building, and their values are 1,600 and 2,400 cm/s^2, respectively. Time history analyses of components having the periods have indicated many cycles of large accelerations. On the other hand, S_d's of both the building base and top floor accelerations almost monotonically increase with the period, suggesting strong dependency of displacement of both building and non-structural component at top floor on the 1st mode period (3.09s) of the building. Note that the broken line in Figure 5b shows the component may move 400cm, if it is flexible enough to resonate with the building's 1st mode. Figure 6 shows move of furniture and falling of ceiling and books due to the high accelerations. By these reasons, effects of the higher modes must be seriously considered when designing tall buildings.

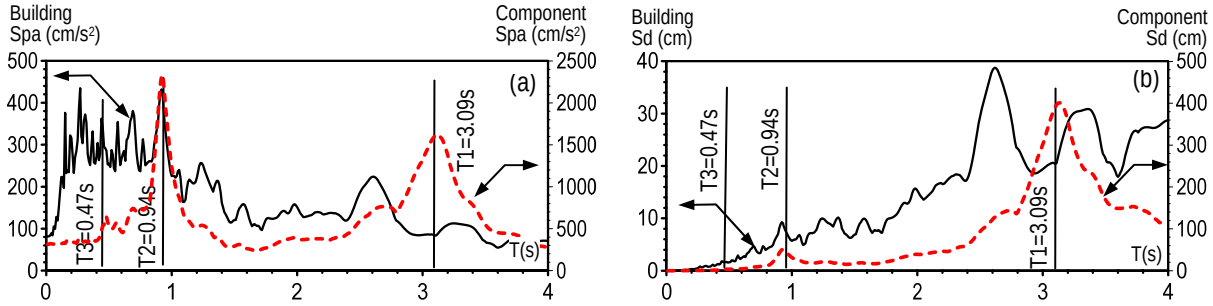

Figure 5. Response spectra (solid lines) of the building base acceleration, and those (broken lines) of the building top floor acceleration

(a) Falling of ceilings (b) Falling of books

Figure 6. Damage to contents of 29-story bldg. (From Prof. Hisada)

Figure 7a compares acceleration records at top floor and base in y-direction. The earthquake duration is long, and is considered to be about 200 seconds (Fig. 7a). For the first 90 seconds of the figure, high frequency response of the top floor is apparent, as confirmed by the large number of cycles per unit time. These are caused by the high-frequency ground shaking, as shown by the base accelerations. In contrast, for the last 110 seconds, low frequency response is dominant. The ground shaking is weak (Fig. 7a), but its low frequency contents excited the first mode and caused resonated response.

Figures 7b compares the top floor acceleration recorded with that calculated by method 2 mentioned earlier. The good agreement suggests that the mode method is effective, and the first three modes are adequate in response calculation for this case. Figure 7c compares relative displacement of top floor obtained by double integration of the record (method 1) with that calculated by method 2. In some cycles the peak values by the both method differ a little, but the displacements agree well overall.

As is known, the contribution of each vibration mode depends on the type of response as well as the story level determining participation vector. Since the properties and responses of each vibration mode have been obtained, it is possible to discuss such contributions:

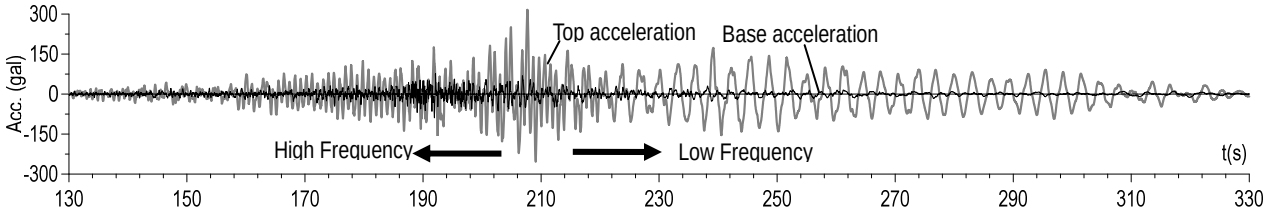

(a) Accelerations recorded at top and base.

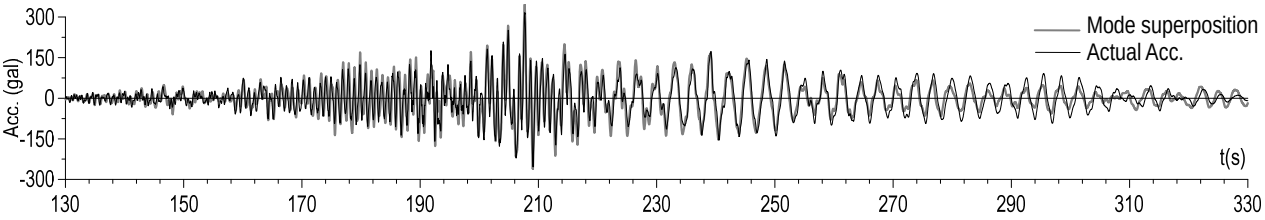

(b) Comparison: acceleration obtained by mode superposition vs. actual recorded acceleration.

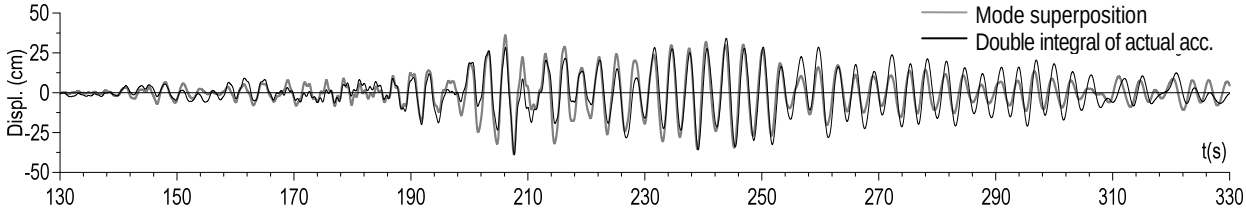

(c) Comparison: dispt. obtained by mode superposition vs. dispt. from double integral of recorded acceleration.

Figure 7. Acceleration records and accuracy of mode superposition method.

Figure 8a shows the acceleration of each mode at the top floor. As mentioned earlier, it is dominated by the 2nd, 1st, and 3rd modes in the order of weight for the first 90 seconds. For the later 110 seconds, the 1st mode response increases and become dominant, with slight contribution from the 2nd mode. As Figure 8b shows, for the 16th floor the 2nd mode is much more dominant, developing almost the same acceleration as top floor. As for the displacement at top floor (Fig. 8c), the 1st mode dominates throughout the entire duration.

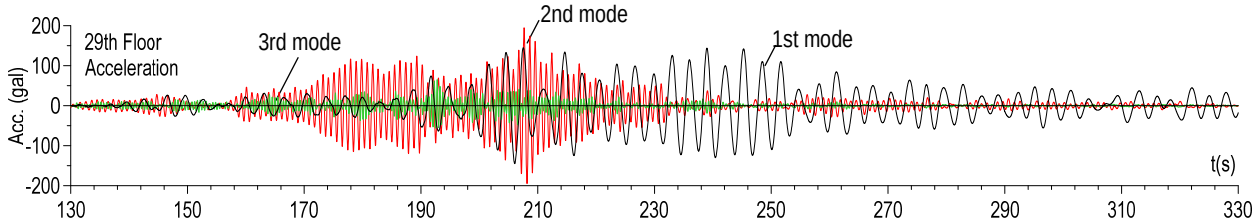

(a) Modal contributions to top floor acceleration.

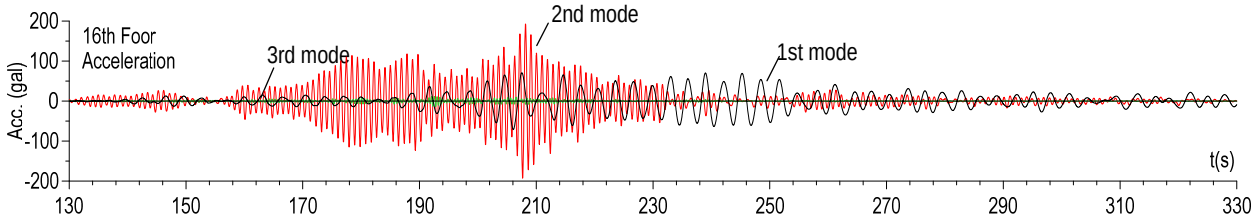

(b) Modal contributions to 16th floor acceleration.

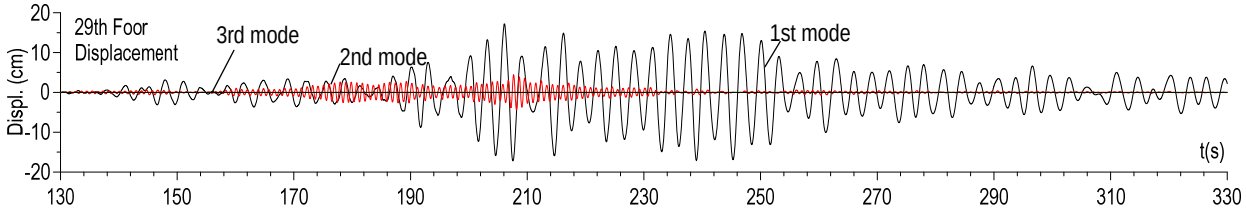

(c) Modal contributions to top floor displacement.

Figure 8. Contributions of the first three modes to acceleration and displacement of Building 1.

Supplementally-Damped Buildings

Response Trends in Kanto Area: Deformation- & Velocity-Dependent Dampers

Ten supplementally-damped buildings investigated by JSSI and located in Kanto area were 5- to 54-Story. Peak accelerations at the building base ranged from 53 to 142 cm/s^2, and those at top of the building ranged from 118 to 435 cm/s^2. The average story drift angle varied from 0.00026 to 0.00372 rad. Note that the buildings with steel dampers showed high accelerations at top, similarly to the seismically-resistant buildings explained earlier. This is because the steel dampers were elastic or barely yielding for the level of the ground shaking in Tokyo, and dissipated little energy.

As a matter of fact, the above-mentioned difference among the deformation-dependent steel damper and three types of velocity dampers, oil dampers, viscous dampers, and viscoelastic dampers, respectively, were demonstrated by the full-scale tests of 5-story supplementally

damped building using the world's largest shake table called E-Defense (Kasai et al. 2009, Kasai 2013). Figure 9 depicts the hysteresis of the four damper types under minor, moderate, and major shaking. The steel damper is elastic at the minor shaking and did not dissipate seismic energy, whereas the three velocity-dependent dampers do even under small deformation. The force of the steel damper was also larger than others. These lead to larger accelerations of the building under minor to moderate shaking.

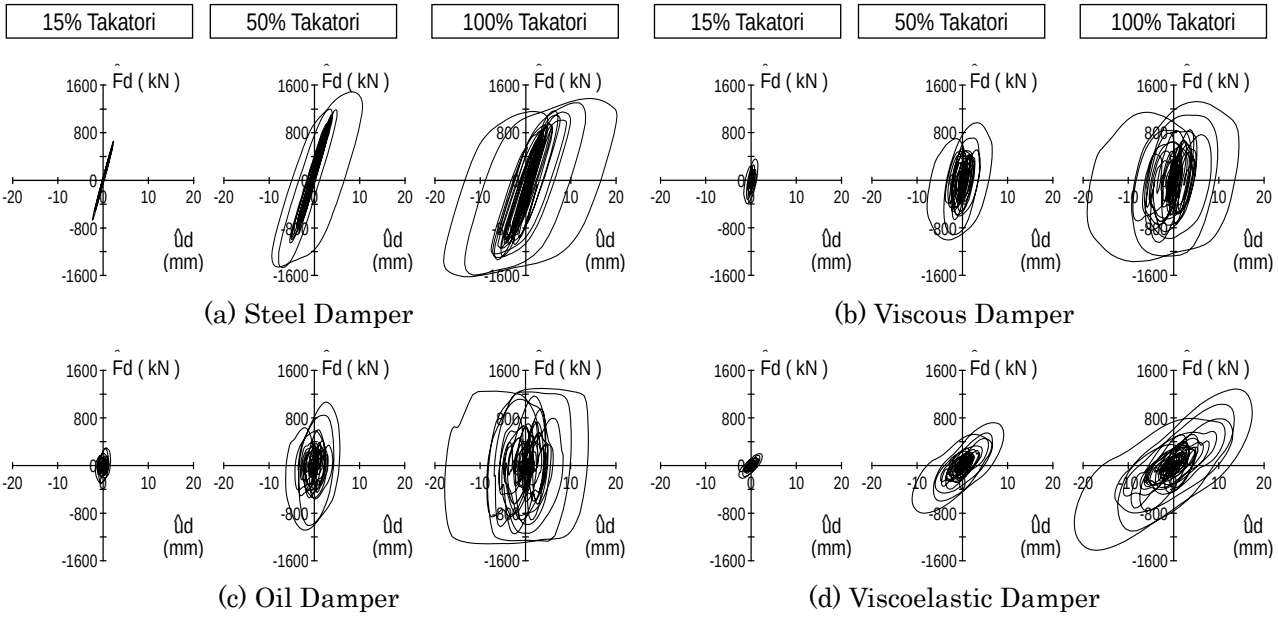

Figure 9 - Damper axial force and stroke, four types of dampers in the full-scale 5-story building tested by the world's largest shake table (used 15, 50, and 100% scale ground accelerations recorded at the JR Takatori station during the 1995 Kobe earthquake)

In Japanese practice to-date, design criteria for supplementally-damped buildings have been set for displacement control, and rarely for acceleration control. The acceleration-induced hazard, however, appeared to be significant during the 2011 Tohoku earthquake, and its mitigation by adding damping seems essential. Therefore, adding velocity-dependent dampers capable of energy dissipation at small to moderate shaking would increase damping ratio.

The observations from the full-scale tests of the 5-story building (Figure 9) appear to be consistent with those of existing tall buildings with dampers. Figure 10 shows the transfer function obtained using the acceleration of building top floor and base for the 38-story building having steel dampers only (Fig. 10a), and the building having both steel dampers and viscous dampers (Fig. 10b). They are located nearby, and were subjected to almost the same ground shaking. The former shows the 1st mode damping ratio of 0.017, similar to the value obtained from the 29-story conventional building explained in the previous section. On the other hand, the latter showed the 1st mode damping ratio of 0.046. The larger damping ratio of the building with steel and viscous dampers can be understood from wider resonance curves (Figs. 10a, b). The damping ratio of 0.046 may not sound very high, but the amount of dampers and viscosity coefficients added are considerable, and still show good vibration control, as will be demonstrated in the subsequent sections.

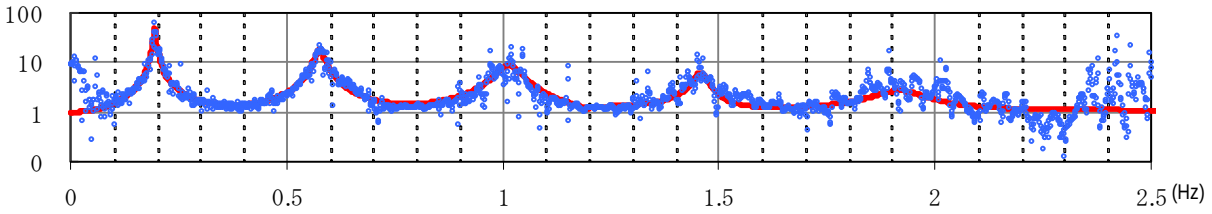

(a) 38-story bldg. (179m) with steel dampers only, 1st mode damping ratio = 0.017, period = 5.08 s

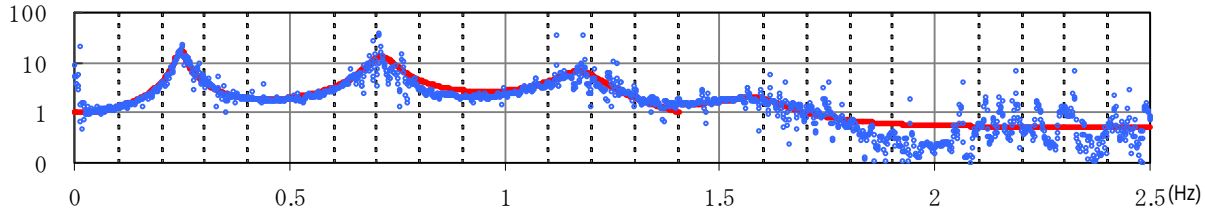

(b) 37-story bldg. (198m) with steel & viscous dampers, 1st mode damping ratio = 0.046, period = 4.05 s

Figure 10 Transfer Functions of Tall Buildings (a) with Steel Dampers Only, and (b) with Steel and Viscous Dampers

21-, 41-, and 54-Story Buildings

Three tall buildings with velocity-dependent dampers will be discussed. They are 21-, 41-, and 54-story buildings as shown in Fig. 11. The first building is a 21-story government office building (Koyoma and Kashima 2011, Kasai 2011a, b, Kasai et al. 2012). It consists of a steel frame and 336 low yield point steel (wall) dampers and 284 viscous (wall) dampers (Fig. 11a). As found from the full-scale test mentioned earlier, a contrasting case of using only steel dampers lead to large accelerations, since the dampers remained elastic for the level of shaking in Tokyo (Kasai 2011a,b, Kasai et al. 2012). The 21-story building had been designed to avoid such a situation, expecting that viscous damper would dissipate energy from a small earthquake, and steel damper, the most economical among all types, would dissipate considerable amount of energy at a large quake, respectively.

The second building is a 41-story office building (Kasai 2011a,b, Kasai et al. 2012). It consists of a frame using concrete-filled tube columns and steel beams, and 688 oil dampers (Fig. 11b) mentioned earlier. The relief mechanism to limit the force was provided, but most likely relief did not occur for the level of shaking.

The third building is a 54-story office steel building constructed in 1979. It was retrofitted in 2009 (Maseki et al. 2011, Kasai et al. 2011a,b) by attaching 288 oil dampers (Fig. 11c). 12 dampers per floor were attached to middle 24 stories of the building. The oil damper is similar to those used for the 41-story building, except that its relief mechanism is modified to reduce forces near peak responses. This aims to reduce the axial force of the column transmitting the damper force, and consequently uplift force of foundation. Most likely, however, the relief did not occur for the level of shaking.

The acceleration magnification ratio (AMR), the largest ratio of both x- and y-directions, was 1.80, 2.38, and 2.51 for the 21, 41, and 54-story buildings, respectively. They are well

below the ratio of 3.55 obtained in the seismically-resistant 29-story building. The three buildings remained elastic, and modal properties are obtained from method 2, and estimated 1st mode damping ratios are about 4%, and those of the 2nd and 3rd modes are almost equal or larger. The 1st mode vibration periods in x- and y-directions are 1.83s and 1.97s fot the 21-story building, 3.97s and 4.10s for the 41-story building, and 5.37s and 6.43s for the 54-story building..

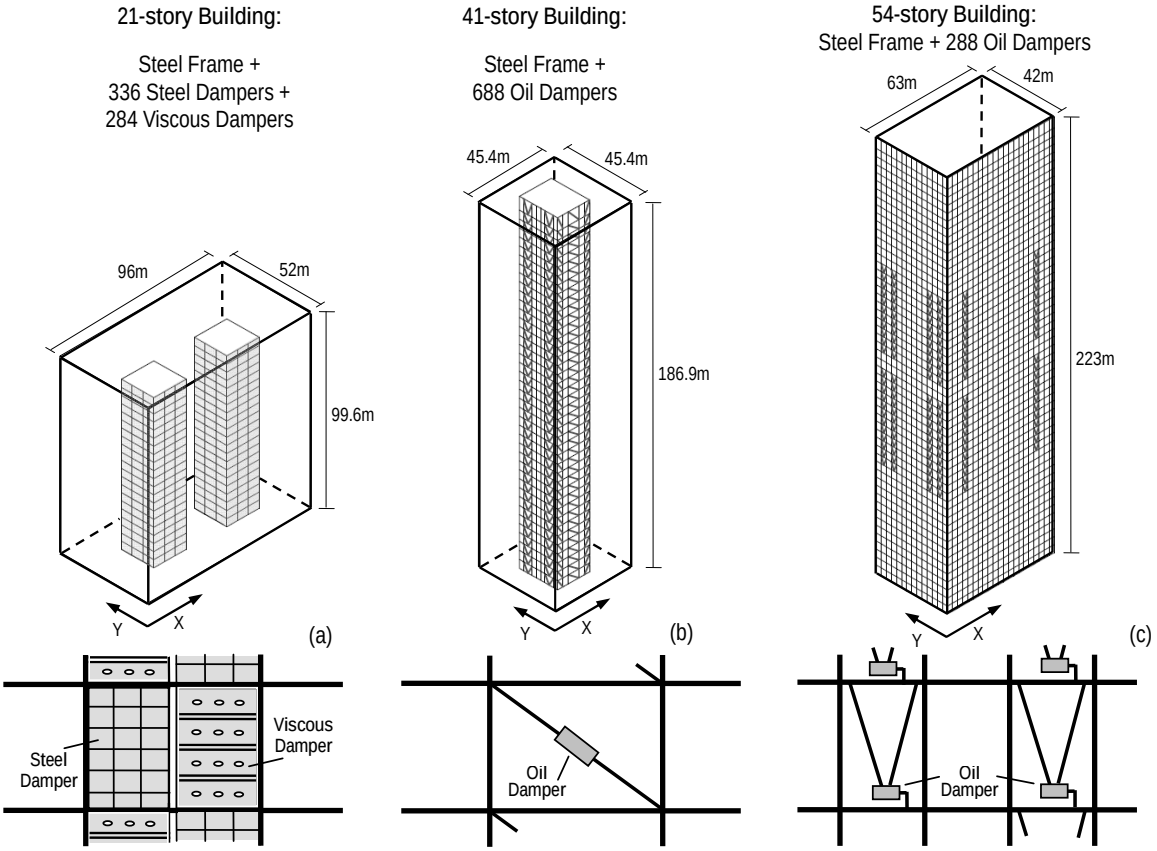

Figure 11 Three buildings with velocity-dependent dampers.

Modal properties were estimated for the three buildings, and their accelerations and displacements are obtained from superposition up to the 3rd mode, and accuracies are confirmed to be even better than those shown in Figs. 7b and c shown earlier. Such responses at top floor are shown by black lines in Figures 12, 13, and 14 for 21-, 41- and 54-story buildings, respectively. In these three buildings, the acceleration is dominated by the 2nd and 3rd modes for about 100 seconds, and by the 1st mode for later 200 seconds. Whereas, the displacement is dominated by the 1st mode throughout the shaking.

This trend is like that of seismically-resistant 29-story building (Fig. 8), but the amplitudes are believed to be smaller due to the supplemental damping. Thus, the responses are compared with those of lower but possible damping ratio representing a hypothetical case of not using the dampers. The modal period is unchanged, assuming small stiffness of the damper. The 1st to 3rd mode damping ratios are uniformly set to 1% and superposition is repeated. The results are shown by gray lines in Figs. 12, 13, and 14 for 21-, 41- and 54-story buildings, respectively.

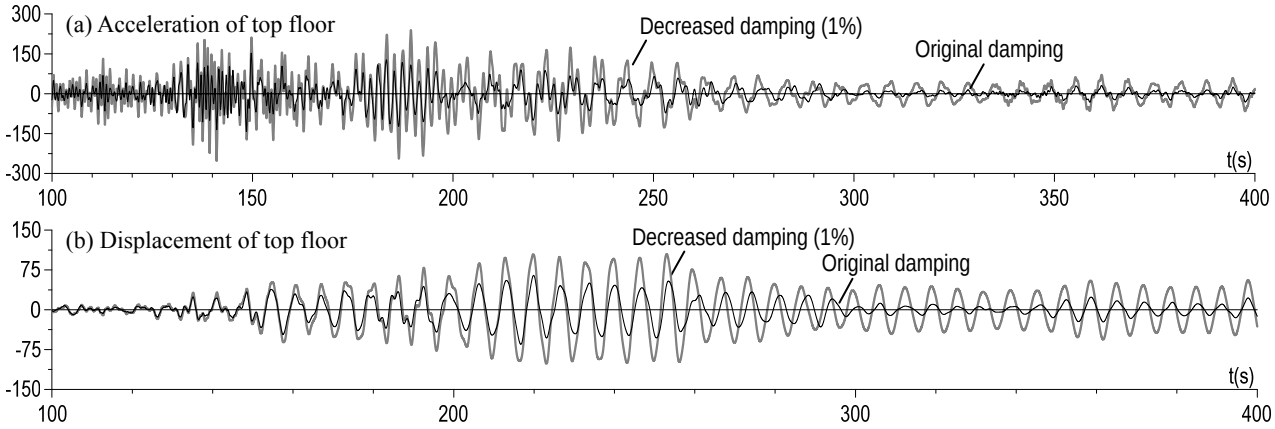

Figure 12. 21-story bldg. responses with original and lowered damping ratios (y-dir.).

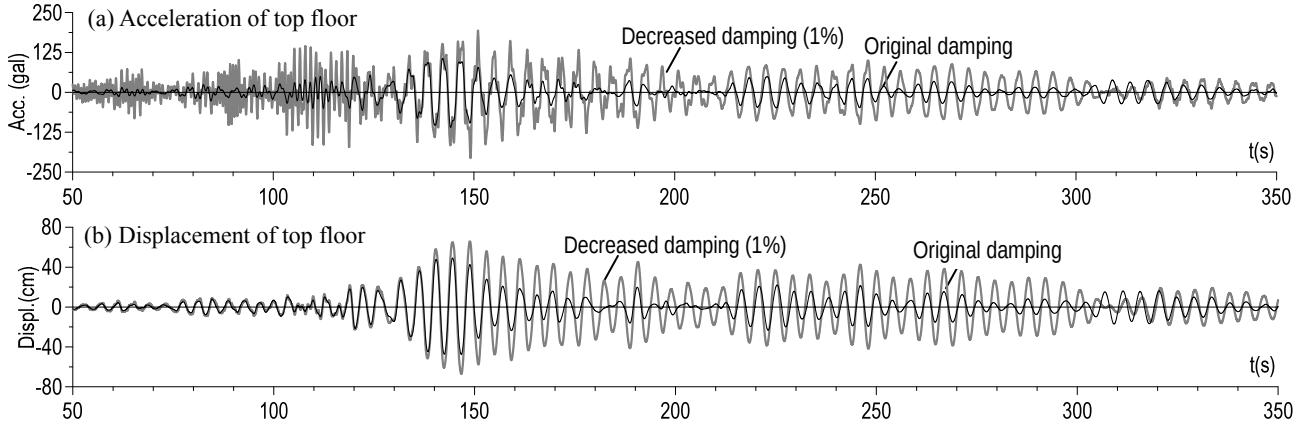

Figure 13. 41-story bldg. responses with original and lowered damping ratios (x-dir.).

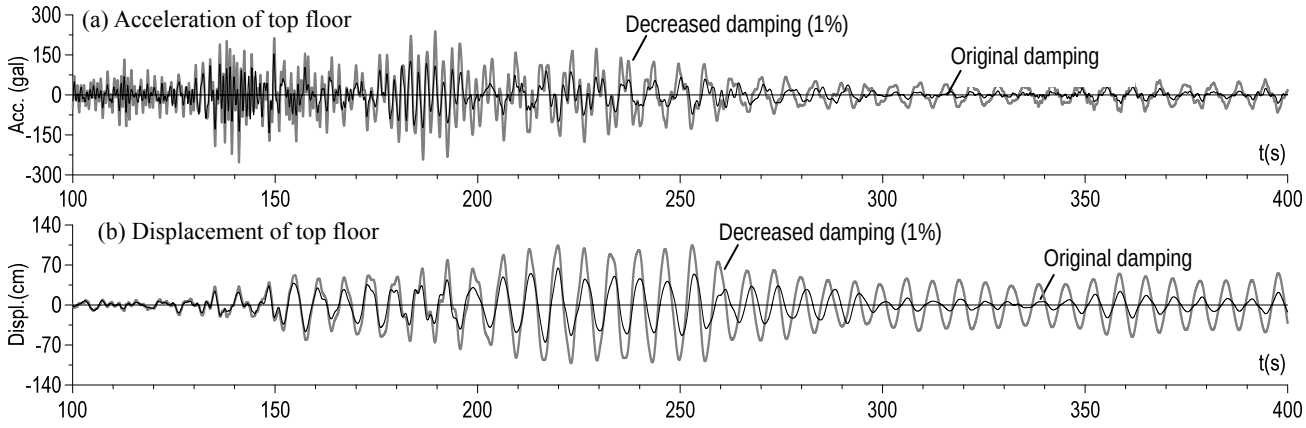

Figure 14. 54-story bldg. responses with original and lowered damping ratios (y-dir.).

In all the three buildings, their responses are considerably smaller (black lines) than those with lowered damping (gray line). The peak accelerations and displacements are about 0.5 and 0.7 times those of the low damping case. Moreover, between significant ground shakings, the

responses decay much faster, and number of large cycles is reduced considerably. These help reducing damage and fatigue of structural and non-structural component as well as fear or discomfort of the occupants. In order to quantify such an effect, root mean square of the acceleration and displacement at top are calculated, and their values appear to be about 0.4 and 0.5 times those with low damping, respectively.

Base-Isolated Buildings

Response Trends in Kanto Area

Sixteen base-isolated buildings investigated by JSSI and located in Kanto area are 2- to 21-Story. About 60% of the buildings use natural rubber bearings with dampers, which is consistent with the nationwide trend in Japan. And, about 40% of the buildings use high damping rubber bearing or lead rubber bearing, without utilizing externally attached dampers. Peak accelerations at the ground level ranged from 45 to 402 cm/s^2, and those at top of the building ranged from 57 to 181 cm/s^2. The maximum displacement at the isolation level, typically estimated from the accelerations and their double integrations, ranged from 59 to 140 mm.

As shown in Figure 15, the acceleration magnification ratio (AMR), is estimated for each horizontal direction and each building, and it is plotted against the PGA (Kasai et al. 2013). Remarkably, AMR and PGA are strongly correlated, and AMR becomes smaller for the larger PGA. The hysteretic characteristic of the base-isolated level is typically a softening type, in which larger excitation results in more deformation, less equivalent stiffness and more energy dissipation, leading to a high damping system. In such a case, better control of accelerations occurs, reducing the AMR. This will be further discussed in a later section by referring to such hysteresis behavior.

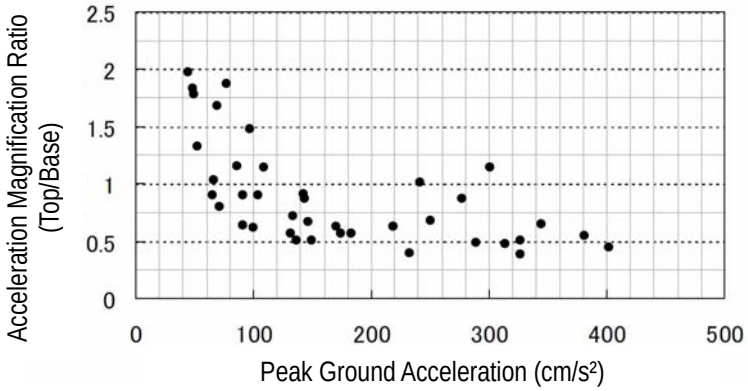

Figure 15. Relationship between acceleration magnification ratio (AMR) and peak ground acceleration (PGA) of base-isolated buildings

20-Story Isolated Building

Figure 16 shows the 20-story base-isolated building of Tokyo Institute of Technology located in Yokohama, Kanagawa Prefecture (Matsuda et al. 2012). The foundation and 1st floor of this building are RC structure, and other floors are hybrid with steel beams and CFT columns. Figure 17 shows the plan of the isolation floor and isolation system: the 1,200 mm diameter rubber bearing with conical spring (Fig. 17a) is installed in position A. Combined steel damper

and 1,100 mm diameter rubber bearing (Fig. 17b) and steel damper alone (Fig. 17c) are installed in positions C and D, respectively. In position E, the 1,000kN oil damper (Fig. 17e) is installed.

The so-called mega-braces (□ - 500mm x 160mm x 19 to 32mm) on both sides of the building stiffen the superstructure. Because of high aspect ratio of 5 (Fig. 16), large uplift force may develop at the rubber bearings due to the large overturning moment. To avoid this, the bearings are allowed to move upward within 20 mm of gap distance (Fig 17a).

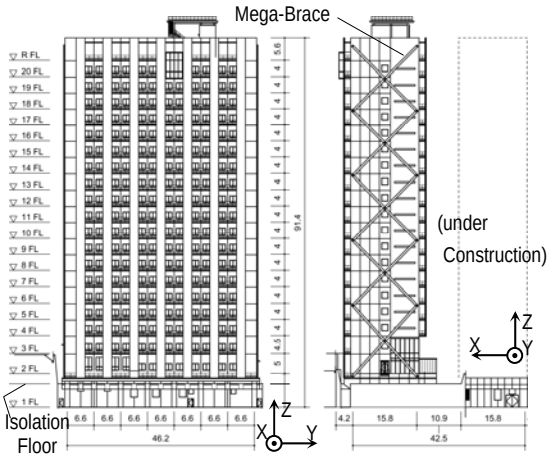

Figure 16 Base-isolated 20-story building (unit: m)

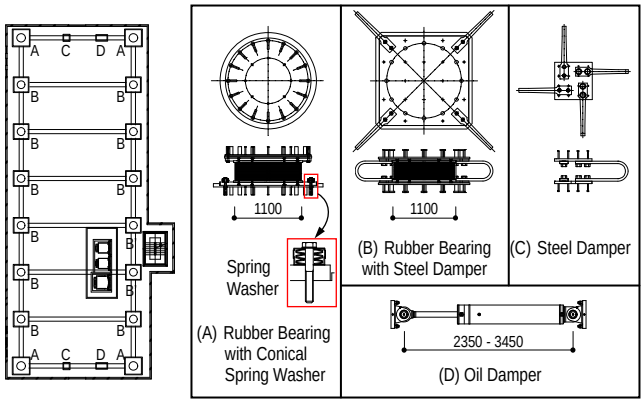

Figure 17 Isolated floor and isolation system

Figure 18 compares the deformations of isolation system obtained from the scratched lines created by the trace recorders, data from wire type displacement sensors, and double integration of the relative acceleration measured by the sensors above and below the isolation system. The deformations obtained from the three distinct methods agree well, validating the measurement method and data. Peak deformations of 69 and 91mm are recorded in X- and Y-directions, respectively, and torsional response appears to be negligible because the two results at the two most remote points are identical (Figs. 18a and b).

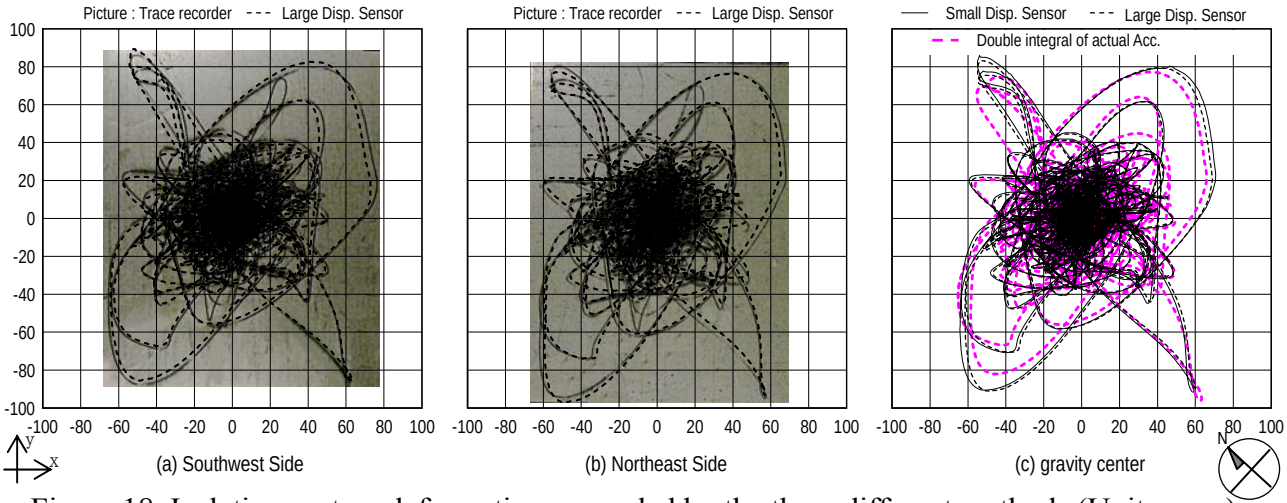

Figure 18. Isolation system deformations recorded by the three different methods (Unit：mm)

Because the whole structure is a non-proportional damping system having high damping concentrated at the isolation floor, the data analysis method 2 discussed earlier is used in two different cases as described below:

(1) Like the proportional damping case, modal period, damping ratio, and participation vector are obtained by the basic system ID technique using the acceleration of ground (1st) level as input and those of other (2nd, 7th, 14th, and 20th) levels as output for the transfer function.

(2) The system ID is applied to superstructure only, using the acceleration of the base (2nd) level as input and those of other (7th, 14th, and 20th) levels as output for the transfer function.

The properties up to the third mode were estimated for the above two cases. The first mode properties are listed in Table 1.

Table 1. Base-isolated 20-story building: the first mode vibration periods and damping ratios estimated for cases (1) and (2), respectively.

	X-direction		Y-direction	
	Period (s)	Damping ratio	Period (s)	Damping ratio
Base-isolated case (total building)	2.92	0.070	2.98	0.105
Seismic resitant case (only superstracture)	2.01	0.021	2.15	0.046

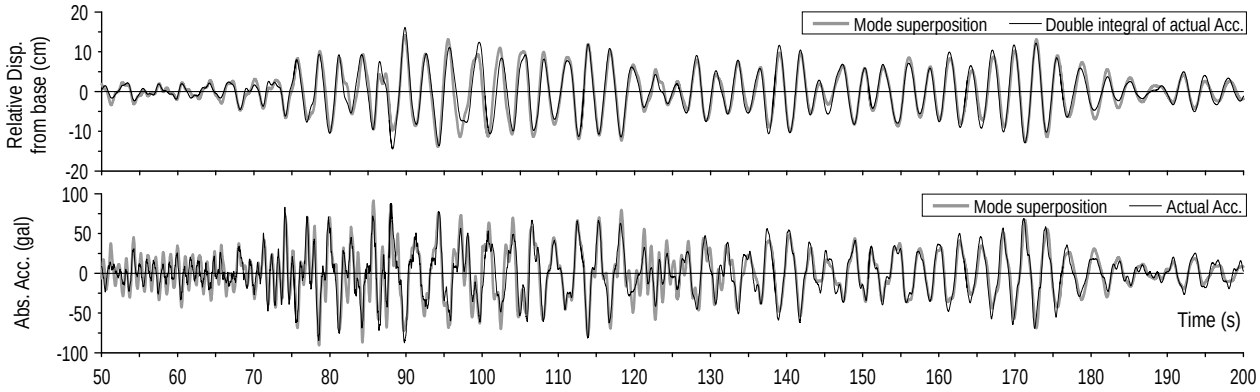

(a) Case 1: Analysis of whole structure (isolation system included), using 1st floor accelerations as input.

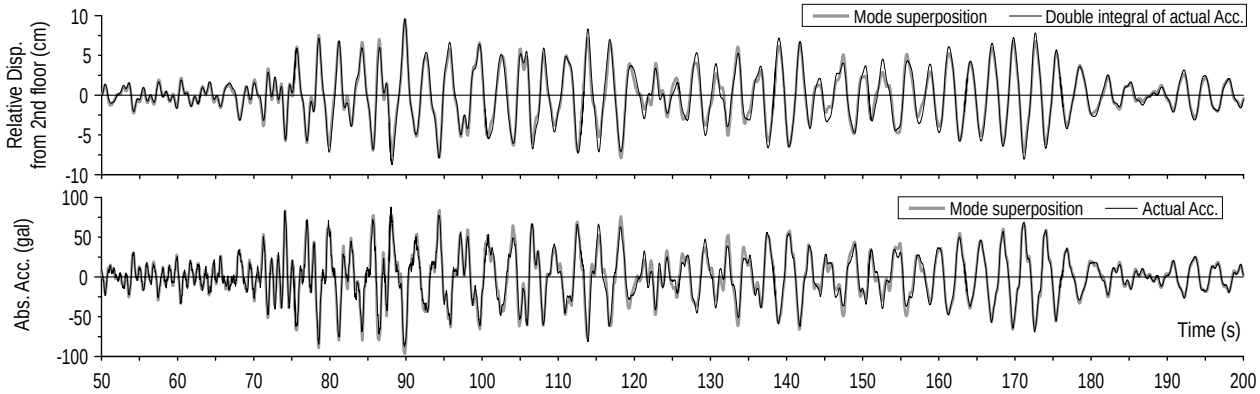

(b) Case 2: Analysis of superstructure only, using 2nd floor accelerations as input.

Figure 19. Comparison of top-level behavior between recorded data and modal analysis using identified modal frequencies and damping ratios in X-direction

Figure 19 compares the building top level displacements and accelerations between the records and mode superposition analysis results. The latter used the modal properties estimated from the basic system ID technique explained above. Even for the non-proportional case (Case (1)), the analysis simulated well the time histories of displacement and acceleration (Fig. 19a). This is because yielding and hysteretic damping of the steel damper was not significant for the level of the deformations noted (Fig. 18). Since yield displacement of the damper is 32 mm, the ductility ratios in X- and Y-directions were only about 2 and 3, respectively. Another reason is that the flexible and tall superstructure contributes more to the displacement and acceleration at the top level, and it is closer to proportional damping system. Therefore, cases of shorter isolated building or significant yielding of damper would produce more errors than reported here. On the other hand, small damping and approximately proportional case (Case (2)) is simulated extremely well (Fig. 19b).

In addition to the mode-superposition time history analyses, more detailed system ID technique called the autoregressive with exogenous inputs (ARX) method (Isermann and Münchhof, 2011) is used to validate the modal properties of the whole building (e.g., Case (1) of Table 1). ARX method gives step-by-step estimate for damping ratio and vibration period, and the average taken between their highest and lowest values over the entire duration seems to agree with the value in Table 1 (Matsuda et al. 2012). Note also that the above methods consistently indicated larger period shift and damping ratio in Y-direction where dampers were yielding more.

Additional Comments on Performance

Based on validations described above, the vibration periods and damping ratios of Case (1) are estimated for the past records from (a) microtremor, (b) March 9 earthquake, (c) March 11 Tohoku Earthquake, (d) March 11 after-shock, and (e) microtremor. The ground motions of (b) and (d) are almost half of the ground motion (c), and the results are shown in Figure 20. It clearly indicates higher damping and longer period for the stronger ground shaking. Therefore, larger isolation effect from the steel dampers could be expected for stronger earthquake.

Note also that the acceleration magnification ratio (AMR) during the March 11 event was about 1.7 (Fig 21), and it was as high as 3.1 for the weaker ground motion considered above. The high-rise base-isolated building whose superstructure is relatively flexible (see Table 1) and the steel damper showing only moderate yielding made equivalent stiffness of the isolation

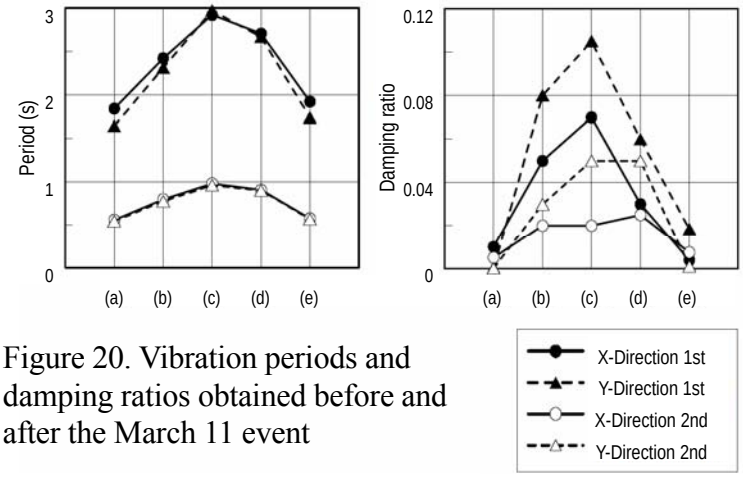

Figure 20. Vibration periods and damping ratios obtained before and after the March 11 event

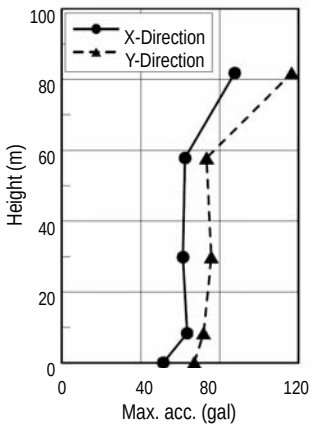

Figure 21. Peak accelerations

system relatively high, causing the building to behave like a seismically-resistant building. However, as noted above the performance is expected to be better fro the stronger ground motions. This point, however, should be carefully examined considering much stronger earthquake that will definitely happen in the near future.

Like the supplementally-damped building cases discussed earlier, observed performance of the base-isolated building will be compared with that of the building without isolation system. The latter uses modal properties of the superstructure (Case (2)) and the ground (1st) level acceleration rather than the base (2nd) level accelerations that were used for the system ID. The result is shown in Figure 22. Although the displacements of the top level are similar in the two buildings, acceleration of the base-isolated building is only about 0.5 times that of the seismically-resistant building.

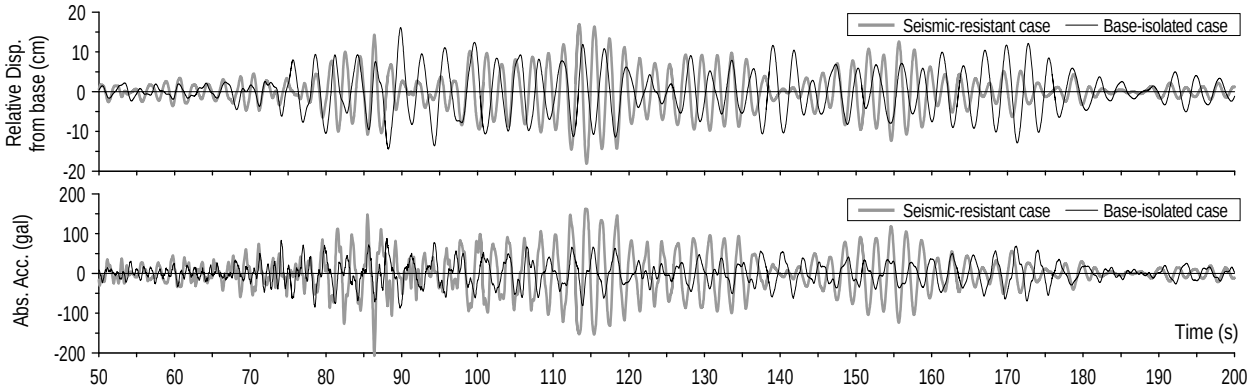

Figure 22. Comparison of base-isolated case and seismically-resistant case by modal analysis

As can be understood from this paper, the writers have been performing data analysis mainly by using the standard modal approach in various ways. However, for some cases of highly concentrated damping and/or nonlinearity in the building, floor-by-floor stick model or member-by-member frame model can provide different and useful information. The most significant advantage of such modeling is direct referencing to the physical responses rather than modal responses. The forces of a particular floor level or member are directly estimated by this model, which has been utilized to interpret the records at Tokyo Institute of Technology.

Figure 23 shows an example for such a model created to clarify the hysteretic responses and properties of the isolation system in the base-isolated 20-story building. Base shear and isolation system deformation are obtained by estimating inertia forces as well as the deformation from the recorded accelerations. The hysteresis is shown for three distinct phases of excitation, and linear and bilinear performance of the steel damper is clearly seen. The envelope curves are in excellent agreement with the design curves, therefore the steel damper has functioned as planned.

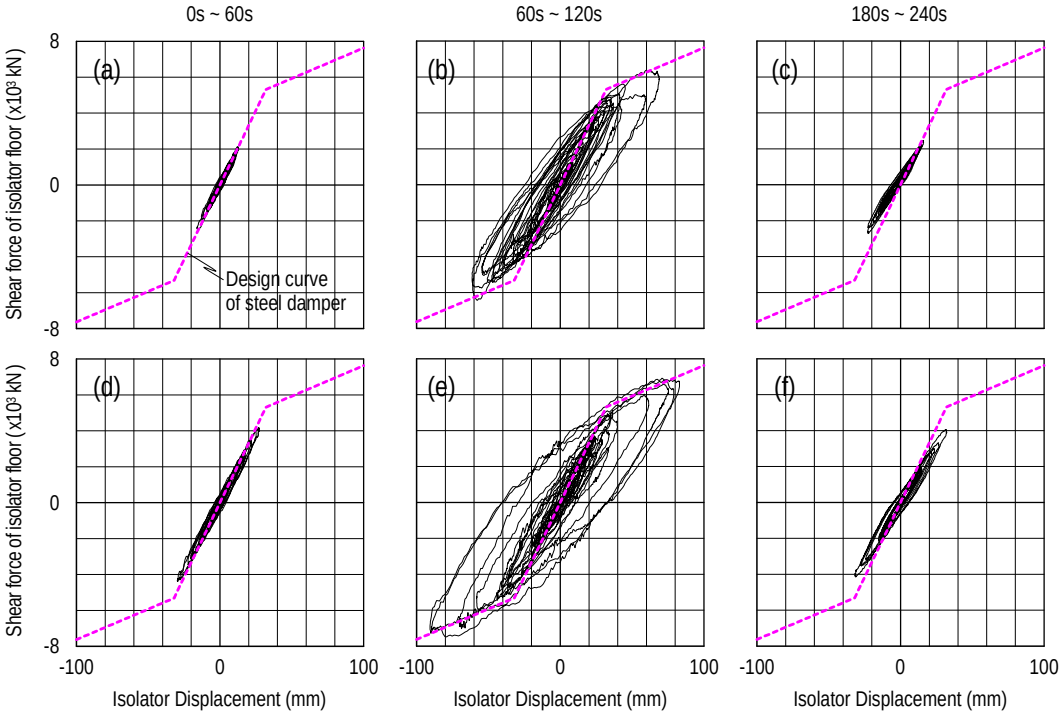

Figure 23. Hysteresis of isolation system in X-direction ((a) ~ (c)), and Y-direction ((d) ~ (f))

Accelerations of Nonstructural Components

Inertia forces against structural and non-structural components including equipment and building content are produced by accelerations in the building. Large accelerations typically developed at upper stories cause falling, overturning, shifting, crashing, rapture, and excessive vibration of a variety of non-structural components. Economic loss due to damage of non-structural components is much more than that of structural damage. Falling of ceilings and other components may also cause death of occupants. Such failures due to the 2011 Tohoku Earthquake were enormous.

Figure 24a-d show component acceleration spectra (CAS) for the top floors of the 29-story seismically-resistant building, and 21, 41, and 54-story supplementally-damped buildings, respectively. Damping ratio of the component is assumed to be 3%. For the 29-story building (Fig. 24a) seismically-resistant, the curve of the broken line is generated from the floor acceleration record, and solid line is generated from floor accelerations that come from the modal superposition time-history analysis by assuming increased damping ratio of 4% for the first three modes. In contrast, for the three supplementally-damped buildings (Fig. 24b-d), the solid line is generated from the top floor acceleration records, and the broken line from floor accelerations that come from the time-history analysis by assuming decreased damping ratio of l% for the first three modes. The plots indicate a merit of increasing building damping for protecting the acceleration-sensitive components.

According to Figure 24, the past belief that short-period components are safer in a tall building is incorrect. They are as vulnerable as the long-period components due to multiple resonance peaks created by different modes of the building. The peaks are extremely high,

even greater than 2,000 cm/s^2 (≈2G). Thus, the resonant acceleration of the components may be greater than 8G at a so-called major quake 4 times or stronger. The problem may become more serious when damage and softening of components cause period shifting from one resonance peak to others. Note that three peaks for each building are shown in Figure 24, since the first three modes were identified. But more peaks may emerge in an actual low damping case.

As a rule of thumb, facilities may overturn when floor acceleration exceeds 0.3G, and ceiling whose vibration period typically ranges from 0.3 to 1s may fall when its acceleration response exceeds 1G. These indicate the needs for an immediate attention to component responses at a major quake that will occur in Tokyo. Figure 24 also clearly indicates that even moderately increasing the building damping ratio by 3% or so would reduce the component acceleration considerably.

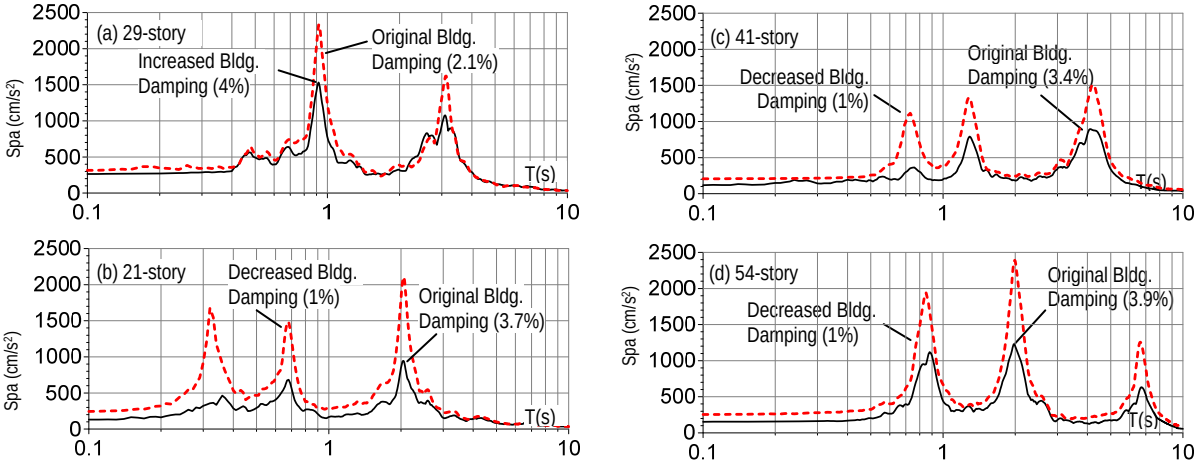

Figure 24. Component Response Spectra (Component Damping Ratio = 3%) at top floors of a seismically resistant building and three supplementally-damped buildings..

Finally, the solid line of Figure 25 shows the CAS at the top floor of the base-isolated 20-story building discussed above. It is generated from the floor acceleration record, and broken line is generated from floor accelerations that come from the modal superposition time-history analysis assuming the seismically-resistant building with no isolation system. Unlike Figure 24, the resonance period as well as the peak CAS vales of the two buildings are very different, and good performance of the base-isolated building for acceleration control is clearly seen.

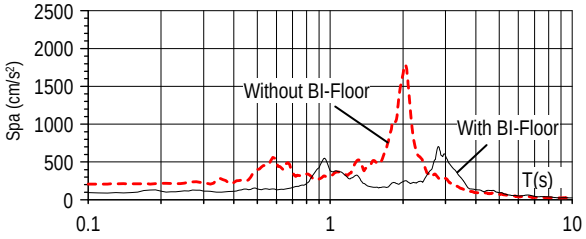

Figure 25. Component Response Spectra (Component Damping Ratio = 3%) at top floor of a base-isolated 20-story building

Conclusions

Responses of the tall buildings in Tokyo during the 2011 Tohoku Earthquake are discussed based on the strong motions recorded. By successfully analyzing contributions of multiple vibration modes, various shaking phenomena in the tall building that had not been experienced are clarified. Moreover, the most significant evidence of response-control effectiveness was presented, and the merits of damping technology as well as base-isolation technology for occupants and contents are explained.

In most seismically-resistant tall buildings of steel construction, the damping ratios were approximately in the range between 0.01 and 0.02. This is believed to be a main reason for higher magnification of acceleration. Excessive accelerations have been found to cause large economic loss due to the damage on non-structural components and facilities. Thus, acceleration magnification should be taken in structural design more seriously.

The tall buildings with velocity dependent dampers had damping ratios of 0.03 to 0.05 typically. Their responses were compared with those generated from hypothetical analyses assuming low damping ratio of 0.01. They show reduction of peak responses, significantly faster decay of vibration, which would lead to reducing damage and fatigue of structural and non-structural components as well as fear of the occupants. In this regard, steel damper, although economical and effective for a major event, could be supplemented with velocity-dependent dampers for better performance.

In Kanto area, tall base-isolated buildings have shown for the first time the special vibration characteristics which had been expected but not observed until the 2011 Tohoku Earthquake. The loss of isolation effects due to slender configuration as well as moderate yielding and small energy dissipation of steel damper lead to magnification rather than reduction of the accelerations in the superstructure. For larger earthquake, the building performance is expected to be much better, but this point must be studied carefully.

Immediate attention must be given to mitigate acceleration-induced hazards in existing and new tall buildings against much stronger shaking likely to occur in the near future. The use of supplemental damping or base-isolation appears to be desirable, since it can reduce not only peak accelerations but also number of large response cycles, and duration of significant shaking.

The present paper has discussed issues related to response-control, focusing on global responses of the system. In order to assure such design, all members must be properly sized. Hence, designs for the components such as beams, columns, connections, and dampers are important and are currently studied by the writer and the colleagues.

References

(1) Kasai, K., Motoyui, S., Ozaki, H., Ishii, M., Ito, H., Kajiwara, K., and Hikino, T. (2009), Full-Scale Tests of Passively-Controlled 5-Story Steel Building Using E-Defense Shake Table; Part 1 to Part 3, Proc. Stessa2009, Philadelphia.

(2) Kasai, K. (2011a). 4.2.3 Acceleration records of buildings, 4.4.5. Behavior of response controlled buildings, Preliminary Reconnaissance Report of the 2011 Tohoku-Chiho Taiheiyo-Oki Earthquake, Architectural Institute of Japan, pp.280-284, pp.345-347.

(3) Kasai, K. (2011b). Chapter 4. Performance of Response-Controlled Buildings, The Kenchiku Gijutsu, No.741, pp.118-123.

(4) Hisada, Y., Kubo, T., and Yamashita, T. (2011), Shaking and Damage of the Shinjuku Campus Building and Shinjuku Campus Report from Kougakuin University, Internet Access: http://kouzou.cc.kogakuin.ac.jp/Open/20110420Event/20Apr11_Kogakuin01.pdf

(5) Koyama, S., and Kashima, T. (2011), Prompt Report on Strong Motions Recorded during the 2011 Tohoku Pacific Ocean Earthquake, Report 5, Building Research Institute (BRI).

(6) Maseki, R., Nii, A., Nagashima, I., Aono, H., Kimura, Y., and Hosozawa, O. (2011), Performance of Seismic Retrofitting of Suoer High-Rise Building Based on Earthquake Observation Records, International Symposium on Disaster Simulation and Structural Safety in the Next Generation (DS'11), Japan

(7) Isermann, R. and Münchhoff, M. (2011) Identification of Dynamic Systems: An Introduction with Applications, Springer, New York.

(8) Hisada, Y., Yamashita, T., Murakami, M., Kubo, T., Shindo, J., Aizawa K., and Arata T. (2012), Seismic Response and Damage of High-Rise Buildings in Tokyo, Japan During the Great East Japan Earthquake, Proceedings, International Symposium on Engineering Lessons Learned from the Giant Earthquake, Tokyo, Japan, March 3 -4.

(9) Kasai, K., Pu, W., and Wada, A. (2012): Responses of Tall Buildings in Tokyo during the 2011 Great East Japan Earthquake, Proc. of STESSA 2012 (Behaviour of steel structures in seismic areas), Keynote Paper, pp.25-35, Santiago, Chile, 9-11 January.

(10) JSSI (2012), Japan Society of Seismic Isolation, "Report of Response-Controlled Buildings Investigation Committee," January 26, 2012, Tokyo, Japan.

(11) Matsuda, K., Kasai, K., Yamagiwa, K., and Sato, D. (2012), Responses of Base-Isolated Buildings in Tokyo during the 2011 Great East Japan Earthquake, 15th WCEE, CD-ROM, Lisbon, Portugal, 2012.9

(12) Kasai, K., Mita, K., Kitamura, H., Matsuda, K., Morgan, T., and Taylor, A. (2013), Performance of Seismic Protection Technologies During the 2011 Tohoku-Oki Earthquake, Earthquake Spectra, Special Issue on the 2011 Tohoku-Oki Earthquake and Tsunami, pp.265-294, 2013. 3

(13) Kasai, K. (2013), Implications for Design of Response-Controlled Buildings from Full-Scale Lab Tests and Actual Earthquake Observations, 13th World Conference on Structural Control (13WCSI), Keynote Paper, Sendai, Japan, 2013.9

OBSERVATIONS FROM THE APRIL 20, 2013 LUSHAN COUNTY, YA'AN CITY, SICHUAN PROVINCE, CHINA EARTHQUAKE

Marshall Lew

AMEC Environment & Infrastructure, Inc.
Los Angeles, California

Abstract

The April 20, 2013 Lushan earthquake followed the 2008 Great Wenchuan earthquake by almost five years. Although the rupture also started in the Longmenshan fault zone, the Lushan earthquake is not an aftershock. Although similar damage and disruptions to infrastructure and society occurred, it was of a smaller scale and not unexpected due to the short time for the lessons from Wenchuan to be applied. There were some examples of lessons learned and the strong motion dataset obtained in this event will prove valuable in assessing how effective the actions taken have been. The visual observations were made on May 27 and 28, 2013 in Lushan.

Introduction

On April 20, 2013, at 8:02 am (Beijing Time), an earthquake occurred in Lushan County of Ya'an City in Sichuan Province in southwestern China. The epicenter was located at 30° 17' 02" N and 102° 57' 22" E, about 120 km from the major city of Chengdu; see Figure 1. Ya'an City is a prefecture level city in the western part of Sichuan Province and has a population of about 1.5 million people and is the location of one of China's main centers for the protection of the endangered giant panda. Sichuan Province is known as the "Province of Abundance." The province is a leading agricultural region of China and the province is also very rich in mineral resources, including large natural gas reserves. Sichuan is one of China's major industrial centers and has developed a high technology industrial base in electronics and information technology, machinery and metallurgy, hydropower, pharmaceutical, food and beverage industries. Sichuan is a major center for aerospace and defense industries in China as well as China's space program.

Earthquake Statistics

The China Earthquake Networks Center estimated the surface magnitude of the earthquake at M_s 7.0 while a moment magnitude (M_w) of 6.6 was assigned by the United States Geological Survey. The earthquake focus was relatively shallow at about 12.3 km below the surface. On the China Seismic Intensity Scale (similar to the Modified Mercalli Intensity Scale), the maximum intensity was assigned a value of IX.

The earthquake occurred in the Longmenshan Mountains, where the Longmenshan fault is a zone of active tectonically-related thrust faults that form the boundary between the high Tibetan Plateau to the west and northwest and the Sichuan Basin lowlands to the east and southeast. The mountain front is known for its extremely steep rise from an elevation of about 600 meters in the basin to about 6,500 meters in the mountains over a horizontal distance of

about 50 km. The Longmenshan Mountains also hosts the headwaters of many rivers that are tributaries to the Yangtze River.

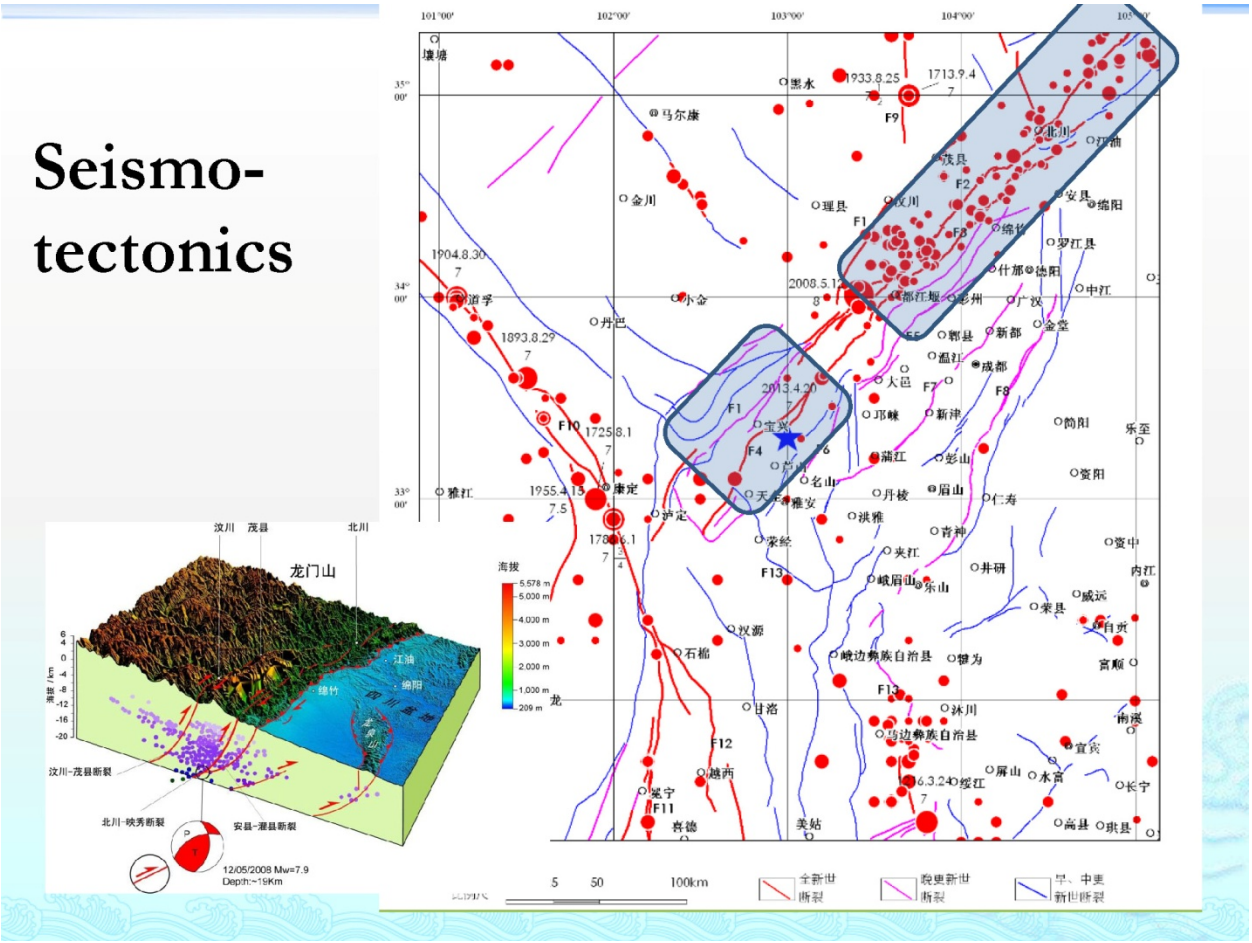

Fig. 1. Location of the Lushan Earthquake; area of 2008 Wenchuan earthquake rupture to the northwest of Lushan. Figure courtesy of Prof. Liu Aiwen of the Institute of Geophysics, China Earthquake Administration.

The causative fault was attributed to the southwestern segment of the Shuangshi-Daichuan fault of the Longmenshan fault zone by Yueqiao et al. (2013); see Figure 2. The principal rupture plane dipped northwest at about 35 degrees; Xu et al. (2013) has inferred that the earthquake might be related to the ramp activity of the basal detachment zone of the Longmenshan fault zone and not related to the Shuangshi-Daichuan fault because of the distribution of aftershocks as shown in Figure 3. The M_w 7.9 Wenchuan earthquake of May 21, 2008 occurred on the Longmenshan fault zone to the northwest of Lushan. The Lushan earthquake is not considered an aftershock of the Wenchuan event as the Lushan rupture occurred on a portion of the fault zone not ruptured by the prior earthquake.

It was reported that there were more than 203 fatalities and over 11,000 injured from the April 20 earthquake. The casualty numbers are significantly lower than for the 2008 Wenchuan earthquake which had over 87,000 fatalities (dead and missing) with almost 375,000 injured.

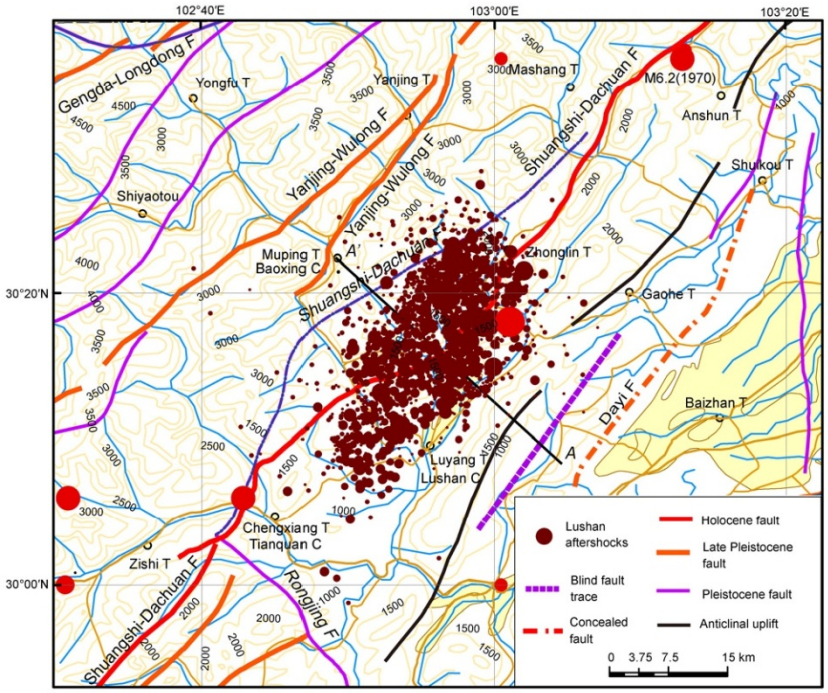

Fig. 2. Spatial Distribution of the Shuangshi-Dachuan fault and aftershocks of the Lushan earthquake from April 20 to 26, 2013 (after Xu et al. 2013)

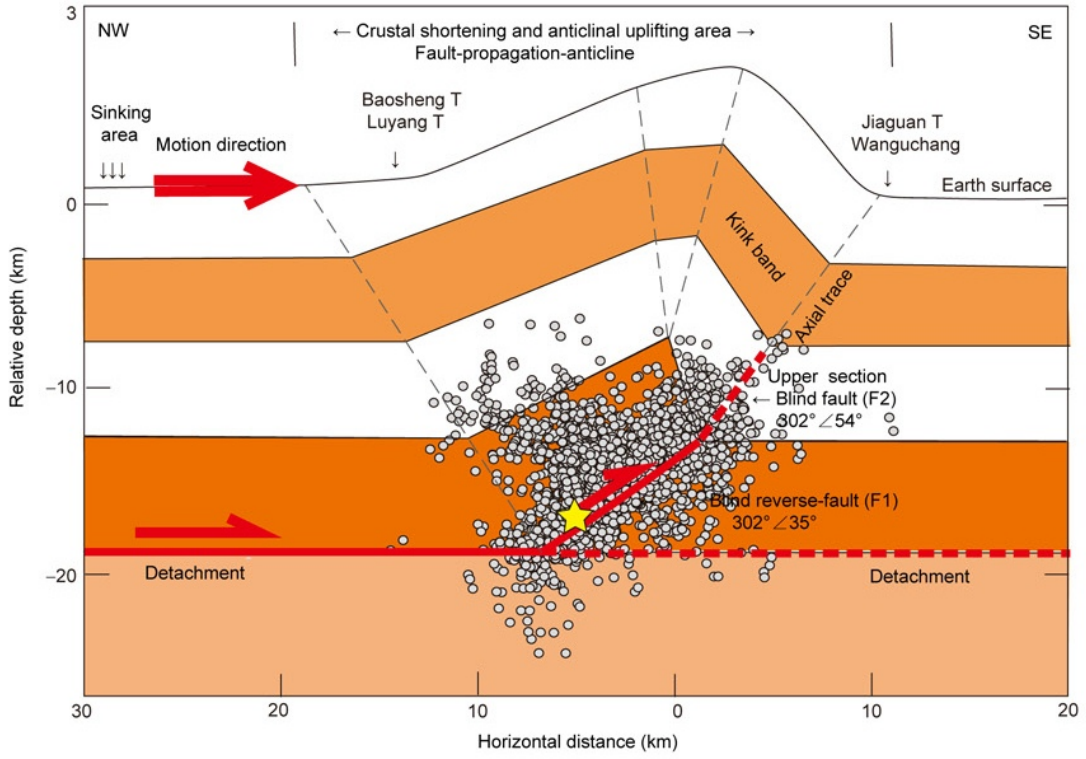

Fig. 3. Cross Section A-A' showing distribution of aftershocks from April 20 to 26, 2013 (after Xu et al. 2013).

Ground Failures

There have been no reports of evidence of surface fault rupture from the April 20 earthquake. Xu et al. (2013) made field investigations along the Dayi, Shuangshi-Dachuan, Yanjing-Wulong and Gengda-Longdong faults of the southern segment of the Longmenshan thrust belt. Thus the Lushan earthquake appears to have occurred on a blind thrust fault in contrast to the Wenchuan earthquake where there was abundant surface fault rupture. Xu and his colleagues also reported that there were NE- and NW-striking tensional ground fissures, landslides, bedrock collapses and occurrences of liquefaction found on the terraces or floodplains and steep piedmont zones. They also report buckled pavement on a concrete road that indicates local crustal shortening. Xu et al. attribute most of these features to the blind thrust faulting which formed a broad arch, or anticline, which results in crustal shortening and anticlinal uplifting as shown in Figure 3.

Strong Ground Motions

China has a strong motion network of ground instrumentation. This system provided a wealth of information from the Wenchuan earthquake. Some 84 stations recorded ground motions (with three components, two orthogonal horizontal and one vertical) at distances ranging from 27.7 to 769 km from the epicenter of the Lushan earthquake according to the China Strong Motion Networks Center (2013). Of these 84 stations, five stations were located within about 50 km of the source as shown in Figure 4.

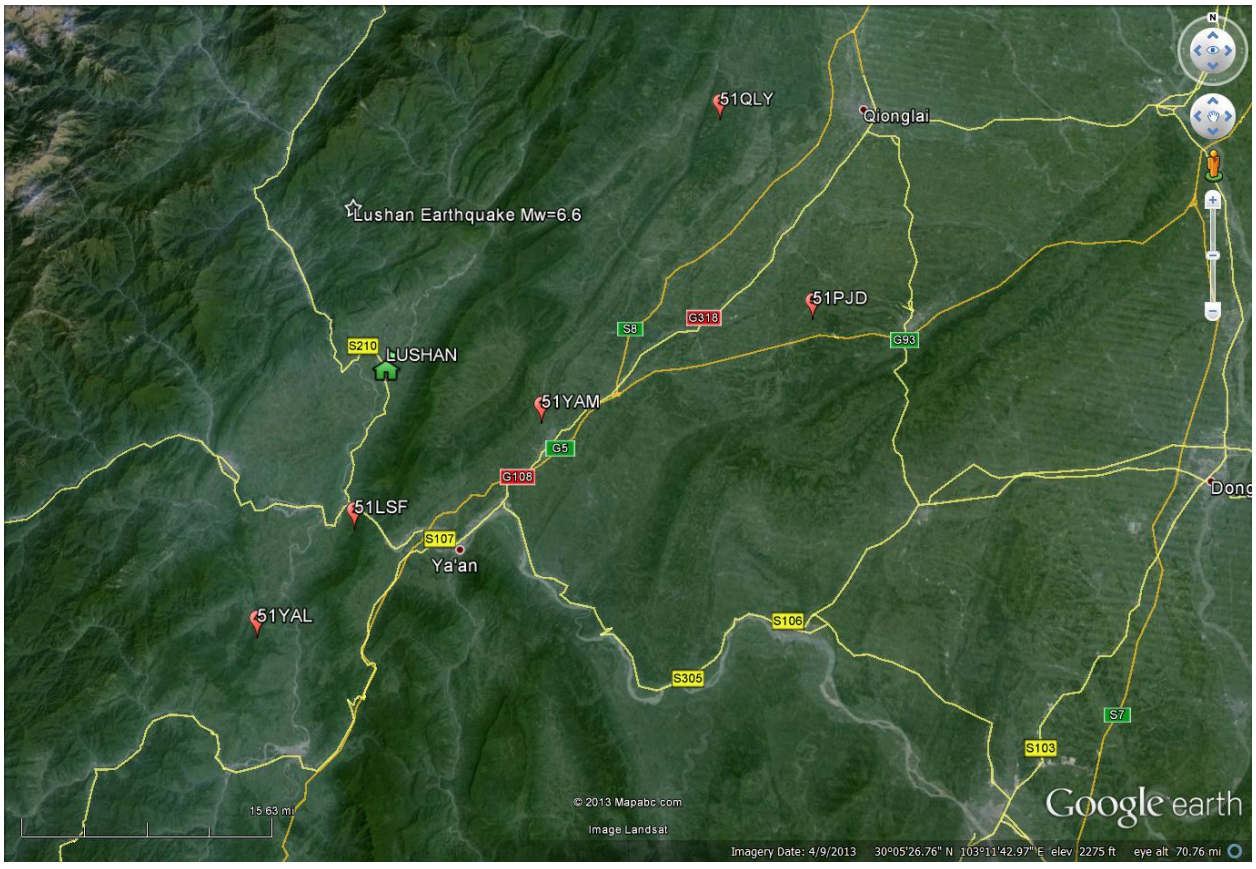

Fig. 4. Locations of five strong motion stations closest to Lushan earthquake source.

A summary of the peak ground motions recorded at the five closest strong motion stations is given in Table 1. Figure 5 shows plots of the acceleration-time histories recorded at the five stations. The acceleration values were uncorrected.

Table 1. Uncorrected Peak ground accelerations recorded at the five closest strong motion stations (after China Strong Motion Networks Center 2013)

Station ID	Station name	Longitude (degrees E)	Latitude (degrees N)	Distance (km)	Direction	Acceleration (cm/sec^2)
51YAM	Mingshan	103.1	30.1	27.7	EW	-400.705
					NS	349.850
					Up	105.102
51LSF	Lushan	102.9	30.0	32.6	EW	387.410
					NS	356.989
					Up	-267.381
51QLY	Qionglai	103.3	30.4	28.2	EW	270.461
					NS	315.486
					Up	111.231
51YAL	Yingjing	102.8	29.9	50.4[(a)]	EW	-400.705
					NS	349.850
					Up	105.102
51PJD	Pujiang	103.4	30.2	40.8	EW	153.581
					NS	-184.318
					Up	-103.518

[(a)] As reported by CSMNC; distance appears to be incorrect and may be about 40 km.

Unfortunately, there was no instrumentation in Lushan town, which is approximately 18 km from the epicenter. Considering the strong motion data from the closest stations which are at greater distances, it would be reasonable to estimate the maximum ground accelerations in Lushan to be greater than 0.4g or even 0.5g.

The preliminary report by CSMNC has been published to the world wide web and was accessed at http://csmnc.net/selnewxjx1.asp?id=797.

Landslides and Rockslides

As in the Wenchuan earthquake, there were many landslides and rockslides in the mountainous terrain (see Figure 6). As the terrain in the Longmenshan Mountains is generally very steep, these slides often damaged and blocked roads that were in canyons, along rivers and on the sides of the slopes. Although the earthquake did not occur during the rainy season, precipitation is common in the mountains and landslides and rockslides occur often even in the absence of strong ground shaking. Slides were also observed to have obstructed rivers; there was early concern about a barrier lake formed on the Yuxi River in Mingshan County (IFRC, 2013). It was not uncommon to encounter huge boulders being dislodged from the steep mountainous

slopes. It was reported that portions of Baoxing, further into the mountains than Lushan, were isolated by landslides and rescue teams were unable to get there for 33 hours (Xinhuanet 2013). During the emergency and recovery period, traffic had to be regulated where most roads were restricted to one-way traffic only as shown on Figure 7; this resulted in long round-trips as circuitous routes were required to return to the starting point.

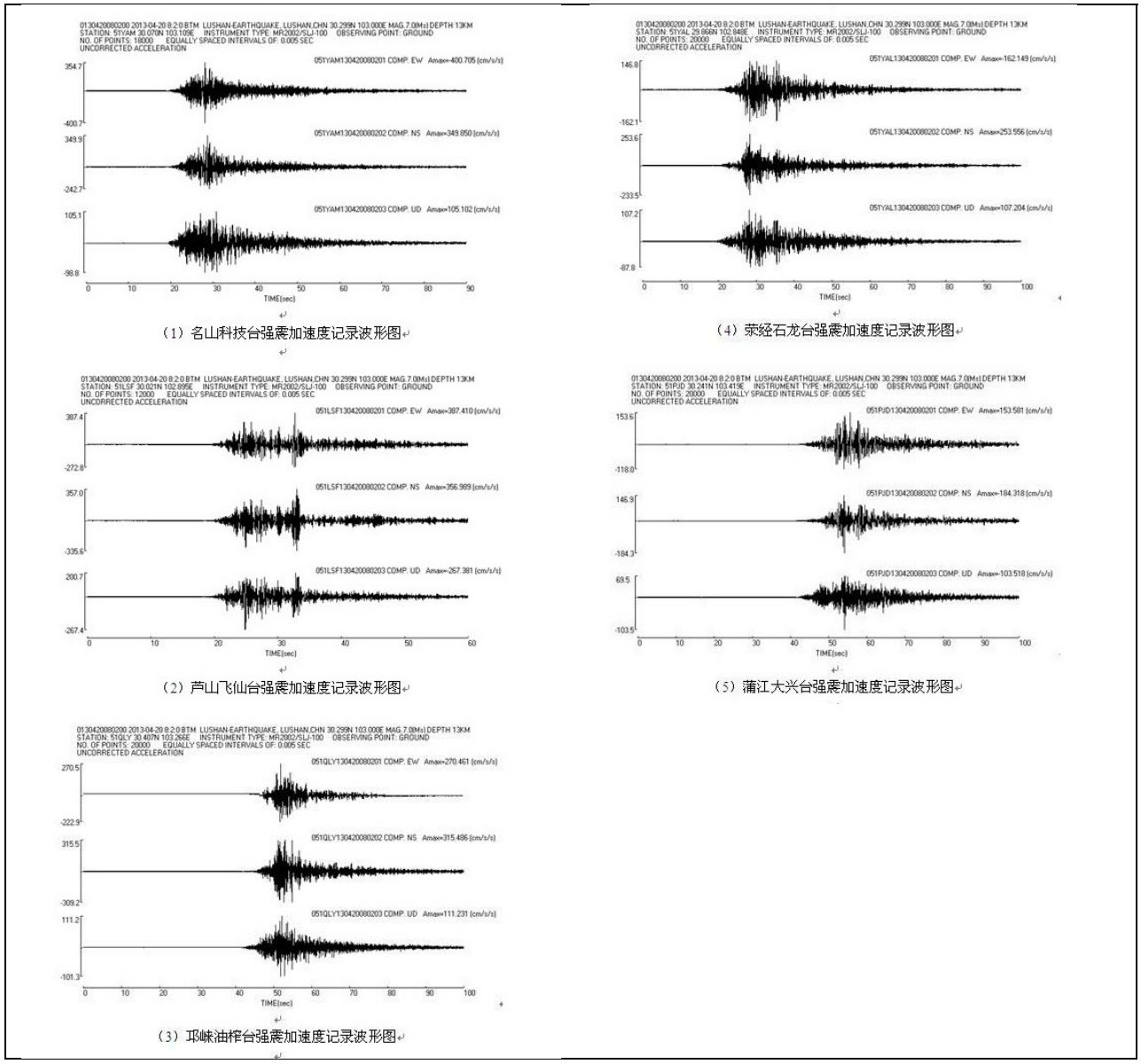

Fig. 5. Acceleration-Time Histories at (1) Station 51YAM, (2) Station 51LSF, (3) Station 51QLY, (4) Station 51YAL and (5) Station 51PJD (after CSMNC 2013).

Fig. 6. Rock and Landslides in Lushan area. Photographs courtesy of Prof. Liu Aiwen.

Structural Performance

From observations in limited portions of Lushan Township, the damages were similar to those observed in the Wenchaun earthquake, although on a smaller scale and much more limited in area. Lushan County has a population of over 110,000 and the main township of Lushan County has a population of about 20,000. According to UNICEF (2013), greater than 90% of the buildings were damaged, while in Baoxing County, to the northwest, greater than 60% of the buildings were damaged. Other seriously affected counties were Yucheng and Tianquan Counties.

As mentioned earlier, the peak ground accelerations in Lushan town are estimated to be in excess of 0.4g or 0.5g. The structures in the old town of Lushan consist of mostly low rise commercial and residential buildings that are typically between two to four stories in height. Typically buildings are constructed with concrete columns and beams with unreinforced brick

used as infill and for interior walls; many buildings are also constructed with just brick and mortar.

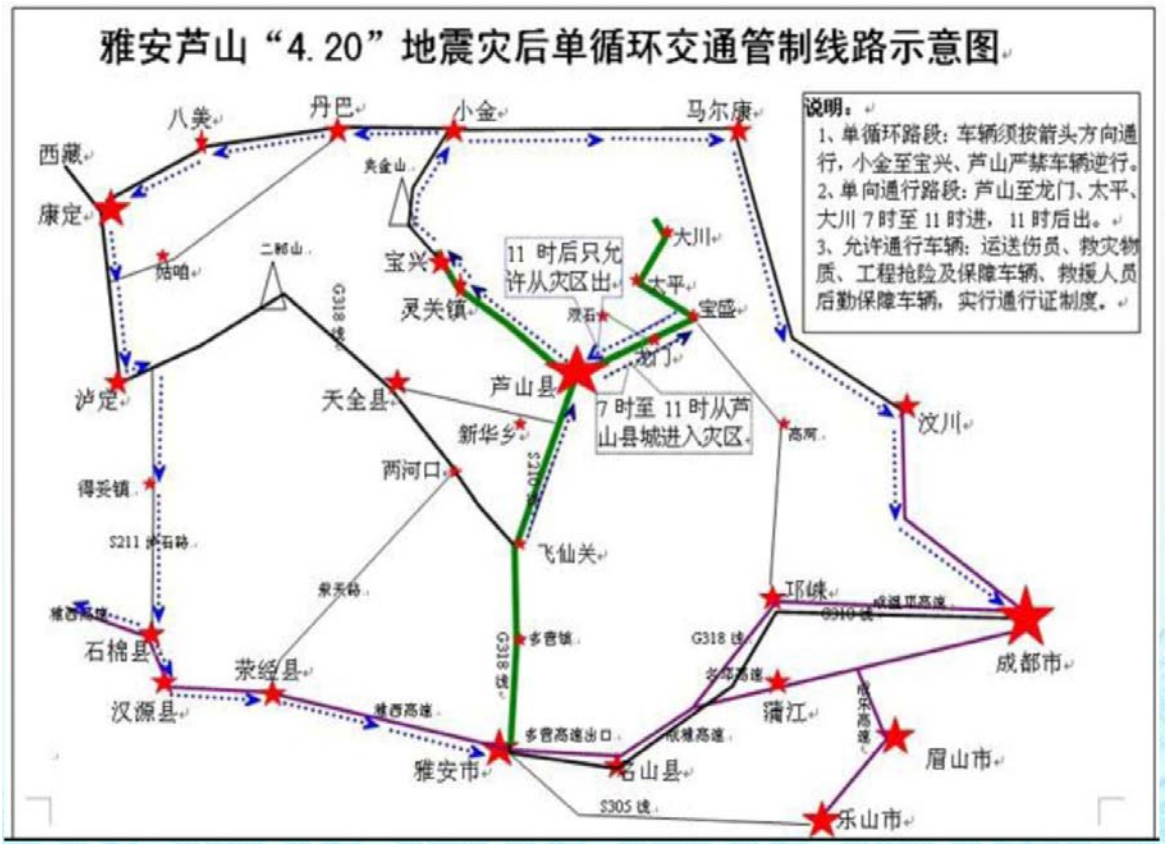

Fig. 7. Traffic control plan for Lushan area implemented after the earthquake due to landslides and rockslides (courtesy of Prof. Liu Aiwen).

Many of these buildings experienced damage, including partial or total collapse; examples of typical damage and partially or completely collapsed buildings are shown in Figures 8 through 11.

Fig. 8. Damage to Lushan County Government Building.

Fig. 9. Debris from collapsed building (Photo by Dr. Craig A. Davis).

Fig. 10. Damaged residential building of brick construction.

Fig. 11. Damaged building with roof collapse.

Older buildings clearly did not perform well in this earthquake. Under the older Chinese Building Code, buildings in the Chengdu region were designed for a ground acceleration of 0.10g. There is also an obvious lack of attention to detailing of connections, such as roof anchorage as shown in Figure 11. There is also common use of brick and mortar without adequate reinforcement or confinement as seen in Figure 12.

Fig. 12. Predominantly brick building without adequate reinforcement or confinement; note shear failures in wall at the second story.

After the Wenchuan earthquake, devastated towns like Beichuan and Yingxiu were essentially rebuilt. The new Beichuan town was relocated out of the mountains to a site on the plain. The new Yingxiu town was rebuilt near the old town. Both Beichuan and Yingxiu were essentially rebuilt. In the case of Lushan town, a new town area was constructed (or is in construction) to the south of the old Lushan town; however, the construction is more limited than in Beichuan or Yingxiu, and consists mostly of new government and institutional buildings as shown in Figures 13 and 14.

Fig. 13. Relatively new government building in New Lushan Town.

Fig. 14. Government building under construction in New Lushan Town.

The construction in the New Lushan Town should be governed by the updated seismic design requirements which were increased after the Wenchuan earthquake. It appeared from the exterior that the newer buildings had relatively less damage; however, as seen in Figure 15, the government building was found to be vacated with visible non-structural and minor structural damage. In the interior of the ground floor, ceiling tiles had fallen from a suspended ceiling and non-structural (infilled) walls were observed to be cracked.

(a) Front of Lushan County Building

(b) Damaged exterior tiles removed

(c) Development of hinges at joints

(d) Distress to ceiling tile and light fixtures; damage to non-structural walls. Photo by Dr. Craig A.Davis.

Fig. 15. Vacated Government Affairs Service Center of Lushan County People's Government Building.

There was one residential tower, about 20 stories in height, under construction with the reinforced concrete framing system essentially completed. This was observed from a distance but the construction did not appear to be affected by the earthquake.

The construction practice of using brick infill between beams and columns is quite prevalent in China. Figure 16 shows a new commercial building under construction which used this system; it can be seen that the infill is subject to out of plane failures as there is lack of reinforcement and inadequate confinement.

Fig. 16. New commercial building under construction with damage to brick infill.

One high point in the observations was the Lushan County People's Hospital Outpatient Building which experienced essentially no structural or non-structural damage during the earthquake; see Figure 17. The building is base isolated on 83 rubber bearings that are 500 to 600 mm in diameter (Best News, 2013a). It is reported that the building was completed in May 2012 and entered service in January 2013; there was no structural damage to the building and minimal impact on non-structural elements, glass or contents (Best News, 2013b). It was reported that some latex paint fell off and a few exterior tiles were shed during the earthquake. It was stated that the building was designed for seismic intensity VII, although it may have experience intensity of up to IX. The design and construction of the outpatient building was funded by the Macau SAR government.

Fig. 17. Base-Isolated Lushan County People's Hospital Outpatient Building. Photograph courtesy of Dr. Craig A. Davis.

Despite the seemingly excellent structural and non-structural behavior of the outpatient building, it was reported by Davis (2013) that water lines servicing the building from the outside were damaged because flexible connections were not provided at the isolation interface; electrical service was reportedly interrupted in the earthquake due to the powergrid going down; however, power cables to the building reportedly had sufficient slack across the isolation interface and did not break. It is unknown if the building had a back-up power system. It is questionable if the repairs to the water service have provided the flexible connections needed for a base isolation system.

In contrast to the outpatient building, other buildings at the County People's Hospital had substantial damage to structural and non-structural elements which caused the buildings to be vacated as shown in Figure 18. Although the structural frames appeared to be relatively intact, the infill and non-structural walls consisting of masonry elements sustained substantial damage. Suspended ceiling systems did not perform well as T-bars sometimes broke causing ceiling tiles and light fixtures to be displaced and sometimes falling down or left dangling.

It should be noted that since the earthquake occurred on a Saturday, classes were not in session and no schools were reported to have collapsed (UNICEF China 2013). However, classes in some parts of Lushan County were meeting in tents after the earthquake.

(a) Exterior of Lushan County People's Hospital

(b) Interior or Lushan County People's Hospital

Fig. 18. Lushan County People's Hospital, adjacent to Outpatient Building. Photos by Dr. Craig A. Davis.

Performance of Lifelines

Water service, electrical power, and telecommuni-cations and were interrupted by the earthquake and recovery was still in progress more than one month after the earthquake.

The underground water system was apparently severely damaged and above ground pipes were laid throughout the town providing water service as shown in Figure 19.

Fig. 19. Temporary above ground water pipe (foreground).

It was reported and observed during this visit that there was damage at water treatment facilities. One of these water treatment facilities had structural damage to support buildings and

walls, but the treatment tanks did not appear to have any major damage although it appeared that some piping had been replaced. The control buildings were apparently reinforced concrete frame structures with masonry infill. The masonry infill failed in shear and sometimes failed out-of-plane. Repairs to these facilities were being undertaken at the time of visitation about five weeks after the earthquake and appeared to be mostly patching and returning the structures to essentially the pre-earthquake conditions at best; see Figure 20.

(a) Exterior of control building (b) Interior of control building

Fig. 20. Damaged water treatment plant control building in Lushan undergoing earthquake repairs.

Control equipment, storage tanks, and water treatment mixing equipment did not appear to have adequate bracing and some equipment showed evidence of displacement from their initial locations. There was no evidence that these facilities would be retrofitted to provide adequate bracing; see Figure 21.

(a) Inadequately braced chemical tank (b) Unbraced control equipment

Fig. 21. Inadequately or unbraced equipment at Water Treatment Plant.

It was reported that electrical power was lost in large parts of the region, including Lushan and Baoxing, as a result of the earthquake. In May 2013, the ASCE TCLEE team visited the State Grid Corporation of China Jinhua 110kV Transformer Substation which is one of several substations which provide power for the Lushan County region. There was severe damage to the structures and transformers at this facility as shown in Figure 22.

Fig. 22. Damage at the Jinhua 110kV Transformer Station. Photographs by Dr. Craig A. Davis.

It was also reported that hydropower plants were also affected (Sichuan Provincial People's Government 2013); Figure 23 shows a hydropower plant that was flooded and rendered inoperable at the time of the earthquake. In the mountains, downed power lines were caused by landslides which caused some transmission tower collapses as shown in Figure 24.

Fig. 23. Hydropower plant made inoperable by flooding. (Photograph by Dr. Craig A. Davis)

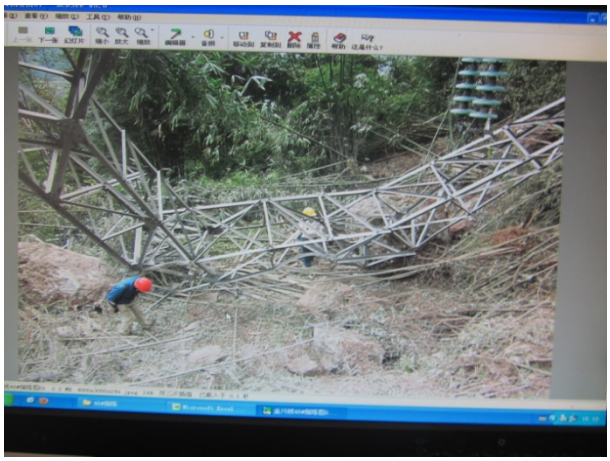

Fig. 24. Transmission tower collapse. (Photograph by Dr. Craig A. Davis)

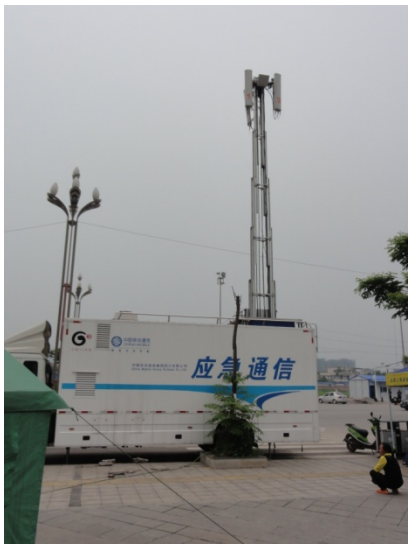

Fig. 25. COW in Lushan Town.

It was reported by Earthquake-Report.com (2013) that electricity was restored to Lushan County on Monday, April 22, two days after the earthquake. Restoration of the power grid to provide electrical service to all the affected counties was accomplished by May 10, 2013 (Newsking.us 2013). Repairs and improvements to the powergrid are on-going.

Mobile telephone service was disrupted by the earthquake. It is reported that China Telecom mobilized teams and equipment from Chongqing to provide service within a few days (Best-news.us, 2013c). As of May 28, mobile phone service in the affected region was still being provided with mobile cell towers, sometimes referred to as COWs or "cell on wheels" as shown in Figure 25.

Emergency Response

The China central government received much criticism during the Wenchuan earthquake for a slow response to the natural disaster. However, in the Lushan earthquake the central government and the People's Liberation Army (PLA) were mobilized within hours (South China Morning Post, 2013). Relief personnel consisted of the military, armed police and central government agencies including personnel from the China Earthquake Administration, the

ministries of civil affairs and public security, and government-backed charities. Almost 7,500 PLA soldiers and armed police were sent to the disaster zone the day of the earthquake and 10,000 others were available on standby. The China Air Force used two reconnaissance aircraft from Beijing to take aerial photographs of the earthquake-ravaged area along with five civilian drone aircraft to survey the area. Civilian aircraft were chartered to bring in relief supplies. The Red Cross Society of China rushed supplies from Chengdu to the affected area, including 1,700 tents. A number of non-government organizations (NGOs) also mobilized quickly, but the leads for relief operations were the central and provincial governments. The new Chinese Premier Li Keqiang arrived in Lushan several hours after the earthquake to direct the emergency response and called for an all-out effort to rescue survivors (NTD News 2013). Efforts to rescue people from collapsed buildings in the affected region were hampered because some more remote communities in the mountains were cut off because of blocked roads, collapsed bridges, fallen boulders and landslides.

Long Term Recovery

In July, the State Council issued the "Lushan earthquake restoration and reconstruction plan" (China Meteorological Administration 2013). This plan is to establish and improve the comprehensive emergency response system; this includes: disaster relief; monitoring, early warning and forecasting; and improving disaster prevention emergency planning. The goal is to improve the management of disaster information collection, transmission and processing as well as to promote information integration, intelligent processing and sharing of services for disaster prevention and mitigation. The plan includes an educational component to "popularize the knowledge of disaster prevention and mitigation." Public awareness of prevention and mitigation are to be improved and disaster emergency drills are included. The plan requires reconstruction of meteorological observation stations and emergency response systems that were damaged. The plan calls for construction of new emergency broadcasting platforms, a national disaster recovery data center, and Sichuan satellite disaster reduction application center.

The plan also states the goal that within three years, every family in the earthquake-hit region will have an apartment, and every family with members capable of working will have a least one job, while living areas in the rebuilt areas will be better than before the earthquake. The funding of the reconstruction plan would come from government fiscal spending, as well as from donations and foreign loans (People's Daily Online 2013). The cost is for the reconstruction is estimated to be up to 86 billion Yuan ($13.9 billion USD). Companies and individuals participating in post-earthquake reconstruction would receive tax breaks and preferential land and financial measures would be available to support the rebuilding.

The reconstruction plan also calls for relocation of families currently living in high risk regions that are subject to "geological disasters." The plan also recognizes the "natural beauty of the landscape and biological diversity of the area." (This is the habitat of the giant panda.) The plan sets tourism as the priority industry in reconstruction and a significant portion of the rebuilt area will also be a "biological protection zone." The reconstruction plan includes a comprehensive study of possible natural disasters in quake-affected regions; these include strong rainstorms and severe drought which can cause "potential geological disasters." An audit plan is also part of the program to assure that reconstruction funds will not be subject to graft and other abuses.

Conclusions

One could easily dismiss the value of the lessons learned from the Lushan earthquake by saying that no new knowledge was gained and that what was seen in this event was déjà vu again. However, with the changes instituted in construction requirements since the Wenchuan earthquake, there is an opportunity to examine what happened and what did not happen as comparisons in behavior are now possible as there are old (pre-Wenchuan) construction nearby the newer (post-Wenchuan) construction. Although the strong motion records stations are not as close to the earthquake source as would be desired, the recordings could be very useful in calibrating the structural performance of old and new construction. The recordings could also be valuable in determining if the changes to the building requirements made after Wenchuan were sufficient or not.

Much can also be learned about the almost immediate Chinese response to the disaster. Hopefully the good things can be applied to emergency response in the United States.

Acknowledgements

Special thanks to Dr. Craig A. Davis, Dr. John Eidinger and Mr. Alex Tang of the ASCE TCLEE Reconnaissance Team for providing the author the opportunity to accompany them on their reconnaissance mission to Lushan County. Greatest appreciation is given to Prof. Liu Aiwen of the Institute of Geophysics, China Earthquake Administration in Beijing, China for providing technical information about the earthquake.

References

Best News (2013a). “Lushan Hospital outpatient building after the earthquake intact.” Accessed on September 7, 2013 at http://www.best-news.us/news-4391701-Photo:-the-Lushan-Hospital-outpatient-building-after-the-earthquake-intact-expert-analysis-isolation-technology.html.

Best News (2013b). “83 rubber bearings dealt with gently from the top-Lushan.” http://www.best-news.us/news-4428683-83-rubber-bearings-dealt-with-gently-from-the-top-Lushan.html.

Best New (2013c). “China Telecom Chongqing rush to the rescue Lushan earthquake zone.” April 29. Accessed on September 8, 2013 at http://www.best-news.us/news-4403072-China-Telecom-Chongqing-rush-to-the-rescue-Lushan-earthquake-zone-rescue-Record.html.

China Meteorological Administration (2013). “Lushan earthquake reconstruction to strengthen disaster monitoring and forecasting.” Accessed on September 9, 2013 at http://www.cma.gov.cn/en/NewsReleases/News/201307/t20130717_220046.html.

China Strong Motion Networks Center (2013). “四川雅安芦山县7.0级地震（第五报）.” [Translated as Lushan County, Ya'an, Sichuan 7.0 earthquake (fifth report)]. Accessed on September 6, 2013 at http://www.csmnc.net/selnewxjx1.asp?id=797.

Earthquake-Report.com (2013). “Deadly earthquake Sichuan (Ya’an), China – Death toll now at 196 dead (21 missing) + April 26 update.” Accessed on September 8, 2013 at http://earthquake-report.com/2013/04/20/very-strong-earthquake-sichuan-china-on-april-20-2013/.

International Federation of Red Cross and Red Crescent Societies [IFRC] (2013). "Disaster relief emergency fund (DREF) – China: Sichuan Lushan Earthquake." April 25.

NTD News (2013). "Difficult rescue efforts in Lushan earthquake epicenter." Accessed on September 9, 2013 at http://www.ntd.tv/en/news/china/20130422/78730-difficult-rescue-efforts-in-lushan-earthquake-epicenter.html.

Newsking.us (2013). "Sichuan – the Lushan earthquake area grid basically returned to the level before the earthquake reconstruction start." Accessed on September 8, 2013 at http://www.newsking.us/news-4465092-Sichuan-the-Lushan-earthquake-area-grid-basically-returned-to-the-level-before-the-earthquake-reconstruction-start.html.

People's Daily Online (2013). "Lushan post-quake work to cost nearly $14b." Accessed on September 9, 2013 at http://english.peopledaily.com.cn/90882/8328007.html

Sichuan Provincial People's Government (2013). "Sichuan provincial government held a second press conference – April 20, 2013." Accessed on September 8, 2013 at http://www.sc.gov.cn/10462/10705/10707/2013/4/20/10257632.shtml.

South China Morning Post (2013). "PLA shows quick response to Lushan earthquake." April 21. Accessed on September 8, 2013 at www.scmp.com/news/china/article/1219509/pla-shows-quick-response-lushan-earthquake.

UNICEF China (2013). "Lushan Earthquake Situation Report #1, 22 April 2013."

Xinhuanet (2013). "Lushan quake prompts disaster preparedness discussion." Accessed on September 8, 2013 at http://news.xinhuanet.com/english/china/2013-04/27/c_124642791.htm.

Xu, X.W., Wen, X.Z, Han, Z.J., Chen, G.H., Li, C.Y., Zheng W.J., Zhang, S.M., Ren, Z.Q., Xu, C., Tan, X.B., Wei., Z.Y., Wang, M.M., Ren, J.J., He, Z.T. and Liang, M.J. (2013). "Lushan Ms7.0 earthquake: A blind reserve-fault event." Chin Sci Bull, 58, doi: 10.1007/s11434-013-5999-4.

Yueqiao, Z., Shuwen, D., Chuntang, H., Jusong, S., Zhonghai, W., Hailong, L., Ping, S., Gang, L. and Jian, L. (2013), "Seismogenic Structure of the April 20, 2013, Lushan Ms7 Earthquake in Sichuan." Acta Geologica Sinica - English Edition, 87: 633–645. doi: 10.1111/1755-6724.12075.

STATUS OF PUBLIC EARTHQUAKE EARLY WARNING IN THE U.S.

Douglas Given

U.S. Geological Survey

Abstract

Earthquake Early Warning (EEW) is a proven use of seismological science that can give people and businesses outside the epicentral area of a large earthquake up to a minute to take protective actions before the most destructive shaking hits them. Since 2006 several organizations have been collaborating to create such a system in the United States. These groups include the US Geological Survey, Caltech, UC Berkeley, the University of Washington, the Southern California Earthquake Center, the Swiss Federal Institute of Technology, Zürich, the California Office of Emergency Services, and the California Geological Survey.

A demonstration version of the system, called ShakeAlert, began sending test notifications to selected users in California in January 2012. In August 2012 San Francisco's Bay Area Rapid Transit district began slowing and stopping trains in response to strong ground shaking. The next step in the project is to progress to a production prototype for the west coast. The system is built on top of the considerable technical and organizational earthquake monitoring infrastructure of the Advanced National Seismic System (ANSS).

While a fully functional, robust, public EEW system will require significant new investment and development in several major areas, modest progress is being made with current resources. First, high-quality sensors must be installed with sufficient density, particularly near source faults. Where possible, we are upgrading and augmenting the existing ANSS networks on the west coast. Second, data telemetry from those sensors must be engineered for speed and reliability. Next, robust central processing infrastructure is being designed and built. Also, computer algorithms to detect and characterize the evolving earthquake must be further developed and tested. Last year the Gordon and Betty Moore Foundation funded USGS, Caltech, UCB and UW to accelerate R&D efforts. Every available means of distributing alerts must be used to insure the system's effectiveness. We have developed an internet-based UserDisplay application and a smartphone app based on Google Cloud Messaging. In addition, USGS has applied for authorization to alert over FEMA's Integrated Pubic Alert and Warning System. We are also working with private companies to develop alert distribution channels and end user implementation capabilities. Finally, because policy makers, institutional users, and the public must be educated about the system, social scientists and communicators are determining how to communicate the alerts most effectively.

Progress is also being made in several related areas. Real-time GPS position data is becoming available on a large scale and algorithms are being developed to use these data to rapidly characterize the fault rupture as it propagates. New, advanced seismological and geodetic algorithms for the Cascadia megathrust and San Andreas fault are being developed. We are

exploring public-private partnerships to develop commercial EEW applications. And Federal, State and local agencies are working out their roles and responsibilities in building, operating and educating users about the system.

There is much more to be done and funding the creation and operation of this new capability is a challenge in the current budget climate. However, our goal is to build an EEW system before the next big earthquake rather than in its aftermath.

USE OF STRONG MOTION RECORDS TO VALIDATE DYNAMIC SOIL-FOUNDATION-STRUCTURE INTERACTION MODELS FOR PILE SUPPORTED WHARVES

Stephen Dickenson[1], Songtao Yang[2], Doug Schwarm[3] and Matt Rees[4]

[1] New Albion Geotechnical, Inc., Corvallis, OR
[2] CH2M Hill, New York, NY
[3] Atlas Geotechnical, Inc., Santa Cruz, CA
[4] CH2M Hill, Swindon, UK

Abstract

This paper provides interim results of an on-going investigation of the seismic response and performance of instrumented pile supported wharves at the ports of Los Angeles and Oakland, California. The first phase of the project has focused on the synthesis of geotechnical, structural, and strong motion data at three port sites instrumented by CSMIP. Geophysical investigations performed for this study provide V_s data in unimproved, liquefiable hydraulically-placed fill at a CSMIP strong motion station and in adjacent zones of fill improved with stone columns. Strong motion recordings obtained at the Port of Oakland Berth 36-38 and Port of Los Angeles Berth 404 have been used to validate a practice-oriented 2D nonlinear, effective stress geomechnical model for low- to moderate-levels of ground shaking and structural response.

Introduction

This investigation addresses the effects of long-duration ground motions on the Soil-Foundation-Structure-Interaction (SFSI) and seismic performance of key port structures in California. The project is examining the effectiveness of current seismic design codes and performance-based provisions (ASCE Seismic Standards, in preparation; CSLC MOTEMS, 2010; POLA, 2010; POLB, 2012) for achieving the defined performance requirements for large magnitude earthquakes that generate long-duration ground motions. The topic is important because: (a) recent experience demonstrates that loss of serviceability at port terminals is strongly correlated with permanent ground deformations, and (b) long-duration ground motions have much greater potential for generating damaging wharf and embankment deformations at lower force levels relative to stronger, but brief, seismic loading. The project is proceeding in two phases that include four primary tasks;

1. Collection and analysis of CSMIP strong motion data at two major ports
2. Validation of a dynamic SFSI model for modern pile supported wharves;
   a. Port of Oakland (Berth 36)
   b. Port of Los Angeles (Berth 404)
3. Application of SFSI model for design-level ground motions
   a. Port of Oakland (Berth 55)
   b. Port of Los Angeles (Berth 404)
4. Application of SFSI model for long-duration ground motions

This paper provides an interim report on the results of the first phase of the project involving Tasks 1 and 2. The collection and synthesis of geotechnical, geophysical, and structural data, as well as construction documentation has been completed for two CSMIP strong motion instrumentation arrays at ports. The extensive characterization of geotechnical and structural conditions at the CSMIP instrumented wharves located at the ports of Los Angeles and Oakland, California has led to the development of models for simulating the nonlinear effective stress response of dynamic SFSI. The model behavior under low- to moderate-levels of ground motion has been evaluated to validate and calibrate modeling procedures for soil constitutive models, cyclic soil-structure interaction for deep foundations, and structural response.

Project Background

Dynamic SFSI of pile-supported wharves represent a complex geotechnical and structural interaction problem. The combination of inertial loading and kinematic effects due to seismically-induced ground displacement (i.e. displacement demand) imposes foundation loads that are commonly out-of-phase and quite variable depending on vertical and lateral location relative to the sloping face of terminal wharves. Observed failures to wharf foundations are often associated with geotechnical failures (liquefaction, cyclic degradation, slope instability). Field reconnaissance and inspection at ports after moderate to large earthquakes routinely finds that damage to waterfront structures is directly related to permanent ground deformation and large displacement demand on pile foundations, cutoff walls and anchor systems, and appurtenant structures (ASCE TCLEE, 1998; PIANC WG34, 2001; ASCE COPRI, in press).

The adoption of performance-based seismic design provisions at major ports and marine oil terminals in California necessitates the reliance in engineering practice on numerical models for simulating dynamic SFSI of wharf and embankment structures. Recent investigations of the seismic performance of pile supported wharves have developed enhanced methods of analysis (e.g.; Chiaramonte et al., 2011; Shafieezadeh et al. 2012); however, the lack of well-documented, instrumented field case histories has precluded thorough validation of analysis methods for simulating dynamic SFSI of these structures. The lack of model validation can lead to a poor understanding of the uncertainty involved in seismic analyses and an over-confidence in the analysis results. The application of performance-based design of pile-supported wharves requires a clear understanding of this dynamic SFSI and methods of analyses for evaluating both inertial and kinematic loads on the wharf structure. Specific aspects of analysis that warrant consideration for long-duration motions include; (a) fatigue and plastic hinge development in piles as a function of row location, (b) stress concentrations at pile-wharf deck connection, and (c) patterns of deformation in the rockfill embankment, backfill and foundations soils.

An important facet of this investigation is the calibration of the numerical SFSI model for the two selected wharves using strong motion records from CSMIP stations for the following cases involving small to moderate levels of shaking;

Port of Oakland, Berth 38, M_w 6.9 October 17, 1989 Loma Prieta Earthquake

The 1989 experience at the Port of Oakland provides a significant case history involving moderate levels of ground motion, extensive liquefaction, and widespread damage to pile foundations, all of which add complexity to the numerical modeling. While Berth 38 was not instrumented in 1989, motions from the CGS-SMIP *Oakland Outer Harbor Wharf* station (Berths 24/25), along with other local motions, have been used by several investigators in validation studies using various dynamic models for both wharves (Norris et al. 1991; Singh et al. 2001a, b; Wang et al. 2001; Roth and Dawson 2003; Donahue, et al. 2005; Dickenson and McCullough 2006).

Port of Los Angeles, Pier 400, M_w 4.7 May 17, 2009 Inglewood Area Earthquake

The 2009 earthquake provides a rich set of recorded motions at Pier 400 at lower levels of shaking (0.113g free-field, 0.21g on the wharf structure) that have been used for validating the SFSI model for elastic response of the wharf.

The CSMIP arrays of strong motion instrumentation at these two locations make them particularly well suited for in-depth seismic performance analysis. Instrumentation in the free-field, at multiple locations on the wharf structures, and in one case within an improved portion of the foundation soils (CDSM treatment in weak soils) has provided opportunities and challenges for numerical modeling. In order to validate the numerical models a major effort has been undertaken to collect supporting information and data required for robust nonlinear SFSI modeling. This has included; port reports on geotechnical site characterization, dynamic soil properties, geotechnical interpretation and design (Fugro West 2001a, b, c), structural seismic design and detailing (Priestley 2000; Weismair et al 2001), construction materials and methods (Degen et al. 2005; Fugro West 2004), as-built drawings (POLA 2002), and large-scale physical model testing of pile-wharf deck connections (Krier et al. 2008; Lehman et al. 2013; Restrepo et al. 2007).

This investigation focusses on both the calibration of a practical dynamic SFSI modeling procedure and the application of the validated model for evaluating the impact of long-duration motions on the seismic performance of modern wharf structures at two major ports in California. The numerical dynamic SFSI modeling is being performed using the commercially available program FLAC. This program has been selected for application due to the wide usage in port engineering practice (e.g., Roth et al. 2003; Roth and Dawson 2003; Arulmoli et al. 2004; Moriwaki et al. 2005, Yan et al., 2005) and the vast experience of the project team with this code for port and waterfront applications. The project team has found by experience that the utilization of an “off the shelf” computed code is not sufficient for port applications without numerous enhancements. Several key aspects of the dynamic SFSI model developed by the project team for use on this project investigation include;

a. The 2D FLAC model is being used for nonlinear, coupled effective stress modeling.
b. Modeling excess pore pressure generation and cyclic degradation in soils is critical for long-duration motions. A recently refined version of the effective stress plasticity model UBCSand (Beaty 2009) is being used for liquefaction triggering and post-liquefaction behavior of sand.

c. Near-surface, lateral pile-soil response will reflect the characteristics of the piles, nature of the inertial loading provided by the wharf deck and contributing loads, the embankment slope, and the nature of the soil and/or rock fill along the upper portion of the pile. Pile embedment through rock armor layers and quarry run fill presents issues related to particle size effects on pile-soil p-y behavior. Physical modeling studies of piles in rock fill have demonstrated the limitations of continuum models for lateral pile response (Boland et al 2001a, 2001b; McCullough 2003; Kawamata 2009). This aspect of dynamic pile behavior is being addressed for the sloping, rock fill and armor conditions at both ports.
d. The mass of a gantry crane will be incorporated in the modeling. While this investigation has not focused on the dynamic response characteristics of the crane a range of dynamic loads on the wharf representing is being evaluated.

The response of the two wharves used as test-bed applications is currently being evaluated (Phase 2) to assess the relative contributions, and phasing, of kinematic and inertial loading on the pile foundations. The progressive and cumulative impact of kinematic loading of the wharf foundations due to foundation deformations is anticipated to be a key consideration for long-duration seismic loading.

Validation of the Numerical Dynamic SFSI Model

Port of Oakland, Berth 38; M_w 6.9 October 17, 1989 Loma Prieta Earthquake

The seismic performance of the Seventh Street Terminal (Berths 35 through 38) pile-supported wharf at the Port of Oakland during the 1989 Loma Prieta Earthquake has been modeled by several investigators, as previously noted. The ground surface motions of approximately 0.25g to 029g, extensive liquefaction with nominal lateral spreading and post-seismic ground settlement, and widespread damage to piles (predominantly batter piles) provide an important case study for seismic loading approaching Operating Level Event (OLE) levels at the Port of Oakland. Field observations indicated permanent ground surface lateral displacement of the rock dike on the order of 15 to 30 cm, with approximately 13 to 30 cm of settlement (Egan et al. 1992, Singh et al. 2001a). In addition, the majority of the batter piles and approximately 20 percent of the vertical piles failed at the pile/deck connection (Singh et al. 2001). It was also noted by Singh et al. (2001) and Oeynuga (2001) that many of the vertical piles probably failed at the approximate interface between the Bay Mud/hydraulic fill and the dense sand, based on the results of pile integrity testing. These failures were likely due to pinning of the piles in the dense sands while lateral forces due to permanent ground deformations pushed on the upper portions of the piles in the rock fill.

This case study was initially evaluated using a simple, yet calibrated and adequate, excess pore pressure generation model for the hydraulically-placed sand fill (McCullough 2003; Dickenson and McCullough 2005). Berth 38 was modeled with the design geometry shown in Figure 1 and numerical model grid, soil layers, and structural elements shown in Figure. The soil and structural properties used in the model are provided by McCullough (2003). The nearest recorded acceleration time history was recorded at the ground surface approximately 1.5 kilometers from Berth 38 at the Port of Oakland Outer Harbor Wharf. The two horizontal components of the recorded motions were vectorally combined to produce a motion

perpendicular to Berth 38. The combined motion was deconvolved to the base of the numerical model (El. –21 m) using the equivalent linear model SHAKE.

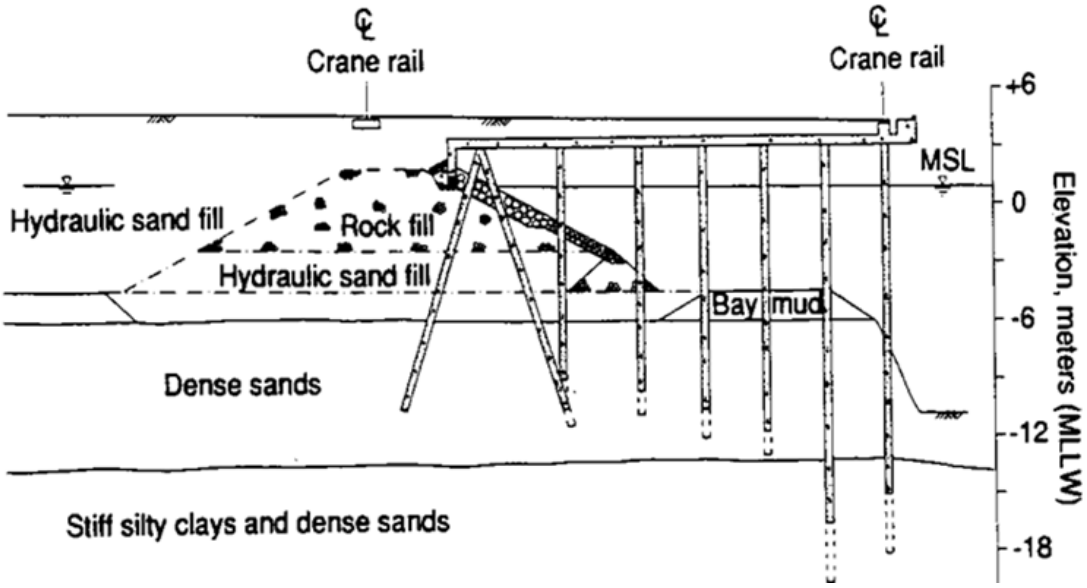

Figure 1. Pile-supported wharf at the Port of Oakland Seventh Street Terminal, prior to the 1989 Loma Prieta Earthquake (Egan et al. 1992).

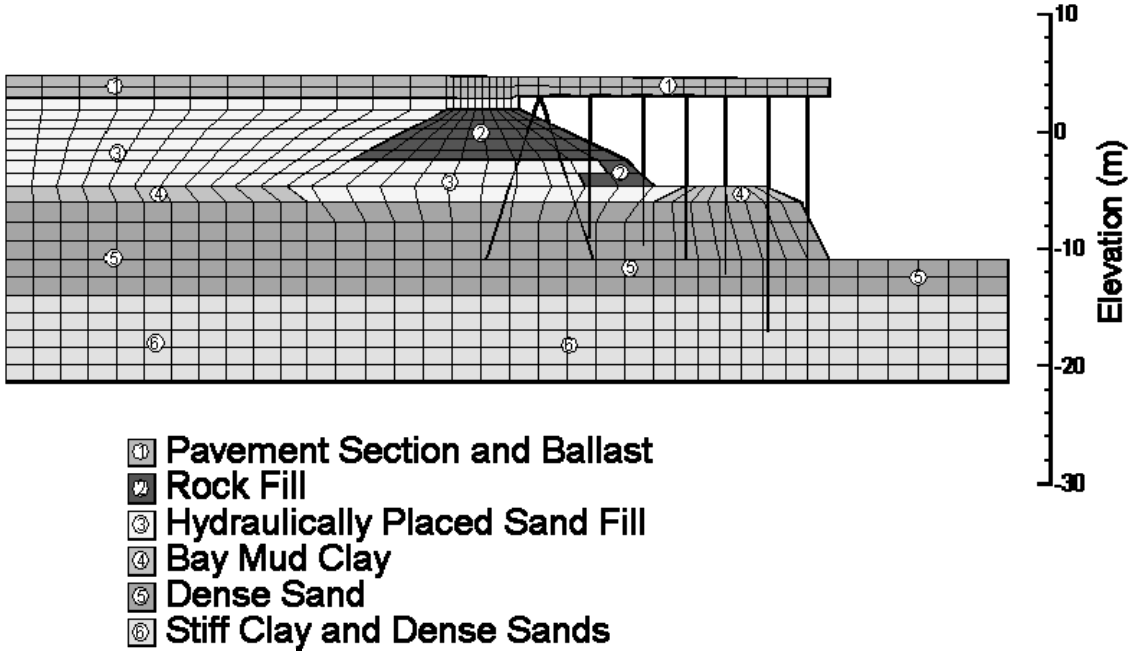

Figure 2. Geometry, grid and structural elements that were used in the numerical model of the Port of Oakland Seventh Street Terminal, Berth 38.

The results of the numerical analysis are illustrated in Figure 3. The analysis predicted a horizontal displacement of the rock dike at the ground surface of 27 cm and a vertical settlement of 22 cm, both in agreement with the observed values of 15 to 30 cm and 13 to 30 cm, respectively. In addition, FLAC predicted plastic hinge development at the top of the all the piles (at the location of the first structural node below the wharf deck). In addition, plastic hinge development at depth was predicted (Figure 3) at the Bay Mud/hydraulic fill and dense sand interfaces. It is significant to note that modeling efforts using FLAC by several groups (Singh et al. 2001a, b; Wang et al. 2001; Roth and Dawson 2003; Dickenson and McCullough 2006) have resulted in computed ground deformations at the top of the crest of the sloping fill ranging from roughly 10 cm to 46 cm; demonstrating the variability of modeling results by experienced practitioners due to reasonable differences in geotechnical and structural material properties, ground motion modeling, and other aspects of the modeling.

The FLAC model has been re-applied in this investigation using an updated pore pressure generation algorithm, UBCSand (Beaty 2009), and slight modifications to the beam elements used to model pile response. The modeling results are comparable with similar patterns of excess pore pressure distribution, ground deformation, and plastic hinge development in piles.

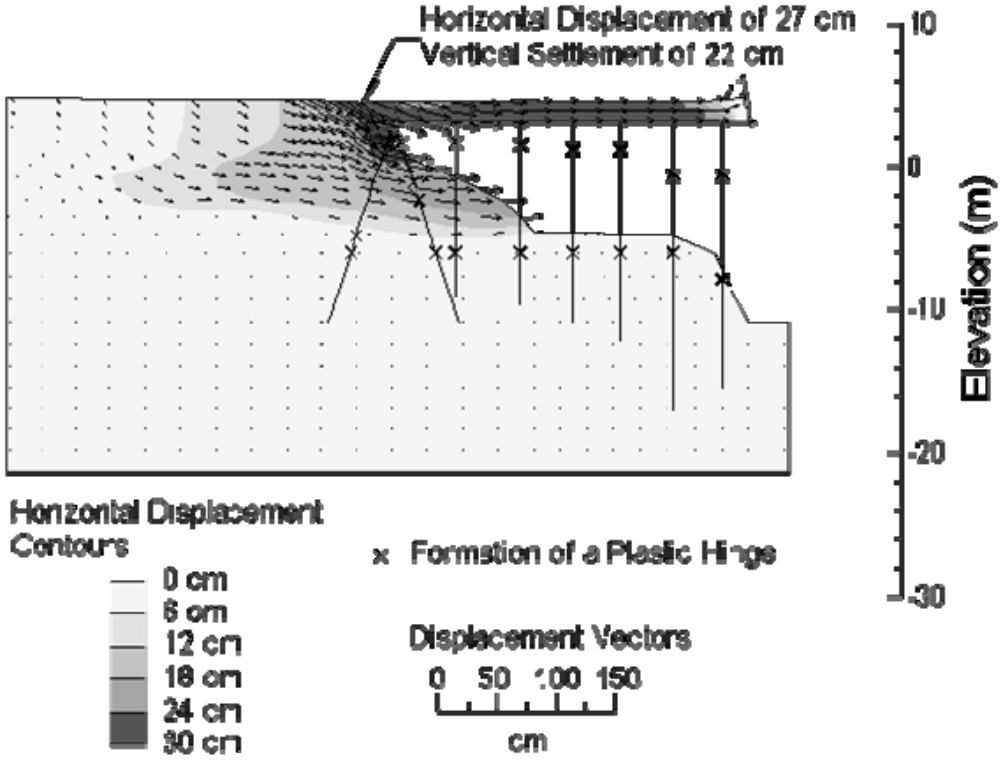

Figure 3. Numerical simulation of seismic performance of Berth 38, Seventh Street Terminal, Port of Oakland during the 1989 Loma Prieta Earthquake.

Port of Los Angeles, Pier 400, Berth 404; M_w 4.7 May 17, 2009 Inglewood Area Earthquake

Pier 400 at the Port of Los Angeles provides an extremely valuable case study for this investigation. The wharf represents recent design and construction practices, and constitutes a very important terminal at the port. The wharf and embankment configuration is similar to other major terminals at the Port of Los Angeles and the adjoining Port of Long Beach, yet the Pier 400 site is particularly valuable due to the extensive CSMIP strong motion array along a portion of the wharf, as shown in the Figure 4. CSMIP stations #14284 and #14256 provide 3 free-field and 15 structural accelerometers, respectively. The type and configuration of the piles (24" octagonal prestressed concrete piles; seven piles per bent) are consistent with contemporary port design in California.

The Pier 400 instrumentation array provides a very worthwhile case study for elastic dynamic response of a new wharf. The wharf SFSI model has been validated using motions from the 2009 M 4.7 Inglewood Area earthquake, an event that produced peak horizontal accelerations of 0.113g in the free-field and 0.21g on the wharf at Pier 400. While this was a relatively low intensity, very short duration event the data from this earthquake provided a valuable opportunity for validating the SFSI model for small- to moderate-strain wharf-embankment interaction.

Geotechnical Site Characterization

The geologic cross section and structural configuration at Berth 404 are provided in Figure 5. As defined by Fugro West (2001a, b, c); from youngest to oldest the soil profile consists of;

1. Hydraulic fill consisting of predominantly silty sand, with layers of sandy silt and silt with clay balls. The construction sequence associated with dredging, characteristics of fill based on borrow area, and the influence of placement techniques on density are addressed by Fugro West (2001a, b) and Foxworthy et al. (1998). A review of post-construction boring logs in the area adjacent to the strong motion arrays at Berth 404 indicates that the SPT penetration resistances of the sand portions of the fill vary with location due to the cumulative influence of; fines content, method of placement, and deposition above or below water level). In the unimproved fill the 33-percentile $(N_1)_{60}$ above the water level (elevation 15 ft to 0 ft) is roughly 23 blows/ft, while the corresponding value below the water level (elevation 0 ft to -34 ft) is 13 blows/ft, indicative of sand vulnerable to liquefiable at design level ground motions.
2. A thin layer of soft harbor bottom sediments (Unit 1 – Harbor Bottom Sediments).
3. An approximately 15- to 35-ft thick layer of generally fine sand and find sand with silt of alluvial deposition (Unit 2 – Younger Channel Sands).
4. An approximately 15- to 20-ft thick layer of sand with silt or silty fine sand of marine deposition (Unit 3 – Marine Sands).
5. A 30- to 35-ft (maximum) thick sequence of paleochannel infill (Unit 4 – Older Paleochannel Infill) composed of very silty fine sand (Unit 4a) overlying silt and clayey silt.
6. A thick, highly layered (sands, silts, clays) sequence of transgressive marine deposits (Unit 7 – Undifferentiated Deposits).

7. An 80- to 100-ft thick sequence of alluvial fine to medium sand with gravel (Unit 8 – Older Allluvial Deposits) that correlates with the onshore Gaspur Aquifer.

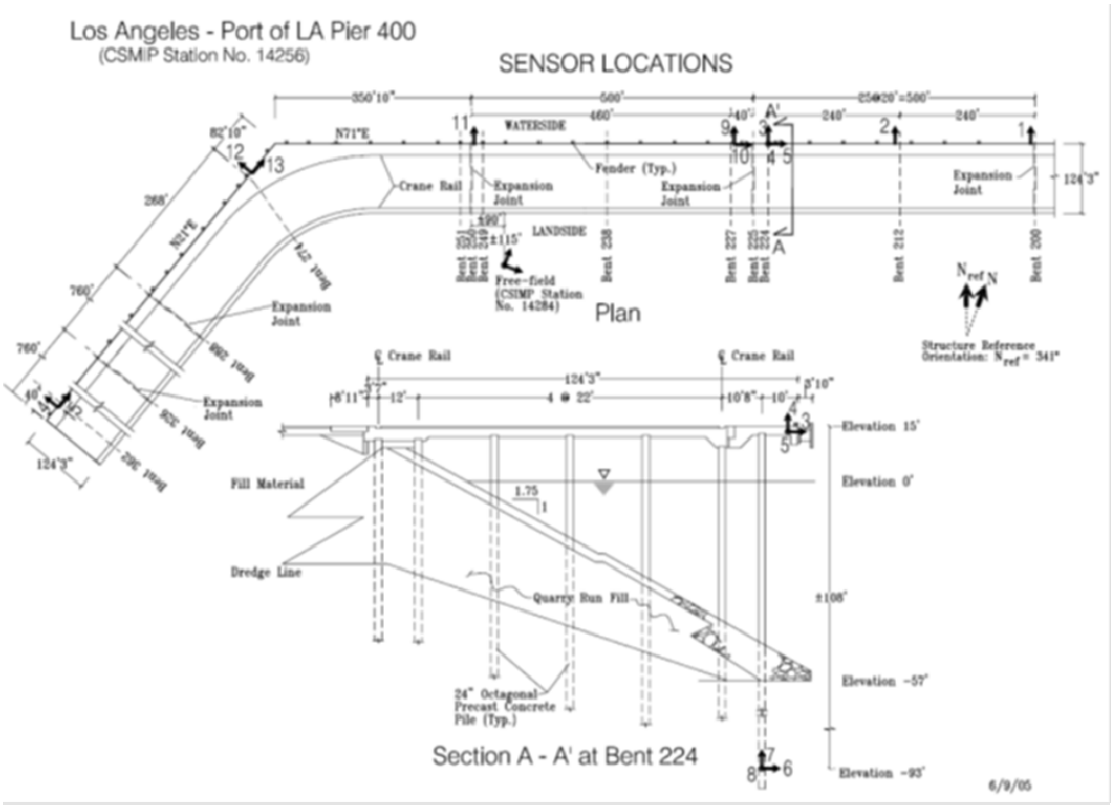

Figure 4: CSMIP Instrumentation Array at the Port of Los Angeles Pier 400 (CGS - CSMIP Station 14256), Center for Engineering Strong Motion Data (CESMD)

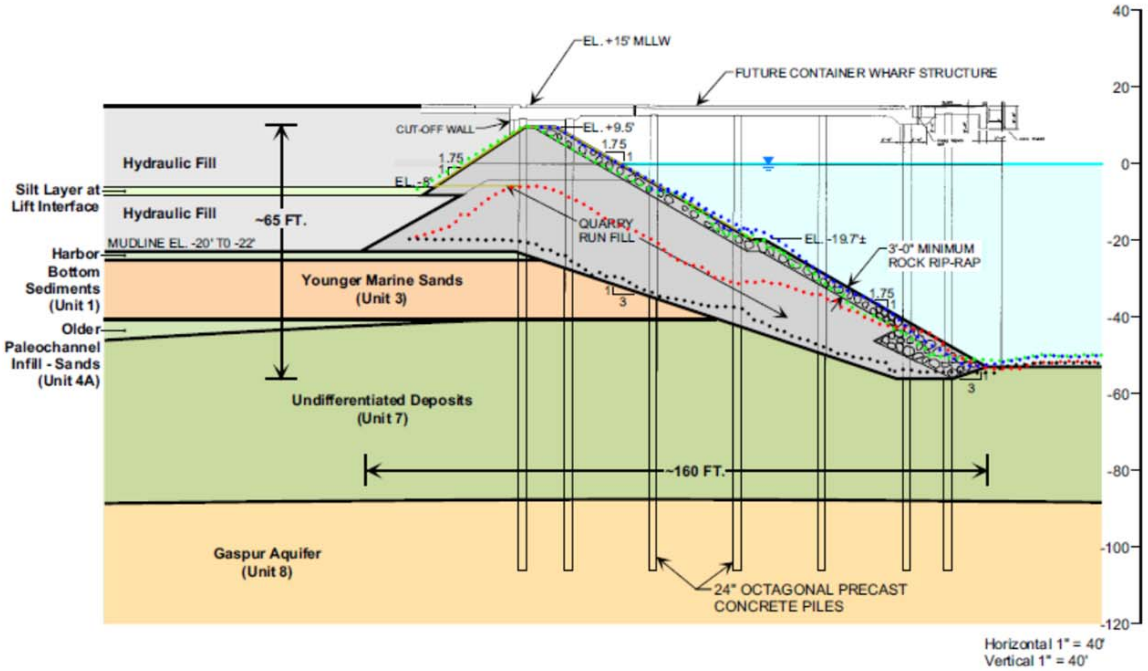

Figure 5: Geologic and structural section at Berth 404, Pier 400, Port of Los Angeles Los Angeles (Fugro West, 2004).

Ground Motions during the 2009 Inglewood Earthquake

Low-amplitude, short-duration ground motions from the M 4.9 Inglewood Earthquake were recorded at the Berth 404 strong motion instrument array. The PGA values in the free-field and on the wharf structure (transverse direction) were 0.11g and 0.21g, respectively. These motions are useful for validating the FLAC model for largely elastic behavior of the soils and structure. In order to model this event the input ground motions can be obtained by the following procedures; (i) the free-field ground surface motion can be deconvolved to the elevation corresponding to the base of the FLAC model (base transmitting boundary), and/or (ii) motions from a local vertical downhole array could be used directly. At this time the analyses have focused on the use of the downhole recordings made at the Vincent Thomas Bridge West Arrays 1 and 2 (CESMD 2013). The arrays are located adjacent to the approach and anchorage to the bridge. At a depth of 100 ft, the depth to the strong motion instruments in both vertical arrays and closest to the depth of the base of the FLAC model, the shear wave velocities at the Vincent Thomas Bridge West and East Arrays bracket (725 to 1050 ft/sec) the Berth 404 site (850 ft/sec) demonstrating somewhat uniform conditions with respect to low-strain stiffness.

This Vincent Thomas Bridge West Array is located approximately 1.8 miles from the Berth 404 site. It is acknowledged that there may be significant changes in the ground motions at prescribed depths (> 100 ft) at the Berth 404 site relative to the Vincent Thomas Bridge site. For the sake of this investigation, which is focusing on the validation of the 2D numerical model, the use of the downhole strong motions records (adjusted for a given depth within firm soil) from the Vincent Thomas Bridge site is considered reasonable as the comparison will be made between the Spectral Amplification Ratios ($SA_{Berth\ 404}/SA_{VT\ Bridge}$) computed using; (i) the recorded motions, and (ii) the ground surface motions computed with FLAC divided by the input motion (i.e. Vincent Thomas Bridge motions). Examples of these Spectral Amplification Ratios for recorded motions are provided in Figure 6a for the Berth 404 ground surface free-field motion, and in Figure 6b for the Berth 404 motions recorded on the wharf deck (transverse component). The orientations of all motions used are within a 20 degree azimuth of each other and no vector manipulation of the records was made (*and not possible due to the lack of recordings in all components during this event*). These two plots are intended to provide a *very approximate* indication of dynamic soil and structural response at Berth 404 for low levels of seismic loading.

Geophysical Investigation at Berth 404

At the outset of this investigation there were no post-construction shear wave velocity measurements at Pier 400. While shear wave velocities could have been estimated in the fill and underlying native soils using correlations with field penetration resistance (SPT, CPT) the research team, POLA, and CSMIP committed to a geophysical investigation using active and passive surface wave techniques (MASW, SASW, and ReMi) to develop the V_s profile across Berth 404 and in close proximity to the CSMIP free-field strong motion instrument station 14284. The geophysical survey provided useful data for seismic site characterization ($(V_s)_{30} \approx$ 207 m/sec) and provided an opportunity to evaluate the V_s profiles through both unimproved fill and zones of fill treated with stone columns. The latter was considered a worthwhile effort for measuring “composite” low-strain behavior of the treated soil mass. This data has been

compared to the results of estimation procedures commonly used to define the equivalent, composite shear stiffness used in 2D dynamic models.

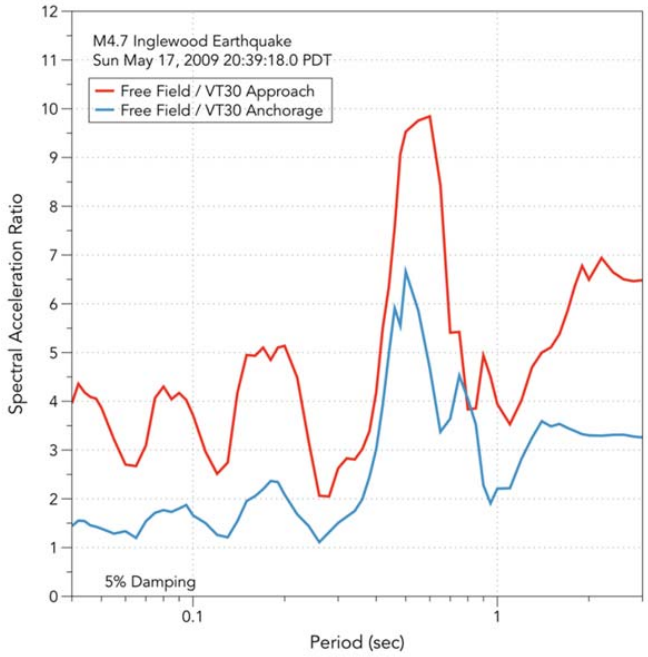

Figure 6a: Spectral amplification ratios for free-field ground surface motion at Berth 404 and motions recorded at a depth of 100 ft at the Vincent Thomas Bridge West Arrays.

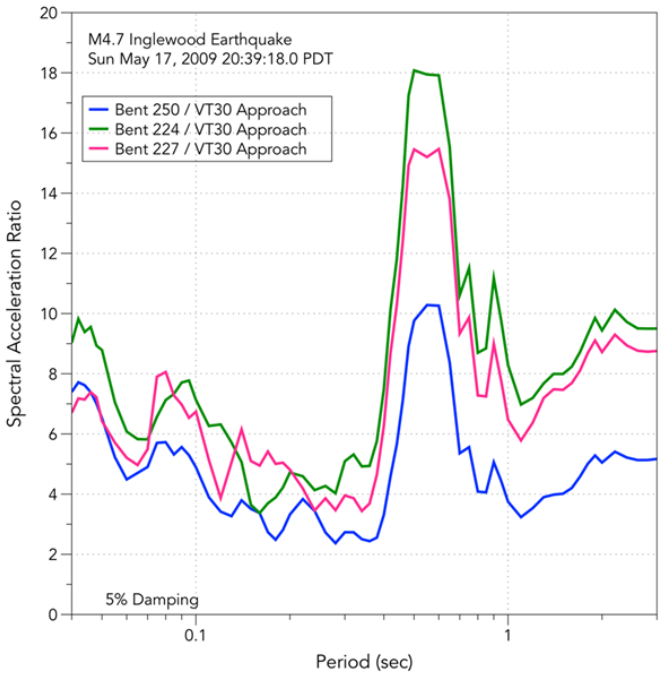

Figure 6b: Spectral amplification ratios for structural response (wharf deck) at Berth 404 and motions recorded at a depth of 100 ft at the Vincent Thomas Bridge West Arrays.

The locations of the geophysical arrays are shown in Figure 7. The arrays located south of CSMIP Free-Field Station 14284 are in areas of the unimproved hydraulically-placed fill. Arrays A-5 through A-8, and A-10 are located in the area of ground improvement by stone columns. The locations of these arrays relative to the stone column layout are provided in Figure 8. The surface wave arrays were located along the mid-points of Rows H – M and M – R, each zone having a different spacing of stone columns and Area Replacement Ratios (ARR). Based on post-construction documentation the approximate average ARR values in the two zones were 14% and 18%, although the diameter of the stone columns was noted to change significantly between the sandy fill and layers of silt-rich soil (Degen et a 2005; Fugro West 2004).

The results of the surface wave investigation are plotted in Figure 9. The agreement in the V_s profiles through native soils beneath the hydraulic fill layers is very good. The V_s trends in the unimproved and improved fill are highlighted in Figure 9a. As expected the "composite" V_s values are greater in the zone of treated soil, although the difference in the values is only roughly 7% to 12%. This data is currently being evaluated to determine the possible influence of geophysical modeling assumptions (plane waves) and 3D nature of the stone column improvement on the "composite" V_s values provide. This is a unique data set that is also being used to assess strain-compatibility concepts as applied for the dynamic behavior of stone column treated soils (Baez 1995; Rayamajhi et al. 2012).

SUMMARY OF OBSERVATIONS DURING PHASE 1 EFFORTS

Several topical lessons have been learned during Phase 1 analysis efforts, including:

1. The geophysical investigation using active and passive surface wave measurement techniques provided a valuable data set for shear wave velocity in hydraulically-placed fill at Berth 404, Port of Los Angeles. Key findings and potential implications are;
    a. The increase in V_s due to stone column placement was roughly 10% for the Area Replacement Ratios (roughly 14% to 18% on average).
    b. The rather low increase in V_s may have implications for modeling composite shearing behavior of ground treated with stone columns.
    c. Additional work is underway to evaluate the applicability of the surface wave techniques (SASW, MASW, and ReMi) in treated soils.
2. The 2D geomechanical model can reasonably predict seismically-induced permanent deformations, accelerations, and excess pore pressure generation for the low- to moderate-levels of shaking experienced in the two case histories. This appears to be true even though a relatively simple Mohr-Coulomb constitutive model was used in conjunction with two different stress-based pore pressure generation models to represent dynamic pore pressure generation.
3. Cyclic lateral behavior of piles in sloping rock fill can be fairly well modeled using a continuum numerical model if the difference between upslope and downslope SSI spring stiffness is accounted for.

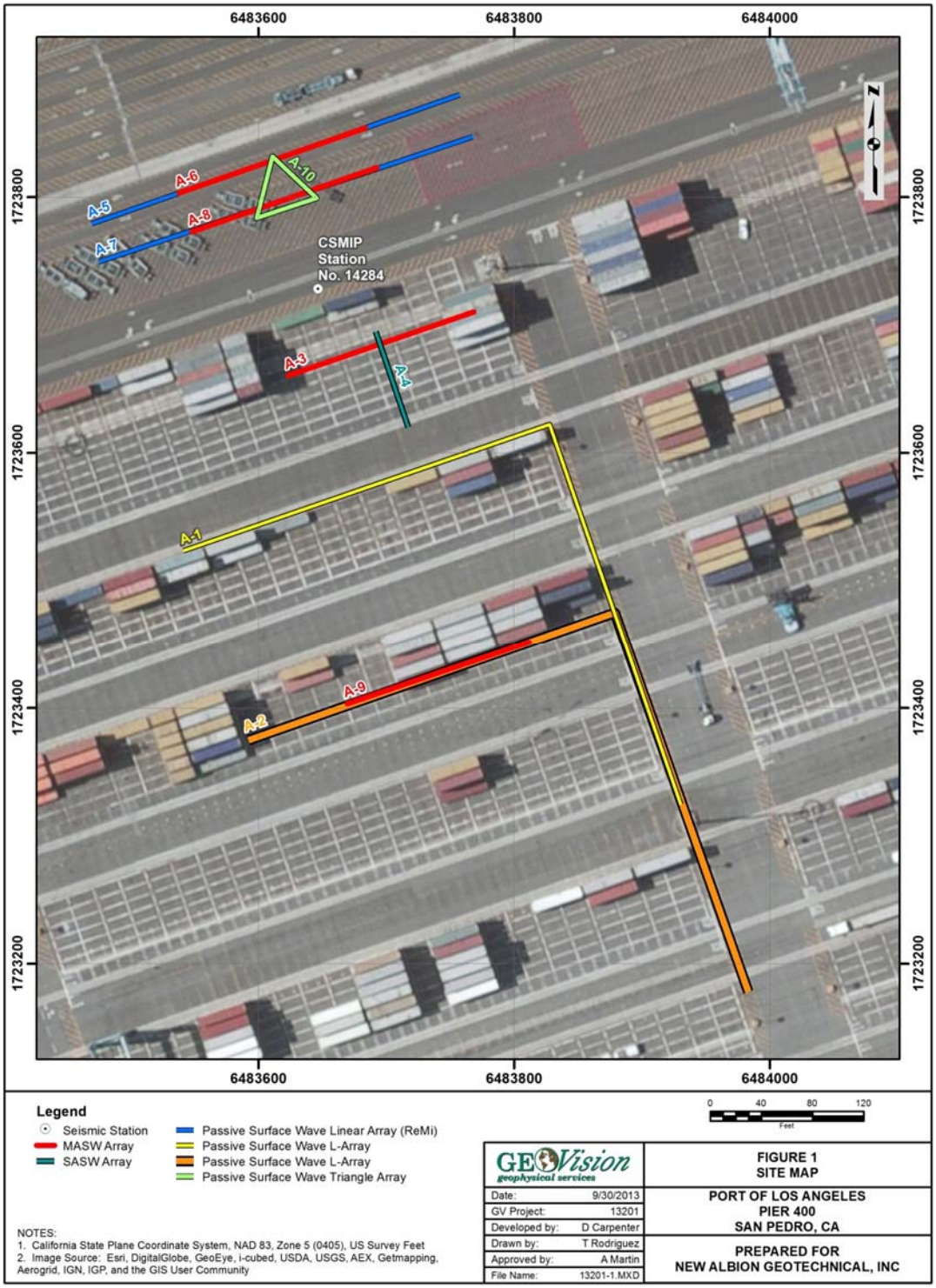

Figure 7: Location of geophysical arrays for surface wave velocity investigation at Port of Los Angeles Berth 404 (GEOVision 2013).

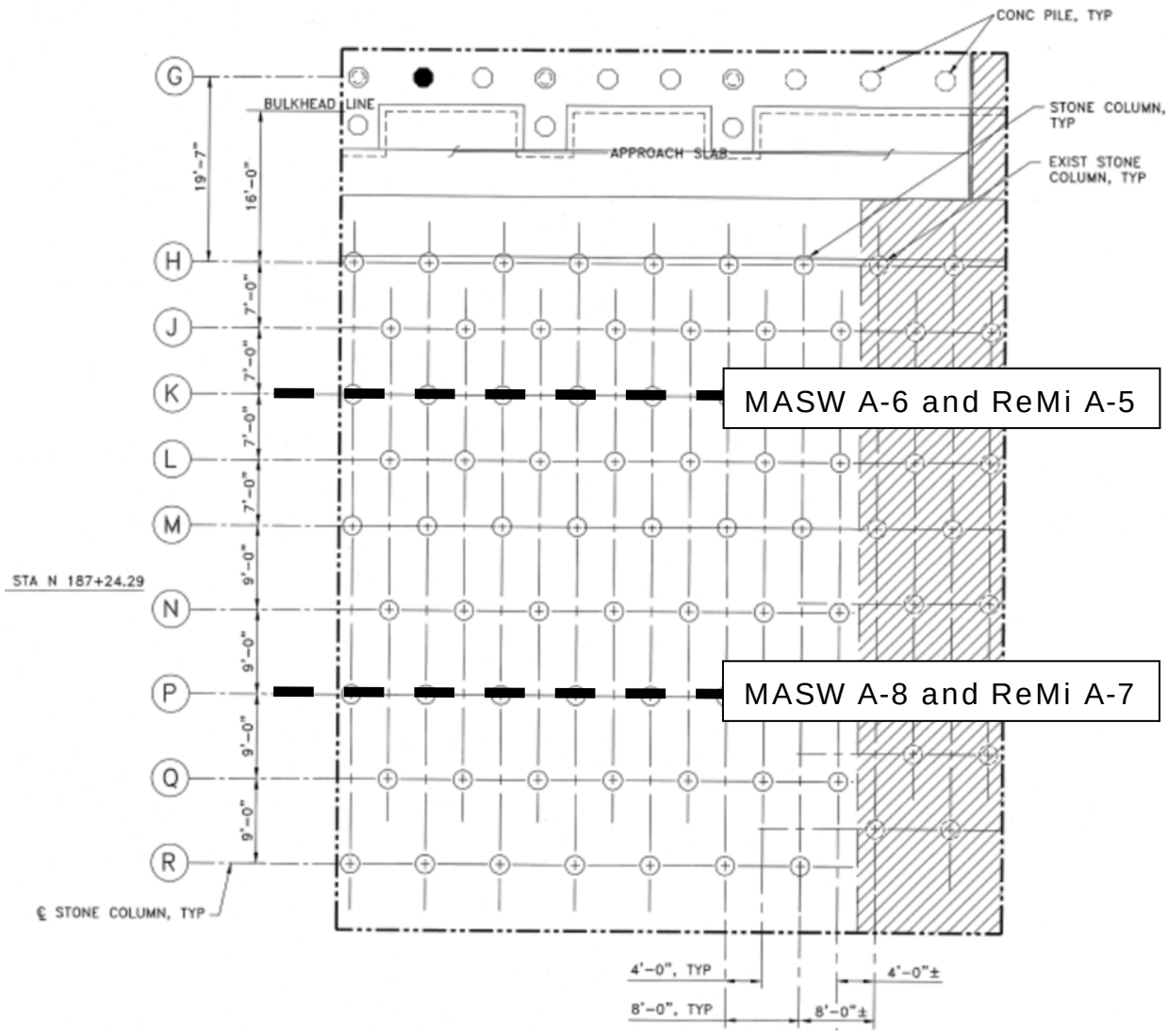

Figure 8: Location of geophysical arrays for surface wave velocity investigation of hydraulic fill treated with stone columns at Berth 404 (after POLA, 2005).

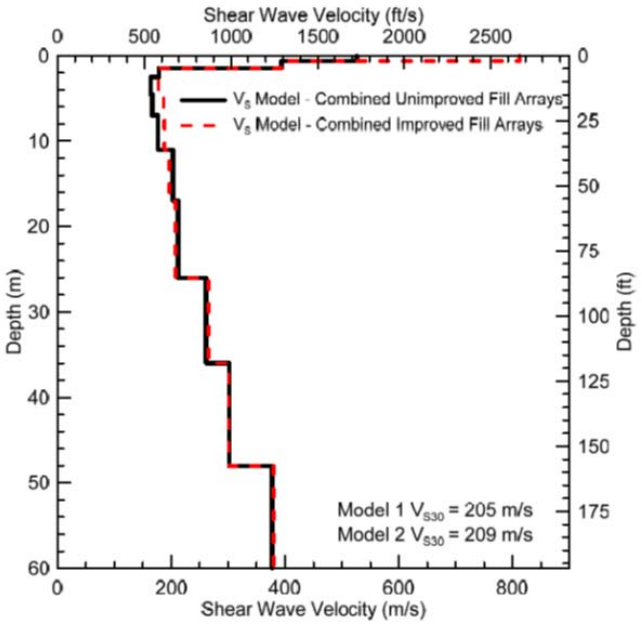

Figure 9a: Comparison of shear wave velocity profiles across the Berth 404 site (GEOVision 2013).

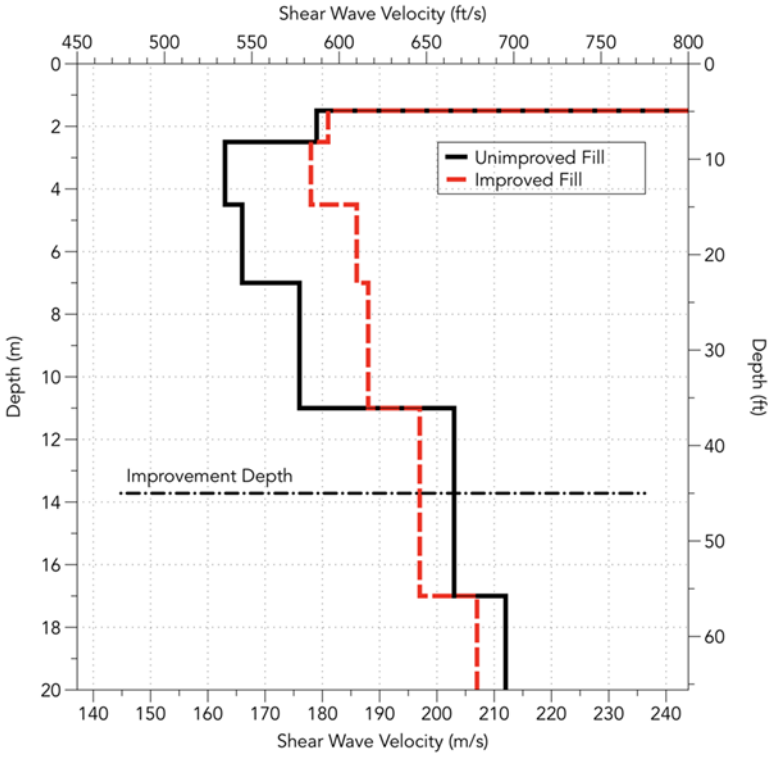

Figure 9b: Comparison of shear wave velocity profiles focusing on zones of unimproved hydraulic fill and adjacent fill improved with stone columns.

4. A simple, practice-oriented procedure for modeling pile response in rockfill includes a nominal "pseudo-cohesion" for the rock to account for the individual rock particle interaction with the pile elements (McCullough 2003; Dickenson and McCullough 2006). This simplification notwithstanding, methods of refining this approximation to account for interlocking and dilation of the rockfill should be pursued (e.g. Kawamata 2009). This is considered an important aspect of the modeling for large-amplitude, long-duration shaking due to significant pile-soil interaction for the "seismic piles" (i.e. rear, landward rows) associated with inertial loading near the pile head, and due to possible deep-seated ground failures (displacement demand) that could provide excessive loads at the interface of the rockfill and underlying soils.
5. It is clear that large pile moments develop at depth when there is even moderate soil displacement due to global behavior of the rock dike and foundation soils. These moments are only-predicted through the use of analysis methods that have the capability to model the global wharf-embankment system.

PROJECT FOCUS FOR PHASE 2 OF THE INVESTIGATION

Calibrating the numerical dynamic SFSI models against recorded behavior is considered a necessary step prior to simulations involving long-duration and higher levels of ground motion. In Phase 2 of this investigation the computed response under long-duration ground motions will be evaluated in light of the seismic performance criteria for wharves at the two major ports. Subsequent tasks involve detailed analysis of the modeling results and seismic performance assessment to identify predicted behaviors that have significant implications for current seismic design methods for wharves. Examples include;

a. Structural failures, particularly those associated with moderate permanent ground deformation caused by long-duration shaking at moderate levels, will be evaluated from initiation through the end of ground shaking using the time histories of forces and displacements. This assessment will incorporate member strength/capacities for the concrete, steel and pre-stress, using the strain limits and plastic hinge lengths, as described in the MOTEMS (2010) and Port of Long Beach Wharf Design Criteria (February, 2012).
b. The relationship between permanent ground deformation and pile response in soils exhibiting excess pore pressure generation that is less than that required for "full liquefaction" (i.e., excess pore pressure ratios of 0.5 to 0.9) will be investigated in detail. The soil constitutive model for excess pore pressure generation and cyclic behavior is well suited to represent shear displacement that would not be indicated in a conventional uncoupled liquefaction susceptibility and slope deformation evaluation.
c. Strain softening of normally consolidated fine-grained soils is a pertinent aspect of the analyses, particularly where soil stiffness is important for deformations in embedded piles. Characteristics of transient and permanent deformations of embankment.
d. Phasing of inertial loads and kinematic loads in the piles and pile-deck connection, and
e. Displacement demand on piles as a function of row location (landside versus waterside).

The sequence of the Phase 2 investigation will include baseline analyses using OLE and CLE motions that are readily available from recent applications at POLA, and which follow

guidelines set forth in the Port-Wide Ground Motion study (EMI 2006). Subsequent analyses will be performed using long-duration motions. A suite of motions will be used with "seed" motions scaled and/or spectrally matched to prescribed Intensity Measures. The dynamic response of the wharf and embankment will be evaluated for each analysis. These analyses will be repeated for the Berth 55 strong motion instrumentation array at the Port of Oakland. It is anticipated that the improved understanding of the relationships between duration of strong shaking, permanent deformation of the ground and pile foundation, and post-earthquake functionality will have practical implications on performance-based design of port structures in California.

Acknowledgements

The authors gratefully acknowledge the significant and on-going contributions made by the following individuals. Collectively, these individuals have provided technical documentation, access to projects archives, acceleration time histories, and research results pertinent to the project. The research team has benefitted from active communication addressing nuances of the analysis and design, construction, and post-construction history at the project sites; Port of LA Berth 404 and Port of Oakland Berth 55.

Tony Gioiello, Peter Yin and Hugo Cisneros; Port of Los Angeles
Matt Pollard, Cornelia Dean and Danya Pollard; Fugro West, Inc. (Ventura, CA)
Imee Osantowski and Steve Low; Port of Oakland
Tony Martin; GEOVision (Corona, CA)
Nason McCullough; CH2M Hill (Corvallis, OR)
Arul Arulmoli; Earth Mechanics, Inc. (Fountain Valley, CA)
Luke Leffingwell; APM Terminals Los Angeles
Moh Huang, Shirley Rowley and Tony Shakal; CSMIP (Sacramento, CA)
Dawn Lehman; University of Washington (Seattle, WA)
Jose Restrepo; University of California (San Diego, CA)

References

Arulmoli, K., Martin, G.R., Gasparro, M.G., Shahrestani, S., and Buzzoni, G. (2004). Design of Pile Foundations for Liquefaction-Induced Lateral Spread Displacements, *Proc. Geo-Trans 2004; Geotechnical Engineering for Transportation Projects*, Vol. 2, 1673-1680, ASCE Geotechnical Engineering Special Publication No. 126, July, Los Angeles.

ASCE (in preparation). Seismic Design of Pile-Supported Piers and Wharves, prepared by the ASCE Standards Committee on Seismic Design of Piers and Wharves.

ASCE COPRI (in press). The March 2011 Great Tohoku Earthquake; Investigation of Port and Harbor Structures, Percher, M., and Dickenson, S. (editors), ASCE, Reston, VA.

ASCE TCLEE (1998). Seismic Guidelines for Ports, Werner, S. (ed.), TCLEE Ports Lifeline Committee, TCLEE Monograph #12, ASCE, Reston, VA.

Beaty, M. (2009). Summary of UBCSand Constitutive Model, Versions 904a and 904aR, Beaty Engineering, LLC, prepared for the short course *Seismic Deformation Analyses of Embankment Dams considering Liquefaction Effects*, Sept. 22 – 24.

Baez, J.I. (1995). A Design for the Reduction of Soil Liquefaction by Vibro-Stone Columns, Ph.D. dissertation, Univ. of Southern California.

Boland, J.C., Schlechter, S.M., McCullough, N.J., Dickenson, S.E., Kutter, B.L., and Wilson, D.W. (2001a), Data Report: Pile-Supported Wharf Centrifuge Model (SMS02), Dept., Civil, Construction & Environmental Engineering, Oregon State Univ.

Boland, J.C., Schlechter, S.M., McCullough, N.J., Dickenson, S.E., Kutter, B.L., and Wilson, D.W. (2001b), Data Report: Pile-Supported Wharf Centrifuge Model (JCB01), Dept., Civil, Construction & Environmental Engineering, Oregon State Univ.

Center for Engineering Strong Motion Data (CESMD). On-line archive for strong motion data. POLA Pier 400 Berth 404; (**http://www.strongmotioncenter.org/cgi-bin/CESMD/stationhtml.pl?stacode=CE14256&network=CGS**) Vincent Thomas Bridge Geotechnical Array West 1 & West 2 (**http://www.strongmotioncenter.org/cgi-bin/CESMD/stationhtml.pl?stacode=CE14783&network=CGS**)

Chiaramonte, M.M., Arduino, P., Lehman, D.E., and Roeder, C.W. (2011). Seismic Analyses of Conventional and Improved Marginal Wharves, *Jrnl. Earthquake Eng. Struct. Dyn.*, 00; 1 -19.

Degen, W., Baez, F., and Rose, M. (2005). Dry Bottom Feed Stone Columns at Pier 400, Phase II – An evaluation of CPT-based soil classification before and after treatment, *Proc. US-Japan Workshop "New Applications & Challenging Soils for Ground Improvement Technologies*, September, Kyoto, Japan.

Dickenson, S.E. and McCullough, N.J. (2006). "Modeling the Seismic Performance of Pile Supported Foundations for Port and Coastal Infrastructure," Proc. of Seismic Performance and Simulation of Pile Foundations in Liquefied and Laterally Spreading Ground, Boulanger and Tokimatsu (eds.), Geotechnical Specialty Publication No. 145, ASCE, 173-191.

Donahue, M.J., Dickenson, S.E., Miller, T.H., and Yim, S.C. (2005). "Implications of the Observed Seismic Performance of a Pile-Supported Wharf for Numerical Modeling," Earthquake Spectra, EERI, 21(3), 617-634.

Egan, J.A., Hayden, R.F., Scheibel, L.L., Otus, M., and Serventi, G.M. (1992). Seismic repair at Seventh Street Marine Terminal, *Proc. Grouting, Soil Improvement, and Geosynthetics*, ACSE Geotechnical Specialty Publication No. 30, Vol. 2.

Earth Mechanics, Inc. (2006). Port-Wide Ground Motion and Palos Verde Fault Study, Port of Los Angeles, California, Final Report, prepared for the Port of Los Angeles, Project 02-131-11, December, 22.

Foxworthy, J., McNeilan, T., and Alcorn, A. (1998) Interim Pier 400 Landfill Status Report, *Proc. Ports '98*, ASCE, Vol. 1., 551 – 560.

Fugro West (2004). Stone Column Ground Improvement Pier 400 Container Wharf Phase 2, Port of Los Angeles, California, prepared for the Port of Los Angeles, March.

Fugro West, Inc. (2001a). Final Geotechnical Framework Report, Pier 400 Landfill Project, Port of Los Angeles, California, prepared for the Port of Los Angeles, April.

Fugro West (2001b). Geotechnical Data Report Pier 400, Stage 2, Post-Fill Investigation, Port of Los Angeles, prepared for the City of Los Angeles, Harbor Department, July.

Fugro West (2001c). Geotechnical Study Pier 400 Container Wharf Phase 2, Port of Los Angeles, California, prepared for the Port of Los Angeles, November.

GEOVision (2013). Report Surface Wave Measurements, Port of Los Angeles, Pier 400, Berth 404, Los Angeles County, California, prepared for New Albion Geotechnical, Inc., Report 13201-01, August 5.

Kawamata, Y. (2009). Seismic Performance of Pile-supported Container Wharf Structures in Rockfill, Ph.D. dissertation, School of Civil & Construction Engineering, Oregon State University, Corvallis, Oregon.

Krier, C.J., Restrepo, J.I., Blandon, C.A. (2008). Seismic Testing of Full-Scale Precast Prestressed Pile to Deck Connections, UCSD Structural Systems Research Project, Report No. SSRP-06/26, Univ. of California, San Diego, Dept. of Structural Engineering, prepared for the Port of Los Angeles, January.

Lehman, D.E., Roeder, C., Stringer, S.J., Jellin, A. (2013). Seismic performance of improved pile-to-wharf deck connections, *PCI Jrnl.*, Summer, 62-80.

McCullough, N.J. (2003). The Seismic Geotechnical Modeling, Performance, and Analysis of Pile-Supported Wharves, Ph.D. dissertation, Dept, of Civil Engineering, Oregon State University, Corvallis, Oregon.

McCullough N. and Dickenson, S. (2004). The Behavior of Piles in Sloping Rock Fill at Marginal Wharves, *Proc. Ports 2004*, ASCE, May, Houston, TX.

Moriwaki, Y., Tan, P., and Choi, Y. (2005). Nonlinear analyses for design of piles in liquefying soils at port facilities, *Proc. of Seismic Performance and Simulation of Pile Foundations in Liquefied and Laterally Spreading Ground*, Boulanger and Tokimatsu (eds.), Geotechnical Specialty Publication No. 145, ASCE, 192-1203.

Norris, G., Siddharthan, R., Zafir, Z., Abdel-Ghaffar, S., and Gowda, P. (1991). "Soil-Foundation-Structure Behavior at the Oakland Outer Harbor Wharf", *Proc. SMIP91 Seminar on Seismological and Engineering Implications of Recent Strong Motion Data*, California Department of Conservation, Division of Mines and Geology, SMIP, held in Sacramento, CA, May 30, p. 11-1 to 11-11.

Oyenuga, D., Abe, S., Sedarat, H., Krimotat, A., Salah-Mars, S., and Ogunfunmi, K. (2001). Analysis of Existing Piles with Missing Data in Seismic Retrofit Design at the Port of Oakland, *Proc. Ports 2001*, Norfolk, VA.

PIANC WG 34 (2001). Seismic Design Guidelines for Port Structures, Iai, S. (ed.), Working Group #34, International Navigation Association (PIANC), A.A. Balkema Publishers, 474 p.

POLA (2002). Pier 400 Container Wharf Phase II – Berths 404-406, Record Set, Stone Column Layout – Bents 200 to 204 (Drawing SC-4), prepared by City of Los Angeles, Harbor Department, Engineering & Construction Division.

POLA (2010). The Port of Los Angeles Code for Seismic Design, Upgrade and Repair of Container Wharves (POLA Seismic Code 2010), City of Los Angeles Harbor Department.

POLB (2012). Port of Long Beach Wharf Design Criteria, Version 3.0 (February).

Priebe, H.J. (1995). The design of vibro replacement, *Ground Engineering*, December.

Priestley, M.J.N. (2000). Pier 400 Strength and Ductility of Wharf Piles, prepared for the Port of Los Angeles, Report #00/01, August.

Rayamajhi, D., Hguyen, T.V., Ashford, S.A., Boulanger, R.W., Lu, J., Elgamal, A., and Shao, L. (2012). Effect of Discrete Columns on Shear Stress Distribution in Liquefiable Soil, *Proc. GeoCongress 2012*, ASCE.

Restrepo, J.I., Yin, P., Jaradat, O.A., and Weismair, M. (2007) Performance of New Pile-Deck Connections Under Earthquakes, *Proc. Ports 2007*, ASCE, San Diego, CA.

Roth, W.H. and Dawson (2003). Analyzing the Seismic Performance of Wharves, Part 2: SSI Analysis with Non-Linear, Effective-Stress Soil Models, *Proc. TCLEE 2003: 6th US Conference & Workshop on Lifeline Earthquake Engineering*, Long Beach, CA.

Roth, W.H., Dawson, E.M., Mehrain, M., and Sayegh, A. (2003). Analyzing the Seismic Performance of Wharves, Part 1: Structural-Engineering Approach, *Proc. TCLEE 2003: 6th US Conference & Workshop on Lifeline Earthquake Engineering*, Long Beach, CA.

Shafieezadeh, DesRouches, R., Rix, G.J., and Werner, S.D. (2012). Seismic Performance of Pile-Supported Wharf Structures Considering Soil-Structure Interaction in Liquefied Soil, *Earthquake Spectra*, EERI, 28(2), 729-757.

Singh, J.P., Tabatabaie, M., and French, J.B. (2001a). Geotechnical and Ground Motion Issues in Seismic Vulnerability Assessment of Existing Wharf Structures, *Proc. Ports 2001*, ASCE, April.

Singh, J.P., Tabatabaie, M., and French, J.B. (2001b). Importance of Seismological-Geotechnical-Structural Handshake in Performance-Based Design of Waterfront Structures, Port of Oakland Wharf & Embankment Strengtheing Program (WESP).

Wang, Z.L., Egan, J., Scheibel, L., and Makdisi, F.I. (2001). Simulation of earthquake performance of a waterfront slope using fully coupled effective stress approach, *Proc. 2nd Intern. FLAC Symposium*, Lyon, France, October, 100-108.

Weismair, M., Shahrestani, S., Lim, A., Priestley, M.J.M., and Lam, I.P. (2001). Seismic Design of Port of Los Angeles Pier 400 Container Wharf, *Proc. Ports '01*, ASCE

Yan, L., Arulmoli, K., Weismair, M., Aliviado, R., and Lam, I.P. (2004). Seismic Soil-Structure Interaction Analyses of an Underwater Bulkhead and Wharf System, *Proc. Geo-Trans 2004; Geotechnical Engineering for Transportation Projects*, Vol. 1, 547-555, ASCE Geotechnical Engineering Special Publication No. 126, July, Los Angeles.

THREE DIMENSIONAL GLOBAL NONLINEAR TIME HISTORY ANALYSES OF INSTRUMENTED BRIDGES TO VALIDATE CURRENT BRIDGE SEISMIC DESIGN PROCEDURES

Anoosh Shamsabadi[1,*] Tom Ostrom[1] and Ertugrul Taciroglu[2]

[1]Office of Earthquake Engineering,
California Department of Transportation, Sacramento, CA

[2]Civil & Environmental Engineering Department
University of California, Los Angeles, CA

Abstract

California Department of Transportation (Caltrans) and California Geological Survey (CGS) have instrumented a number of bridges, and have been collecting their strong motion response measurements for more than two decades (Hipley and Huang, 1997). The deployed instrument sets usually include down-hole sensor arrays, and accelerometers installed on piles, pile-caps, and decks. These bridges are located relatively close to faults identified on the Caltrans Seismic Hazard Map (Mualchin, 1996). The intent has been to select different bridge types, ranging from standard ordinary bridges to those such as toll bridges with unique features.

This paper presents three-dimensional *global* high-fidelity numerical (finite element) models for three representative bridges—namely, a standard ordinary non-skewed bridge, a skewed bridge, and a non-standard long-span bridge. There are multiple sets of acceleration records due to nearby earthquakes for each of the selected bridges. We carefully, albeit heuristically, calibrate the parameters of these models to improve the agreement between the measured and predicted responses. Upon model calibration, the calculated displacement responses of the simulation models match remarkably well with those obtained from the acceleration records at major locations on the specimen bridges.

Introduction

The main objective this paper is to explore the recorded seismic responses of various types of instrumented bridges, and to improve the current seismic analysis procedures and guidelines through comparisons of recorded responses with predictions from forward simulation models. The primary metrics in these comparisons are the natural frequencies, vibration modes and damping.

Herein, two “standard ordinary” bridges and a “nonstandard bridge” (Caltrans SDC, 2013) are selected for detailed analysis. The *Meloland Road Overcrossing* (MRO)—located near El Centro, California—is the selected non-skewed ordinary standard bridge; the *Painter Street Overcrossing* (PSO)—located in Rio Dell, California—is the selected ordinary standard bridge with a high (39^o) abutment skew angle; and the *Samoa Chanel Bridge* (SCB)—located in

* Presenting Author (Email: anoosh_shamsabadi@dot.ca.gov).

Humboldt County, California—is the selected long-span nonstandard bridge. MRO was constructed in 1971. It is a two-span reinforced concrete box-girder bridge supported on a single-column bent and integral (monolithic) abutments. PSO is a two-span cast-in-place prestressed reinforced concrete box-girder bridge supported by integral abutments and a two-column bent. The SCB consists of 20 spans with four pre-stressed reinforced concrete I-girder supported on single-column bents, and seat-type non-skewed abutments.

Description of Investigated Bridges

MRO is approximately 208 ft long and 34 ft wide with each span measuring 104 ft. The depth of the deck is 5.5 ft. The height of its 5ft-diameter column is approximately 21 ft, which is supported on 25 timber piles with a square concrete cap. The monolithic abutment backwalls have a height of the approximately 13 ft. Each abutment is supported on a single row of 7 timber piles. A photograph of MRO and a schematic showing the locations of its seismic sensors (on deck and abutments) are displayed in Figure 1. Figure 2 displays an idealized soil profiles for MRO along the piles and behind the abutments that were used in our analyses.

Figure 1. Meloland Road Overcrossing (top) and its seismic instrumentation (bottom).

PSO is approximately 265 ft long and 52 ft wide with spans measuring 146 ft and 119 ft with a 39^{o} skew angle. The depth of the deck is 5.67 ft. The average height of the columns is approximately 24 ft, and each is supported on a 4×5 arrangement of concrete piles. The average height of the monolithic abutment backwall is approximately 12 ft. The west abutment wall rests on a neoprene bearing strip lubricated with grease to allow thermal movement between the abutment wall and the backfill. There is a 1 inch gap between the abutment wall and the abutment backfill. The west abutment is supported on a single row of 16 concrete piles. The east abutment backwall is monolithic—i.e., the wall is cast to the deck and the pile-cap, and it is supported on a single row of 14-ton driven concrete piles. The locations of the seismic sensors on the bridge deck and abutments are shown in Figure 3. Figure 4 displays the idealized soil

profile along the piles and behind the abutments. Table 1 summarizes the engineering properties of the existing backfills and natural soils for PSO that were used in the analyses.

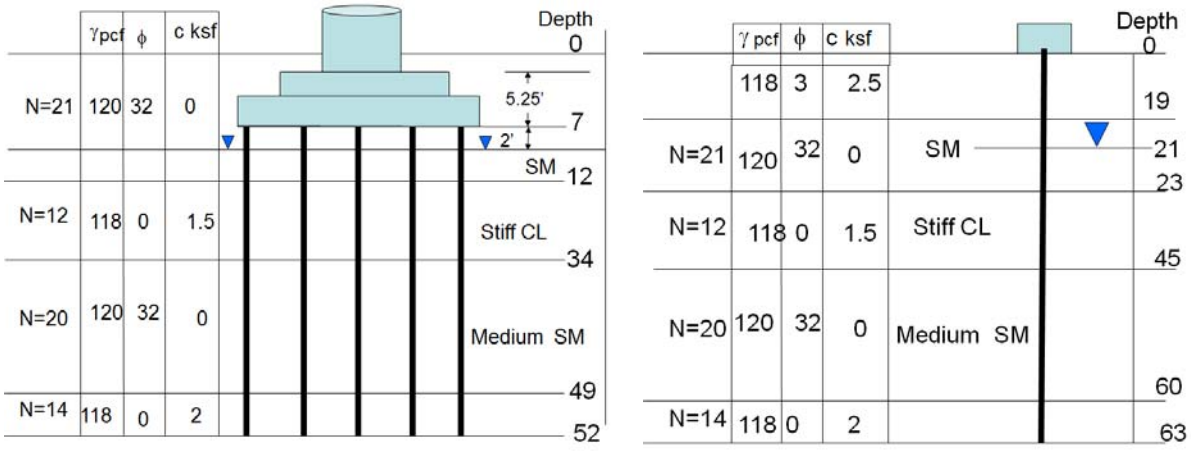

(a) Soil profile along pile group at the bent (b) Soil profile along pile group at abutments

Figure 2. Idealized soil profile for the Meloland Road Overcrossing.

Figure 3. The Painter Street Overpass (top) and its seismic instrumentation (bottom).

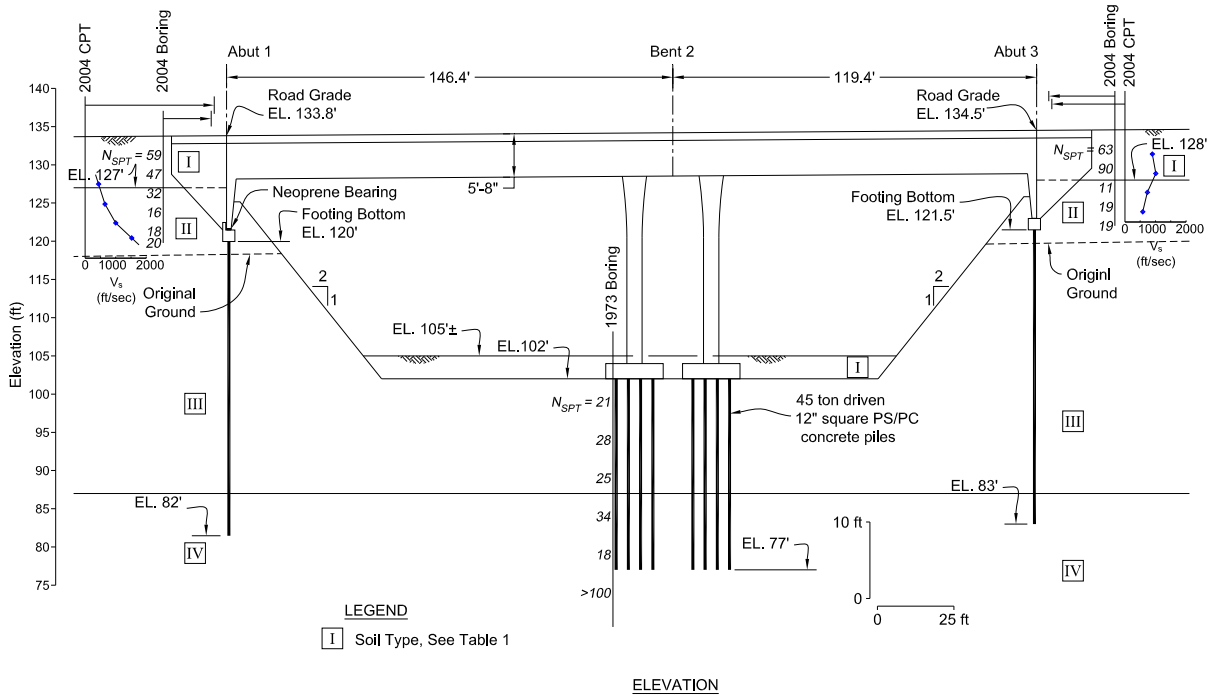

Figure 4. The geometry and idealized soil profile for the Painter Street Overpass.

Table 1. Soil properties for the Painter Street Overpass.

Type	Soil Type (USCS Symbol)	Soil Properties					*p-y* Curve Parameters			Soil Stiffness		
		γ' pcf	ϕ deg	c psf	ν -	v_s fps	k pci	ε_{50} -	J -	E_s ksf	E_{50} ksf	E_r ksf
I	Compacted Sandy Fill (SP, GP)	130	38	50	0.35	670	60	-	-	n/a	n/a	n/a
II	Stiff Silt and Clay (ML/CL)	128	11	3,300	0.40	1,000	-	0.005	0.5	90	110	300
III	Medium dense Sand (SP)	57	34	0	0.35	n/a	60	-	-	n/a	n/a	n/a
IV	Dense Sand with Gravel (SP)	63	36	0	0.35	n/a	80	-	-	n/a	n/a	n/a

Notes: γ' = Effective Unit Weight, ϕ = Friction Angle, c = Cohesion, ν = Poisson ratio, ε_{50} = Strain Parameter for p-y curve, J = Empirical Coefficient for *p-y* curve, v_s = Shear wave velocity, k = Modulus of subgrade reaction, E_{50} = Stiffness at 50% of Ultimate Stress, E_r = Unloading/ Reloading modulus.

The SCB carries Route 225, linking the city of Eureka to Samoa Peninsula (Figure 5). It was constructed in 1971 (construction started in 1968) and underwent a seismic safety retrofit in 2002 (Caltrans, 2002). The bridge is approximately 2506 ft long and 34 ft wide. The locations of the seismic sensors on the bridge deck and the piers, and the basic soil profile at the bridge site are shown on Figure 5. Detailed soil profile data for the SCB are omitted here for brevity, but can be accessed through the California Strong Motion Instrumentation Program's (CSMIP) internet-accessible database (cf. CSMIP Station No. 89734).

The SCB superstructure comprises 6.5in-thick concrete deck slabs resting on four pre-stressed precast concrete I-girders with intermediate diaphragms. The composite deck is supported on concrete bent-cap and hexagonal single-columns and seat-type abutments. The bridge consists of 20 spans. The typical span length is 120 ft except the main channel, which is

225ft-long, and extends from the centerline of pier 8 to the centerline of pier 9. The 150ft-long concrete I-girders of the superstructure begin at pier 7 and pier 10, and are cantilevered 30ft past piers 8 and 9 into the main-channel crossing span. The 165ft-long pre-stressed precast concrete I-girders resting atop the cantilevered portions cross over the main-channel (Figure 5, bottom).

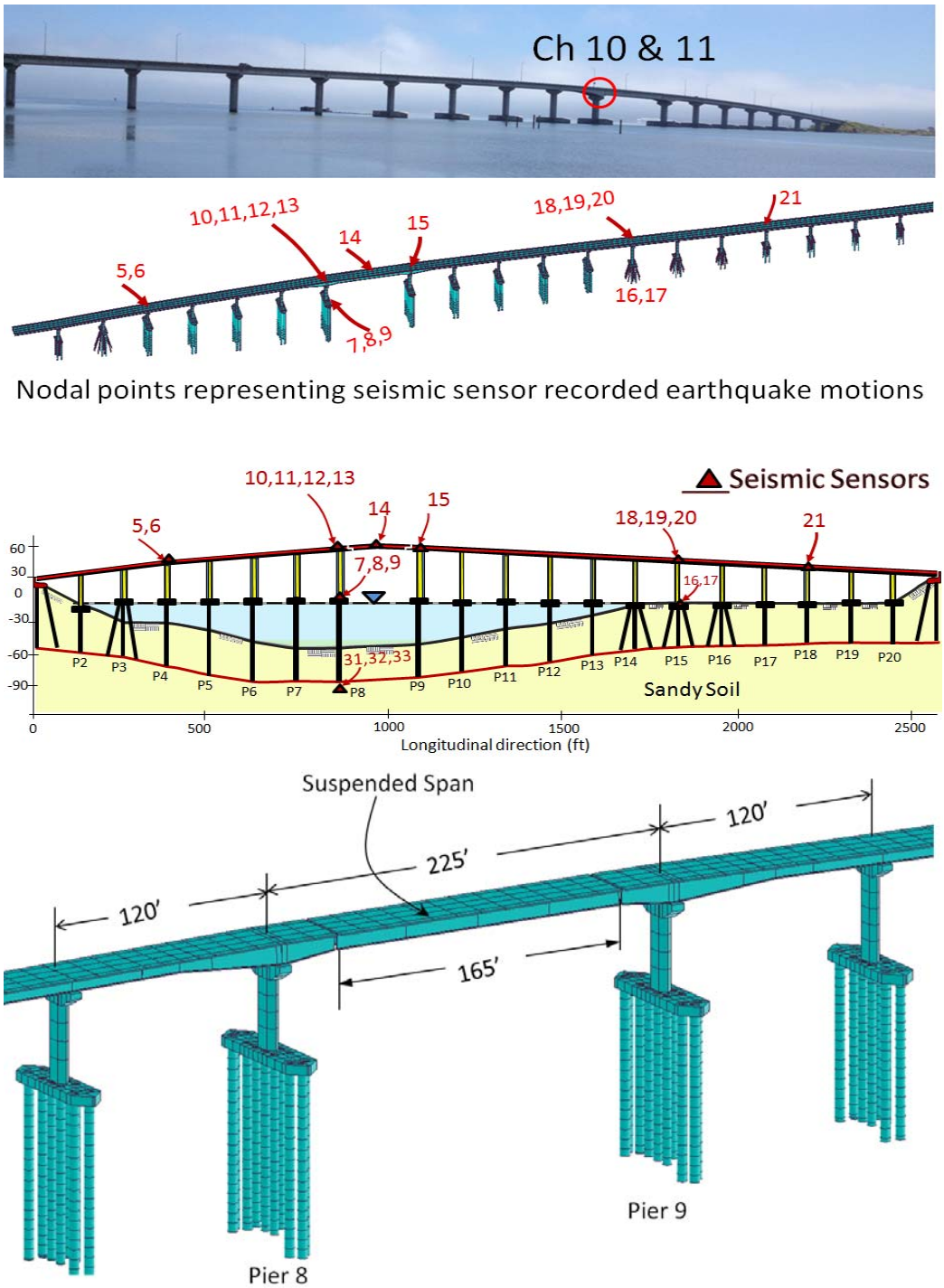

Figure 5. Samoa Channel Bridge (top), its seismic instrumentation (middle), and a close-up view of its finite element model at the main channel crossing.

Bridge Finite Element Models

Detailed global three-dimensional finite-element models of all three bridges were developed (see Figure 6) using the *Midas Civil* (MIDASoft, 2012) computer program. These models featured macroelements to simulate the nonlinear foundation-soil-interaction effects at the abutments and the pile foundations, as well as elements for abutment shear keys. The bridge deck and the abutment walls were modeled as shell elements with appropriately chosen structural properties.

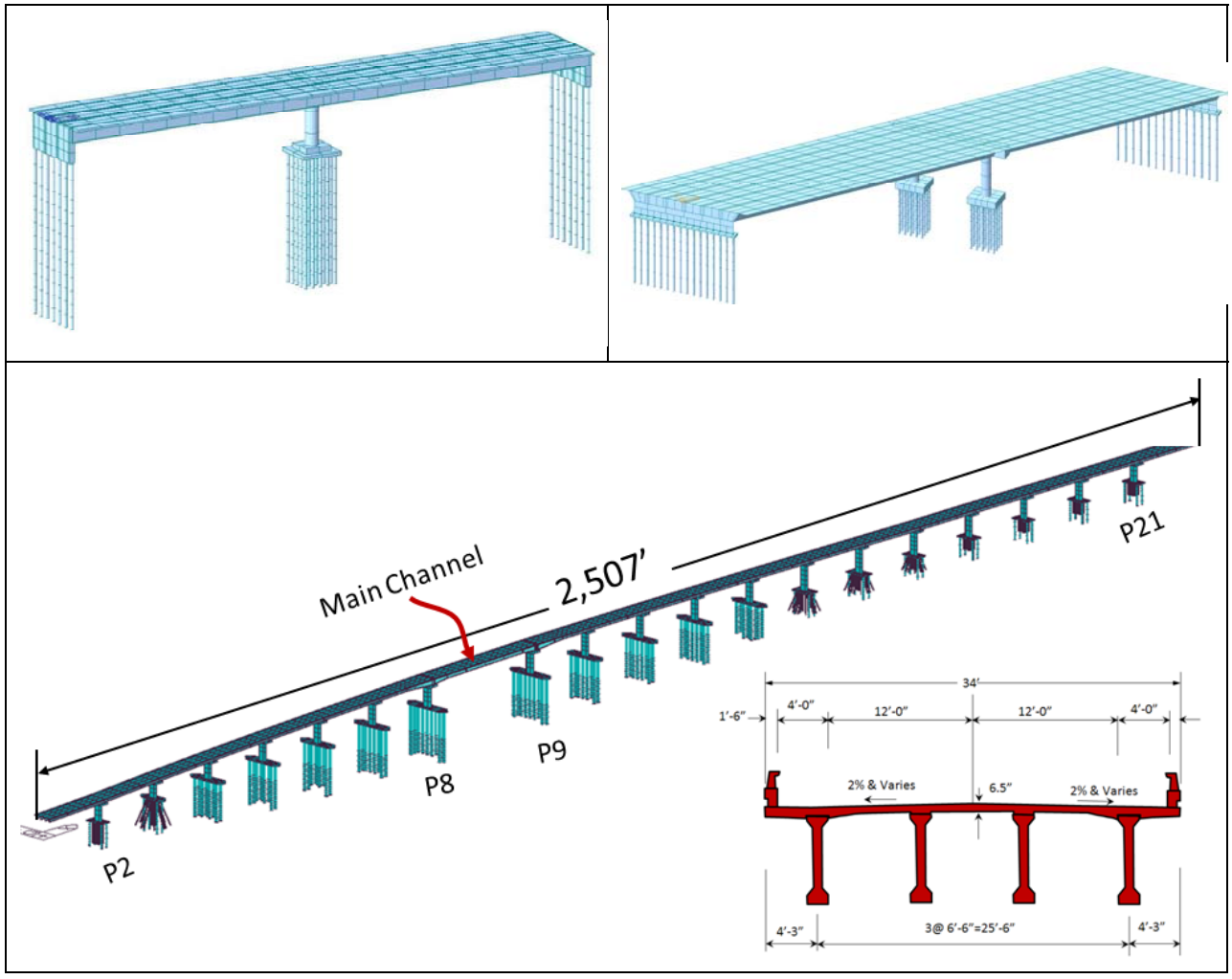

Figure 6. The three-dimensional finite element models of the Meloland Road Overcrossing (top left), Painter Street Overpass (top right), and the Samoa Channel Bridge (bottom).

Abutment and Pile Models

The bridge abutments play a significant role in the global seismic behavior of bridges. This is especially true for ordinary, short-span, bridges like MRO and PSO. For the longitudinal nonlinear spring at the abutment-embankment soil interface, a separate continuum finite-element

model was developed using the computer code PLAXIS with a strain "hardening-soil" model (Vermeer and Brinkgreve, 1998) to develop abutment backbone curves and cyclic unloading-reloading rules (Figure 7a,b) for both the MRO and PSO (a 39^o skew angle was used for PSO).

The behavior of the abutment shear keys in the transverse direction was developed based on a prior Caltrans-UCSD field experiment dataset (Bozorgzadeh et al., 2006, Shamsabadi A, 2007). The nonlinear backbone curve was scaled to produce the structural shear-key capacity of the abutment as a function of displacement between bridge deck and abutment pile-cap (Figure 7b). At the tail-end of the curve, a fourth segment was added to account for the tangential component of the abutment-backfill passive capacity due to deck rotation and the passive capacity contribution of the exterior embankment soil.

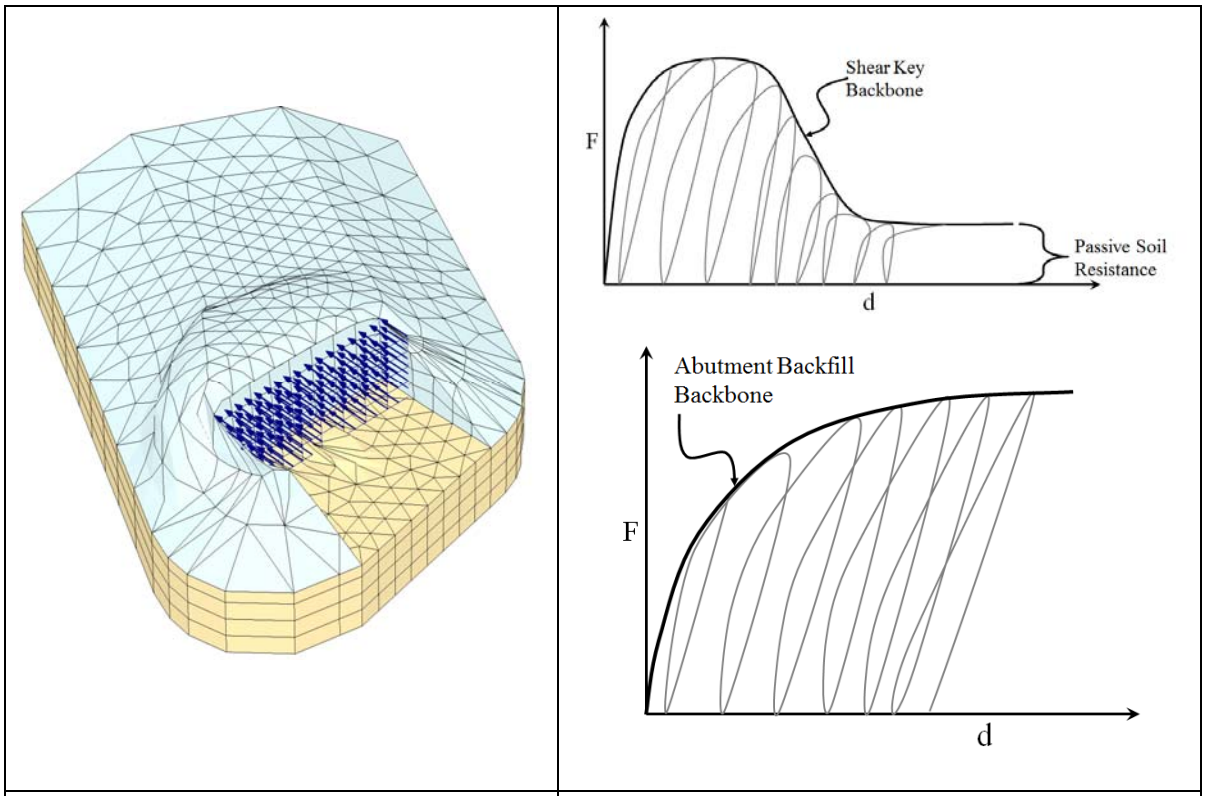

(a) 3D abutment-embankment FEM mesh with the PLAXIS "Hardening-Soil" model.	(b) Transverse and longitudinal backbone and hysteretic cyclic loading-unloading curves.

Figure 7. Ingredients used in modeling the abutment systems.

The hysteretic behavior of the backbone curves both in transverse and longitudinal directions were modeled using a multi-linear plasticity model with the tension side of the curve set to zero. The transverse shears keys were modeled using a single spring attached at each corner of the abutment. The longitudinal abutment-backfill was modeled by a series of nonlinear link elements distributed along each abutment backwall in the bridge global models as shown in Figure 8.

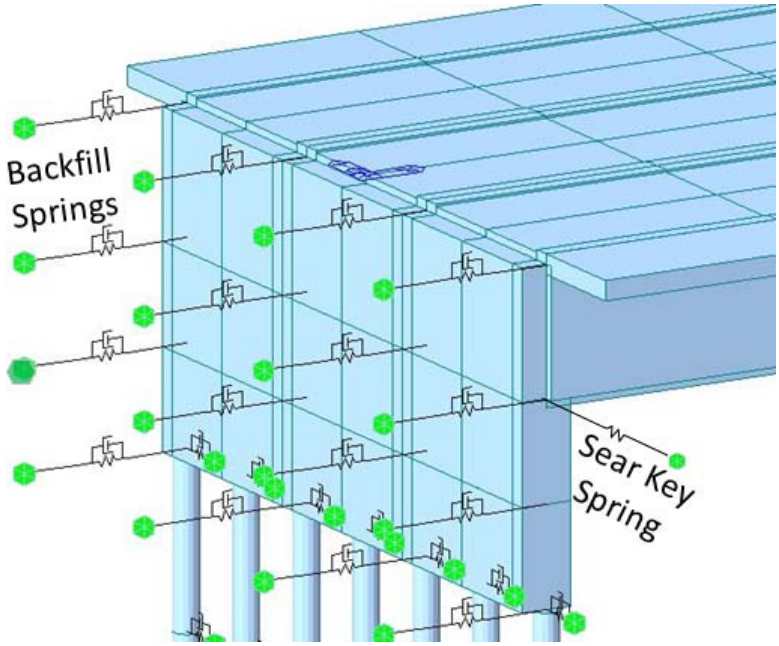

Figure 8. Distributed longitudinal and transverse abutment springs in the bridge models.

The support provided by the west abutment of PSO was modeled using a friction isolator to simulate the neoprene pad, and to decouple the superstructure and abutment backwall from the pile-cap. The isolator is fixed in the vertical direction only. The support provided by the east abutment is fixed to the pile-cap.

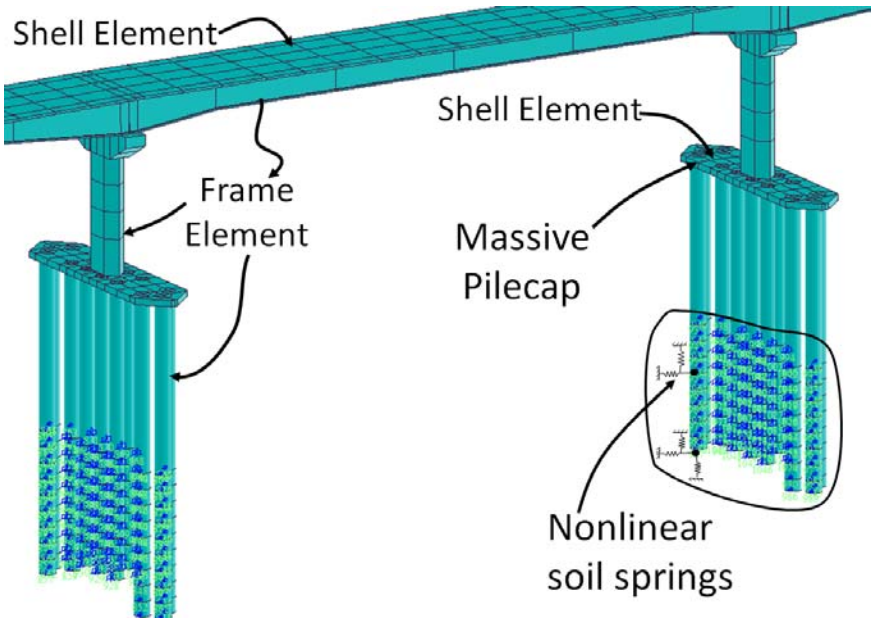

Figure 9. The nonlinear soil springs used in the finite element model of the SCB.

The pile foundations were modeled as beam elements with depth-varying nonlinear springs to represent the interaction between the piles and surrounding soil. Figure 9 displays a close-up view of the global bridge model for of Piers 8 and 9 for the SCB. The fully three-dimensional nonlinear model includes all structural components, foundation components and three-component nonlinear soil support springs. The nonlinear soil springs (Matlock 1970; API 1993) were developed using site-specific geotechnical data (CSMIP, 2012). The soil springs are not only nonlinear but also inelastic upon unloading to allow for hysteretic behavior of the soil. Because the pile caps are massive, the seismic response of the foundations to the earthquake has been found to be an important factor when matching the response of the 3D global model with the recorded seismic response of the bridge.

Input Motions

For dynamic analyses of the MRO, the recorded free-field accelerations from the April 4, 2010 Baja California earthquake were used as the input motions (CGS Station 01336). For PSO, input motions were the free-field records of the 1992 Cape Mendocino/Petrolia earthquake (CGS Station 89324). For the Samoa Channel Bridge, free-field accelerations from the magnitude 6.5 January 2010, Ferndale Area earthquake were used (CGS Station 89686). These acceleration records were obtained from the Center for Engineering Strong Motion Data (CESMD) website, which provides public access to acceleration records from a variety of seismic networks (www.strongmotioncenter.org).

Representative Results

On April 2, 2010, the Caltrans Office of Earthquake Engineering and researchers from University of British Colombia (UBC) collected ambient vibration data from various locations on MRO. Those data were subsequently to for estimated the mode shapes and the natural frequencies for the bridge. The modal data calculated using the finite element model versus those extracted from recorded ambient vibration records are shown in Figure 10.

While the various further refinements can be iteratively made to the model, the agreement between the two sets of modal properties is already observed to be remarkably well. This finite element model was subsequently used to predict the displacement time histories obtained from the earthquake acceleration records to further validate the finite element model. Transverse and longitudinal displacements at a representative location on MRO (Channels 9, and 27) are shown on Figure 11, where, again, the agreement between the actual (recorded) and predicted displacements are observed to be excellent for this two-span ordinary bridge.

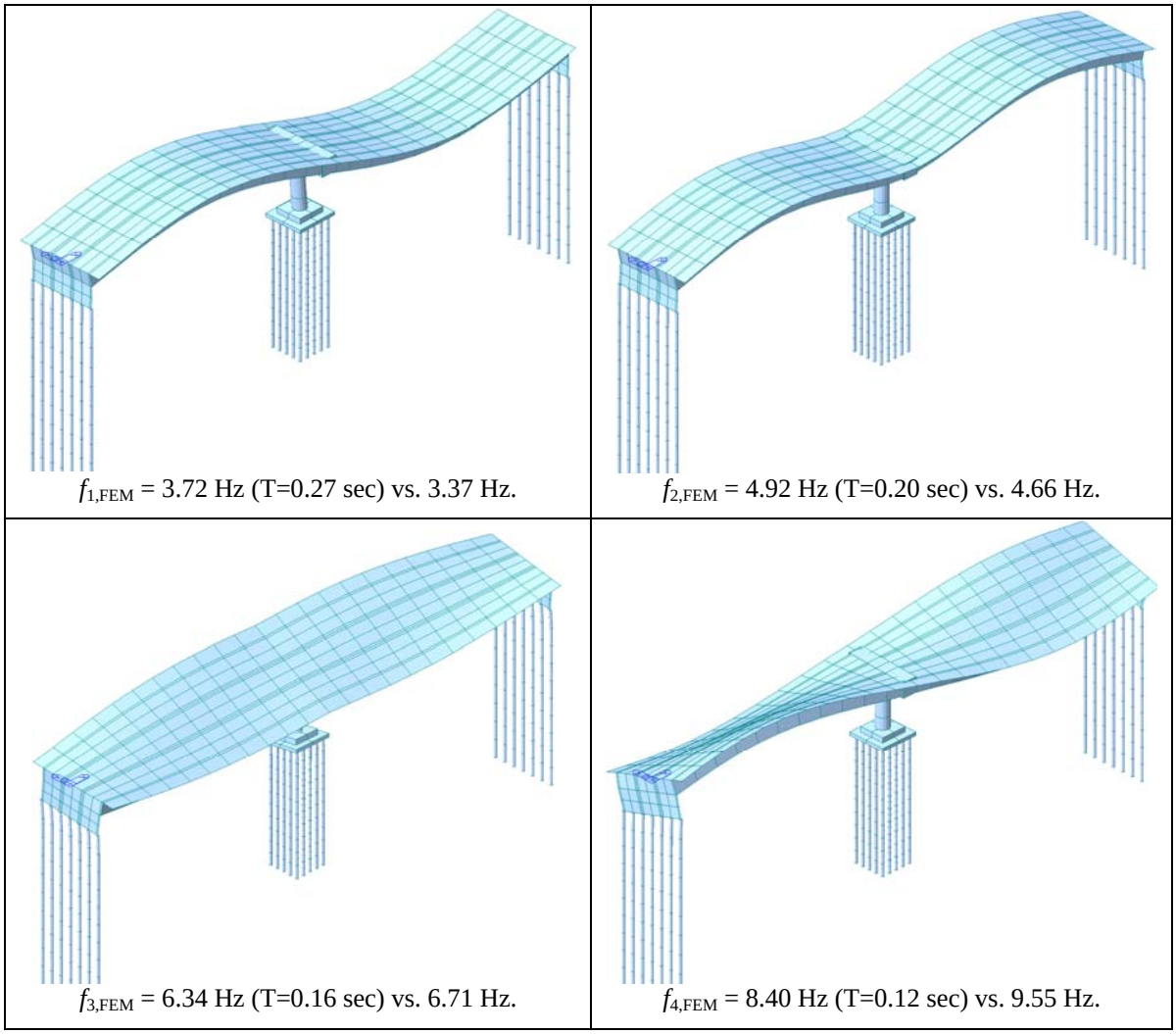

Figure 10. Mode shapes and natural frequencies of the Meloland Road Overcrossing obtained from the initial finite element model versus those extracted from ambient vibration data.

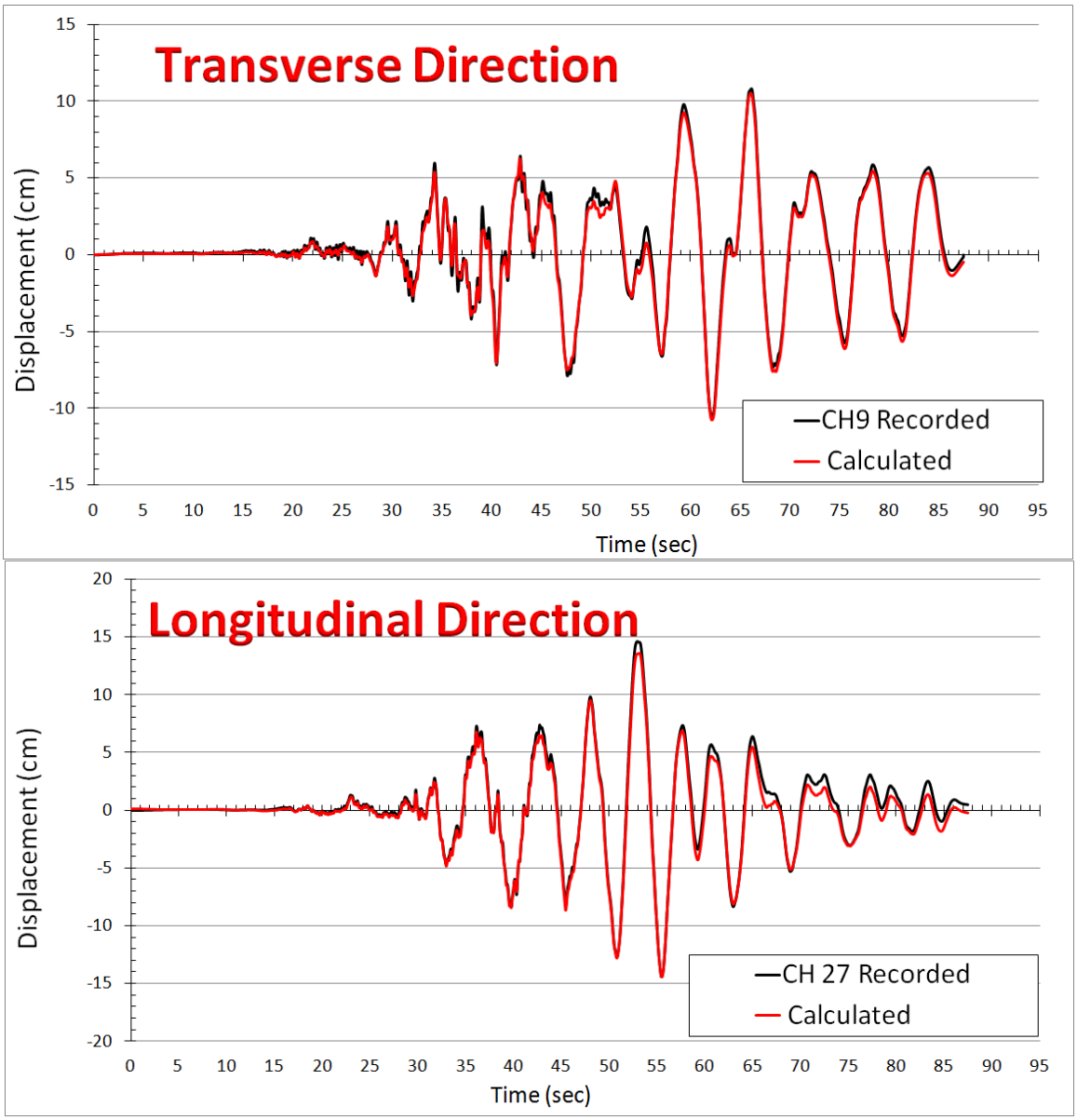

Figure 11. Computed and recorded displacements for the Meloland Road Overcrossing.

The calculated mode shapes and natural frequencies for the Painter Street Overpass are shown in Figure 12. Unlike MRO, we did not have ambient data for the PSO. Therefore, the finite element model was directly used to predict the displacement time histories obtained from earthquake acceleration records for model validation. Transverse and longitudinal displacements at a representative location on PSO (Channels 7, and 11) are shown on Figure 13. Again, the agreement between the actual (recorded) and predicted displacements is observed to be excellent for this two-span ordinary bridge that has a skew abutment. While the considered earthquake motions—*viz.*, recorded motions due to the 1992 Cape Mendocino/Petrolia earthquake—were not severe enough to induce inelastic/permanent deformations, the aforementioned agreement between the predicted and measured responses validate—albeit indirectly—the elastic loading/unloading portions of the abutment-backfill interaction macroelement besides the model of the super-superstructure.

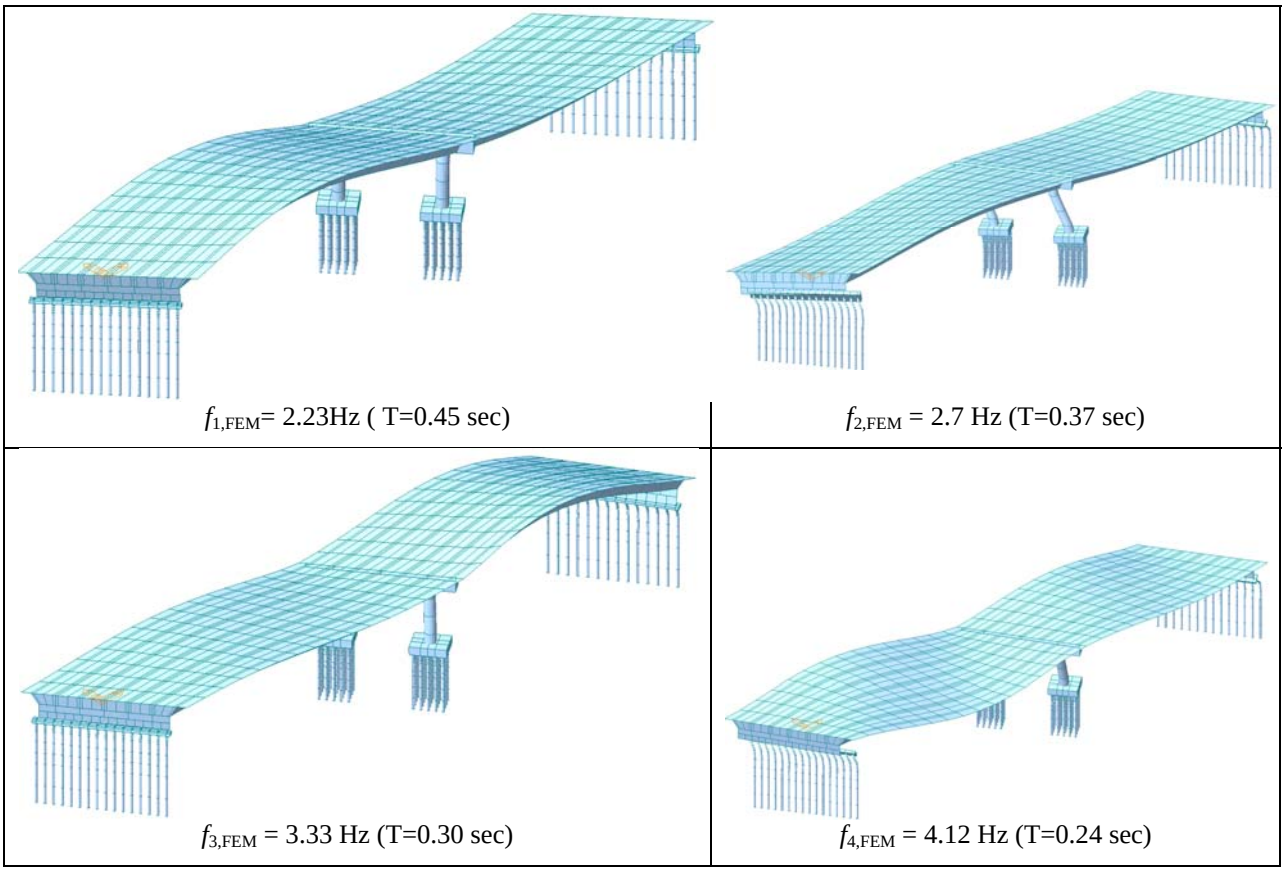

Figure 12. Mode shapes and natural frequencies of the Painter Street Overpass obtained using the initial finite element model.

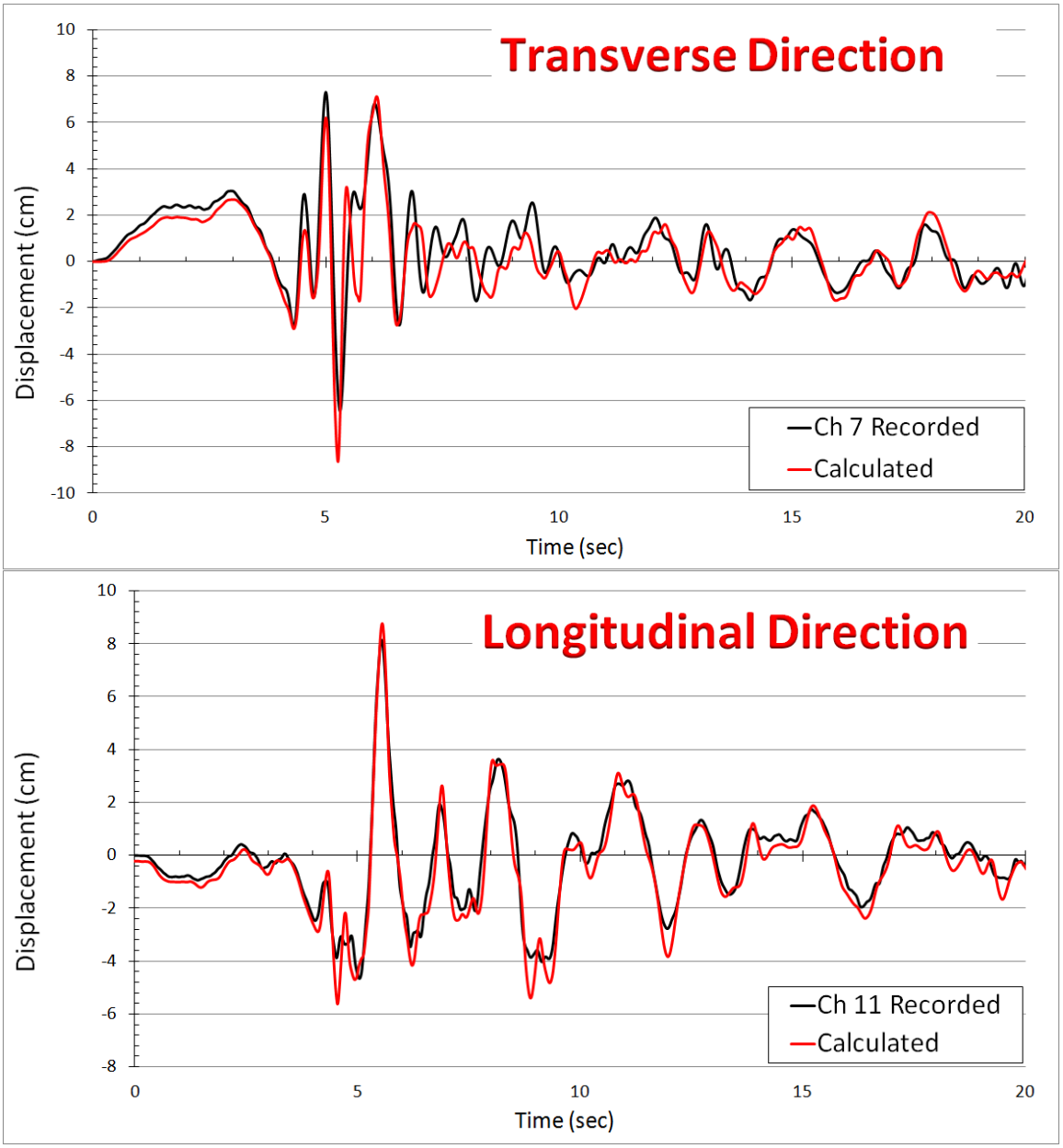

Figure 13. Computed and recorded displacements for the Painter Street Overpass.

The calculated transverse and longitudinal modal data for the Samoa Channel Bridge are shown in Figure 14 (only the first two modes are presented here, for brevity). Unlike the ordinary bridges, the SCB model required multiple iterations from the initial finite element model so that the computed motions matched the recorded motions. The key ingredients in these model-updating studies were the use of cracked section stiffness values for the superstructure elements, the correct values for the mass of the pile caps, and the pile-foundations' lateral stiffnesses. Details of these iterative model-updating studies are omitted for brevity, and may be found in (Shamsabadi et al., 2012). The updated finite element models ultimately displayed very

good agreement with the earthquake-recorded motions. Representative results (Channels 10 and 11) are shown in Figure 15.

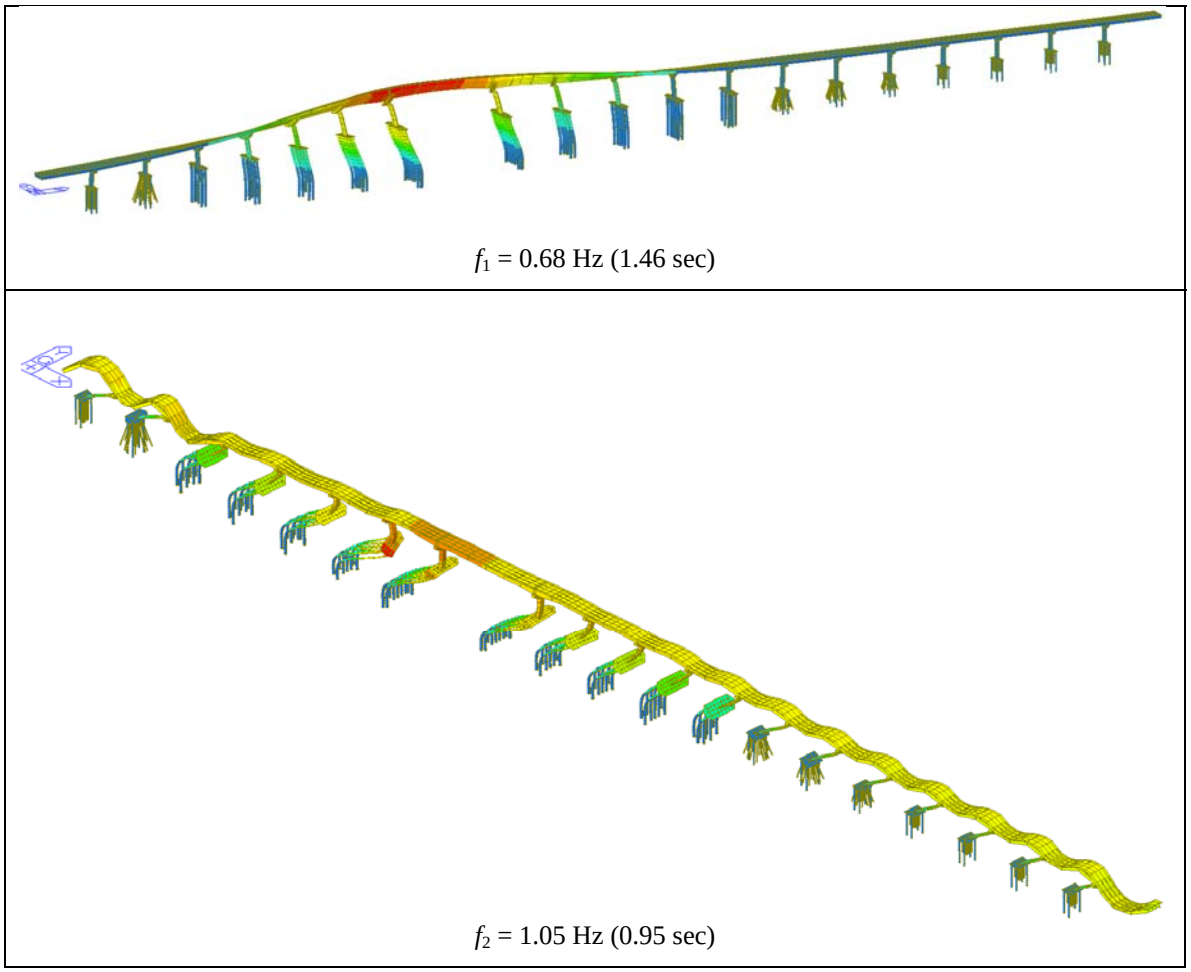

Figure 14. The first two modes of the Samoa Channel Bridge computed using *Midas Civil*.

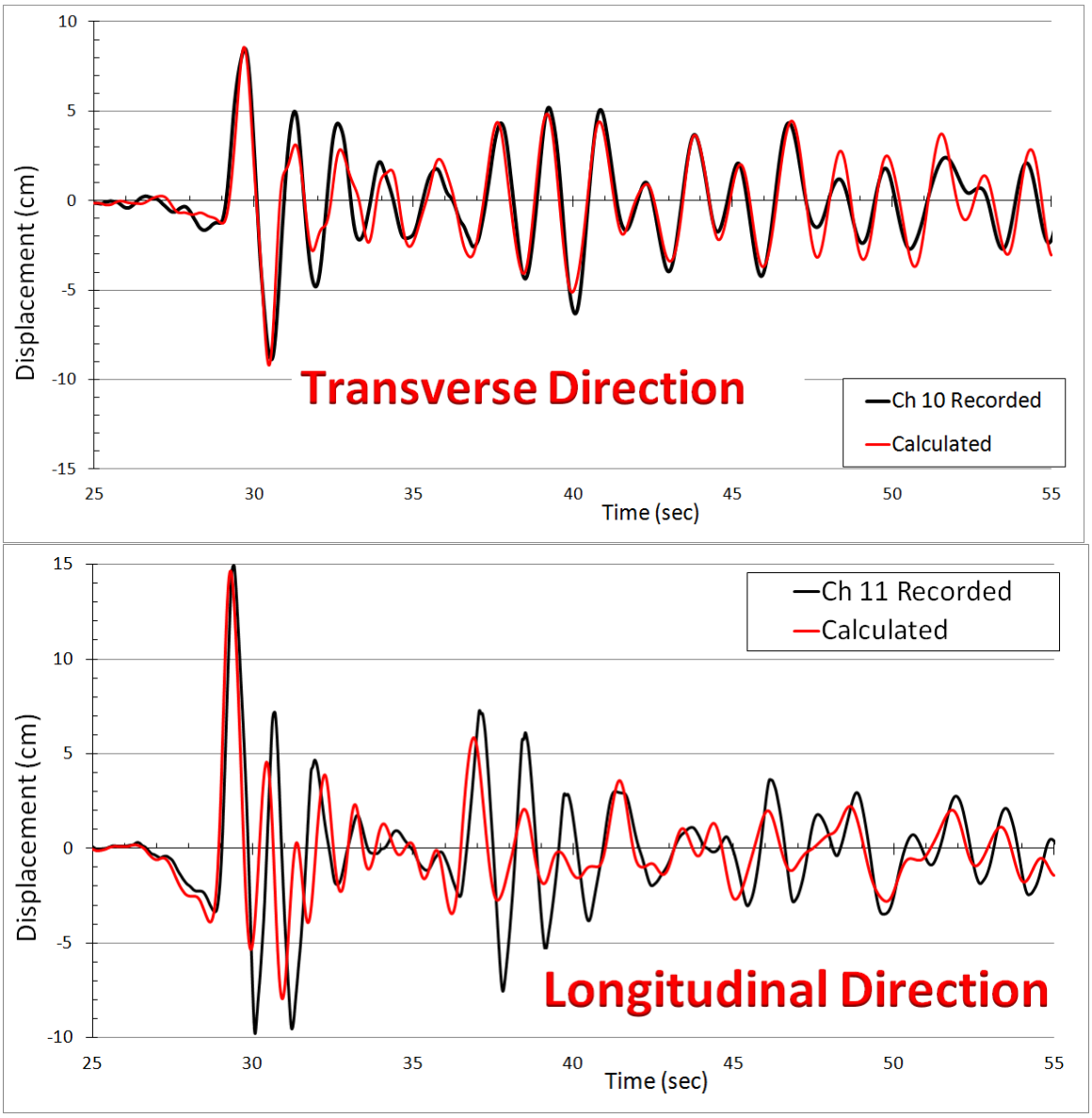

Figure 15. Computed and recorded displacements for the Samoa Channel Bridge.

Conclusions and Recommendation for Future Studies

The ability of finite element models created from structural drawings and geotechnical data in predicting the response of bridges during strong motion events were explored. To this end, three instrumented bridges that are representative of California's bridge inventory were selected. Two of the bridges were ordinary bridges one of which has an abutment with a large (39^{o}) skew angle. The other bridge was a long-span non-ordinary bridge.

Three-dimensional detailed finite element models were developed for the three bridges, which were constructed and analyzed using the *Midas Civil* computer program. These models featured nonlinear/inelastic macroelements that represented the soil-structure interaction at the abutments and pile foundations, as well as the behavior of abutment shear keys. The passive

cyclic response of backfill soils for skew abutments that were used in the macroelements were calibrated using high-fidelity three-dimensional continuum finite element models developed and analyzed using PLAXIS computer program.

The results obtained for the all of the bridges studied suggested that—provided that the abutment and pile foundations are accurately modeled, the finite element models could predict the response observed in strong—albeit non-damaging—earthquakes. The calibration of the finite element model for the long-span bridge was found more challenging, and required more careful consideration of the superstructure properties in comparison to the ordinary bridges. Further studies are needed to clearly delineate the influence of soil-foundation-structure effects in both ordinary and non-ordinary bridges. This can be achieved through parametric studies using validated/calibrated finite element models such as those presented in this study. Moreover, studies are required to investigate the expected behavior of these (and similar) bridges under damaging earthquakes in order to determine the influence of soil-structure effects on the seismic demands that these bridges will be experience.

References

API—American Petroleum Institute (1993), *Recommended Practice and Planning, Designing, and Constructing Fixed Offshore Platforms – Working Stress Design (RP 2A-WSD*), Washington, D.C.

Bozorgzadeh A, Megally S, Restrepo JI, Ashford SA (2006). Capacity evaluation of exterior sacrificial shear keys of bridge abutments, *ASCE Journal of Bridge Engineering*, 11(5): 555-565.

Caltrans SDC (2013). *Caltrans Seismic Design Criteria, v.1.7*, April 2013.

CSMIP (2012). *California Strong Motion Instrumentation Program*, http://www.conservation.ca.gov/cgs/smip.

Hipley P, Huang M (1997). Caltrans/CSMIP bridge strong motion instrumentation. *Second National Seismic Conference on Bridge and Highways*, Sacramento, California.

Matlock, H. (1970), "Correlation for Design of Laterally Loaded Piles in Soft Clay," 2nd Annual Offshore Technology Conference, Paper No. 1204.

Mualchin, L (1996). *A Technical Report to Accompany the Caltrans Seismic Hazard Map 1996 (Based on Maximum Credible Earthquakes)*, California Department of Transportation, Engineering Service Center, Office of Earthquake Engineering, Sacramento, CA 95816.

MIDASoft (2010). *Midas Civil: Integrated Solution System for Bridge and Civil Engineering*, MIDAS Information Technology Co., Ltd. (www.MidasUser.com)

Shamsabadi A. Three–dimensional nonlinear seismic soil–abutment–foundation-structure interaction analysis of skewed bridges, Ph.D. thesis, Department of Civil and Environmental Engineering, University of Southern California (USC), Los Angeles, CA (2007).

Shamsabadi A, Mitchell S, Hipley P, Zha J, Omrani R, Ghahari SF, Abazarsa F, Taciroglu E (2012). Assessment of seismic soil-foundation-structure interaction analysis procedures for

long-span bridges using recorded strong motion data, *Proc. 10th Int. Congress on Advances in Civil Engineering*, Ankara, Turkey, 17-19 October.

Vermeer PA, Brinkgreve RBJ (1998). *PLAXIS: Finite-element code for soil and rock analyses* (version 7.1), Balkema, Rotterdam, The Netherlands.

INSTRUMENTATION REQUIREMENTS FOR TALL BUILDINGS PER THE LOS ANGELES TALL BUILDINGS STRUCTURAL DESIGN COUNCIL 2011 ALTERNATIVE ANALYSIS AND DESIGN PROCEDURE

Farzad Naeim

John A. Martin & Associates, Inc.
Los Angeles, California

Abstract

Seismic instrumentation can provide valuable insight into performance of structures and help us assess the validity, or lack thereof, of assumptions used and methods applied. It is precisely for this reason that the Los Angeles Tall Building Structural Design Council (LATBSDC) mandates extensive seismic instrumentation of tall buildings designed according to the provisions of its alternative analysis and design procedure that has been adopted by the Department of Building and Safety of the city of Los Angeles. This paper describes 2011 LATBSDC seismic instrumentation requirements and provides an example of their application.

Introduction

Performance based design of tall buildings is in its early stages of application and development. The funding necessary to experimentally validate performance of various components and systems utilized in tall buildings probably will not be available for a long time. Analytical simulations, as detailed and elaborate as they may be, cannot replace the need for experimental results and observed performances. It is imperative that we maximize every opportunity at our disposal to learn as much we can and as quickly as possible about performance of tall buildings designed according to these procedures during major earthquakes so that we can improve our design practices and produce more efficient and safe buildings.

Seismic instrumentation can provide valuable insight into performance of structures and help us assess the validity, or lack thereof, of assumptions used and methods applied. It is precisely for this reason that the 2011 LATBSDC mandates extensive seismic instrumentation of tall buildings designed according to its provisions.

A Brief History of the LATBSDC Document

LATBSDC was formed was formed in 1988 to provide a forum for the discussion of issues relating to the design of tall buildings. The Council seeks to advance state-of-the-art structural design through interaction with other professional organizations, building departments, and university researchers as well as recognize significant contributions to the structural design of tall buildings. LATBSDC is a nonprofit California corporation whose members are those individuals who have demonstrated exceptional professional accomplishments in the structural design of tall buildings. The annual meeting of the Council represents a program for engineers,

architects, contractors, building Official and students. The annual meeting program includes research reports on areas of emerging importance, case studies of current structural designs, and consensus documents by the membership on contemporary design issues. LATBSDC criteria documents are published under a unanimous consent requirement, which makes publication of them laborious process.

The first criteria document published by LATBSDC in the late 1980s covered the topic of application of site-specific design spectra and dynamic analysis, which were hot topics during that time. The first performance-based alternative analysis and design criteria document was published in 2005 and has been since updated every three years. The current document is the 2011 edition. Every edition of LATBSDC has contained mandatory extensive instrumentation requirements.

Why a Document on Tall Buildings?

A tall building represents a significant investment of human and material resources and may be occupied by hundreds, if not thousands, of occupants. Building codes' reaction to this fact, at least in the United States, has been twofold. First, application of certain structural systems has been limited to certain heights and second, buildings with high occupancy are required to be designed for higher lateral forces via the use of an importance factor (I) which is taken as unity for ordinary buildings. Numerous studies and evaluations [1, 2, 3] have shown that it is possible and economical to design tall buildings as safe or safer than code designed buildings while ignoring code imposed height limits. Furthermore, even a strict imposition of arbitrary premiums on elastic design forces may not do much to address the issues of damage and potential collapse, which are inherently inelastic and nonlinear.

Prescriptive codes by in large contain a collection of empirical rules and experimental results that have evolved over many years of practice and in a sense provide a "one size fits all" approach to seismic design. Tall buildings as small class of specialized structures will perform better during earthquakes if special attention is afforded to their individual seismic behavior and engineers are provided with ample opportunities to explore new frontiers, utilize state of the art technologies and latest research results in order to improve the performance, feasibility, and constructability of their designs.

There are other reasons why performance-based design of tall buildings and production of documents to guide such design has gathered momentum [4]. The overwhelming majority of construction in United States and worldwide consists of low-rise buildings. According to Portland Cement Association [5], buildings with one to three floors represent 93% of floor area of construction in United States while buildings with 14 floors or more represent only 1% of floor area of construction. With so much of the construction effort concentrated on low-rise construction it is not surprising that the code writers have these buildings in mind when crafting code provisions. As a result, one can often find a provision or two in the building code that either do not have relevance to tall building design, or even worse, do not make much sense for design of tall buildings. For example, until just a few years ago, the Los Angeles Building Code had a very peculiar drift design provision [6] requiring story drift not to exceed $0.020/T^{1/3}$ where T is the fundamental vibration period of the building. This provision, which was later retracted,

probably did not have a serious effect on design of low-rise buildings but was a huge straightjacket for design of tall buildings with long vibration periods.

LATBSDC was the first professional group in the United States to publish a performance-based alternative seismic analysis and design criteria specifically intended for tall buildings [7, 8, 9] and to obtain approval by the city's building officials in 2010 for its use in lieu of using prescriptive code provisions for buildings of all types and heights.

LATBSDC Building Performance Objectives

The 2011 edition of LATBSDC criteria [9] sets two performance objectives: (1) serviceable behavior when subjected to frequent earthquakes defined as events having a 50% probability of being exceeded in 30 years (43 year return period); and (2) a low probability of collapse under extremely rare earthquakes defined as events having a 2% probability of being exceeded in 50 years (2,475 year return period) with a deterministic cap. This earthquake is the Maximum Considered Earthquake (MCE) as defined by ASCE 7-05 [10].

LATBSDC Instrumentation Requirements

2011 LATBSDC seismic instrumentation requirements are contained in Section 5 of that document which states: buildings analyzed and designed according to the provisions of this document shall be furnished with seismic instrumentation as described therein.

Instrumentation Objectives

The primary objective of structural monitoring is to improve safety and reliability of building systems by providing data to improve computer modeling and enable damage detection for post-event condition assessment. Given the spectrum of structural systems used and response quantities of interest (acceleration, displacement, strain, rotation, pressure), the goal of these provisions is to provide practical and flexible requirements for instrumentation to facilitate achieving these broad objectives. The instrumentation used on a given building should be selected to provide the most useful data for post-event condition assessment." It further states that the "recent advances in real-time structural health monitoring and near real-time damage detection may be extremely useful in rapid evaluation of status of the building after an event and deciding whether the building is fit for continued occupancy or not" [11].

Instrumentation Plan and Review

An instrumentation plan shall be prepared by the EOR and submitted to SPRP and Building Official for review and approval. SPRP Approved instrumentation plans shall be marked accordingly on the structural drawings. If the building is intended to be included in the inventory of buildings monitored by the California Geologic Survey (CGS) then the recorders and accelerometers must be of a type approved by CGS.

Minimum Number of Channels

The building shall be provided with minimum instrumentation as specified in the document (see Table 1 below). The minimum number of required channels maybe increased at the discretion of the peer review team and building officials. Please note that for reliable real-time structural health monitoring and performance evaluations a substantially larger number of channels may be necessary [11]. Each channel corresponds to a single response quantity of interest (e.g., unidirectional floor acceleration, interstory displacement, etc.).

Table 1. Minimum tall building instrumentation levels

Number of Stories Above Ground	Minimum Number of Sensors
10 – 20	15
20 – 30	21
30 – 50	24
> 50	30

Distribution

The distribution or layout of the proposed instrumentation shall be logically designed to monitor the most meaningful quantities. The sensors shall be located at key measurement locations in the building as appropriate for the measurement objectives and sensor types. The sensors shall be connected by dedicated cabling to one or more central recorders, interconnected for common time and triggering, located in an accessible, protected location with provision for communication.

Installation and Maintenance

The building owner shall install and maintain the instrumentation system and coordinate dissemination of data as necessary with the Building Official

Example Application

The instrumentation requirements of 2011 LATBSDC can be rather easily satisfied by development of simple instrumentation plans which are very similar to CSMIP produced sketches for its instrumented buildings. The owners and engineers of new tall buildings in Los Angeles region are often advised by their peer review panel to contact CSMIP for up to date information and relevant specifications and to enquire whether their instrumented building may become part of the CSMIP database of instrumented buildings.

Several tall buildings designed according to the provisions of the 2011 LATBSDC are in various stages of design and construction. The 34-story 888 Olive, which is currently under construction in downtown Los Angeles, is one example of such buildings. The lateral system for the tower consists of a core shear wall buildings. The tower sits on a podium on its lowest several floors some of which are subterranean and it is flanked by a seismically separated parking structure (Figure 1).

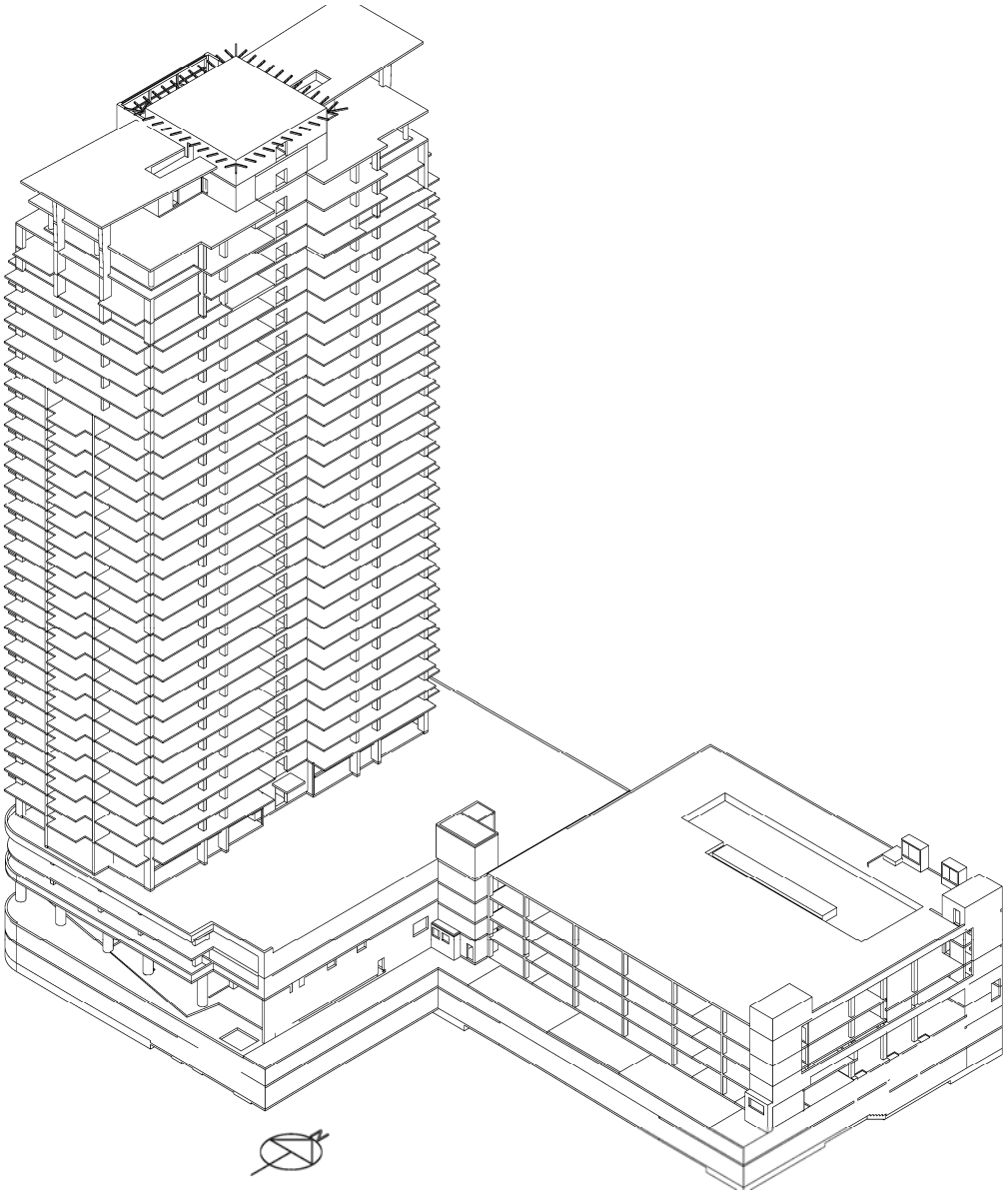

Figure 1. A 3D sketch of the 888 Olive Project with its tower, Podium and the adjacent parking structure (illustration courtesy of Glotman-Simpson and Onni Group).

The building is being instrumented with 24 accelerometers all connected to a central processing unit and once completed will become a part of SMIP database of instrumented buildings. The entire set of instrumentation plans produced for this project is presented in the Appendix of this paper.

Conclusions

Instrumentation is inexpensive and nonintrusive if planned during the design process and implemented during the construction of a tall building. Given the recent advances in sensor technology, now it is possible to install sensors not only to measure accelerations but to measure

and record relative or overall displacements (building tilt), and various stresses and strains throughout the structure. Modern information technology has made real-time or near real-time measurements and remote transmission of sensor data and engineering interpretation of them not only possible, but feasible. Integration of seismic instrumentation with broad building health monitoring which includes monitoring buildings during more frequent events and malfunctions (such as wind storms, fires, floor vibrations, flooding, elevator functions, HVAC problems), may finally produce enough tangible benefits for tall building owners and developers to cause them to willingly and enthusiastically embrace the modest cost of building instrumentation and health monitoring.

Acknowledgment

The author is grateful to Onni Group (developers) and Glotman-Simpson (engineers of record) for the 888 S. Olive project for allowing the author to reproduce the schematic view of the building (Figure 1) and their instrumentation plans (Appendix) as a part of this paper.

References

1. Los Angeles Tall Buildings Structural Design *Council, Proceedings of the 2007 Annual Meeting*, Los Angeles, California. May 2007.
2. Los Angeles Tall Buildings Structural Design *Council, Proceedings of the 2008 Annual Meeting*, Los Angeles, California. May 2008.
3. Los Angeles Tall Buildings Structural Design *Council, Proceedings of the 2009 Annual Meeting*, Los Angeles, California. May 2009.
4. Naeim, F. (2010), *Performance Based Seismic Design of Tall Buildings*, in Earthquake Engineering in Europe, Garevski, M. and Ansal, A. (Eds.), Springer.
5. Portland Cement Association, *Concrete Structural Floor Systems and More*, CD013, 2000.
6. International Conference of Building Officials, *2002 City of Los Angeles Building Code*, Sec. 1630.10.2, Whittier, California.
7. Los Angeles Tall Buildings Structural Design Council (LATBSDC), *An Alternative Procedure for Seismic Analysis and Design of Tall Buildings located in the Los Angeles Region*, 2005 Edition, May 2005.
8. Los Angeles Tall Buildings Structural Design Council (LATBSDC), *An Alternative Procedure for Seismic Analysis and Design of Tall Buildings located in the Los Angeles Region*, 2008 Edition, May 2008.
9. Los Angeles Tall Buildings Structural Design Council (LATBSDC), *An Alternative Procedure for Seismic Analysis and Design of Tall Buildings located in the Los Angeles Region*, 2011 Edition, May 2011.
10. American Society of Civil Engineers (2005), *ASCE 7-05 Minimum Design Loads for Buildings and Other Structures Including Supplement 1*, Reston, VA.
11. Naeim, F. (2011), *Near Real-Time Damage Detection and Performance Evaluation for Buildings – A White Paper*, John A. Martin & Associates, Inc. Report No. 13115-2011, Los Angeles, CA.

APPENDIX – Instrumentation Plans for 888 Olive Tower located in downtown Los Angeles

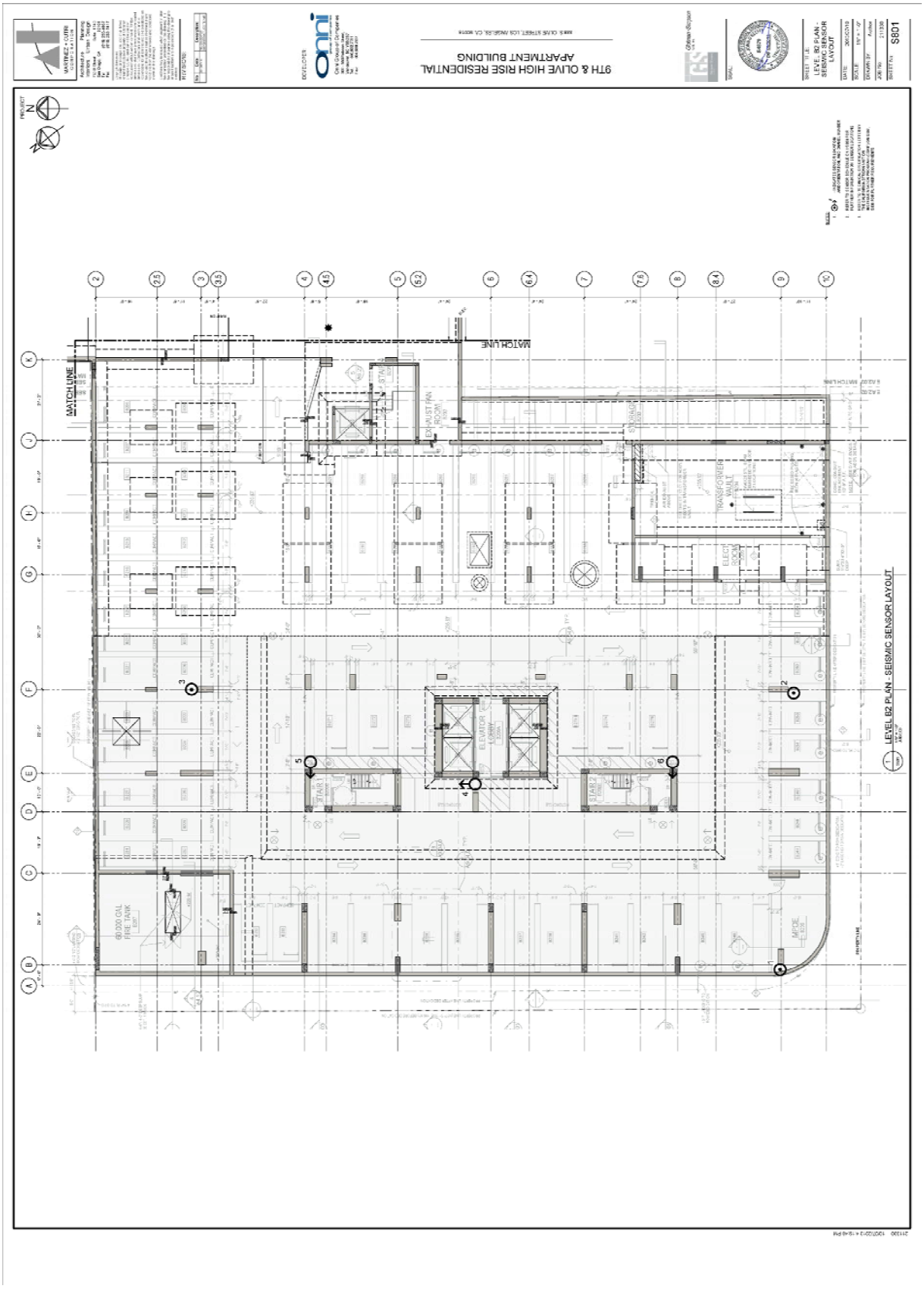
9TH & OLIVE HIGH RISE RESIDENTIAL
APARTMENT BUILDING
LEVEL B2 PLAN - SEISMIC SENSOR LAYOUT
S801
MATCH LINE
LEVEL B2 PLAN - SEISMIC SENSOR LAYOUT

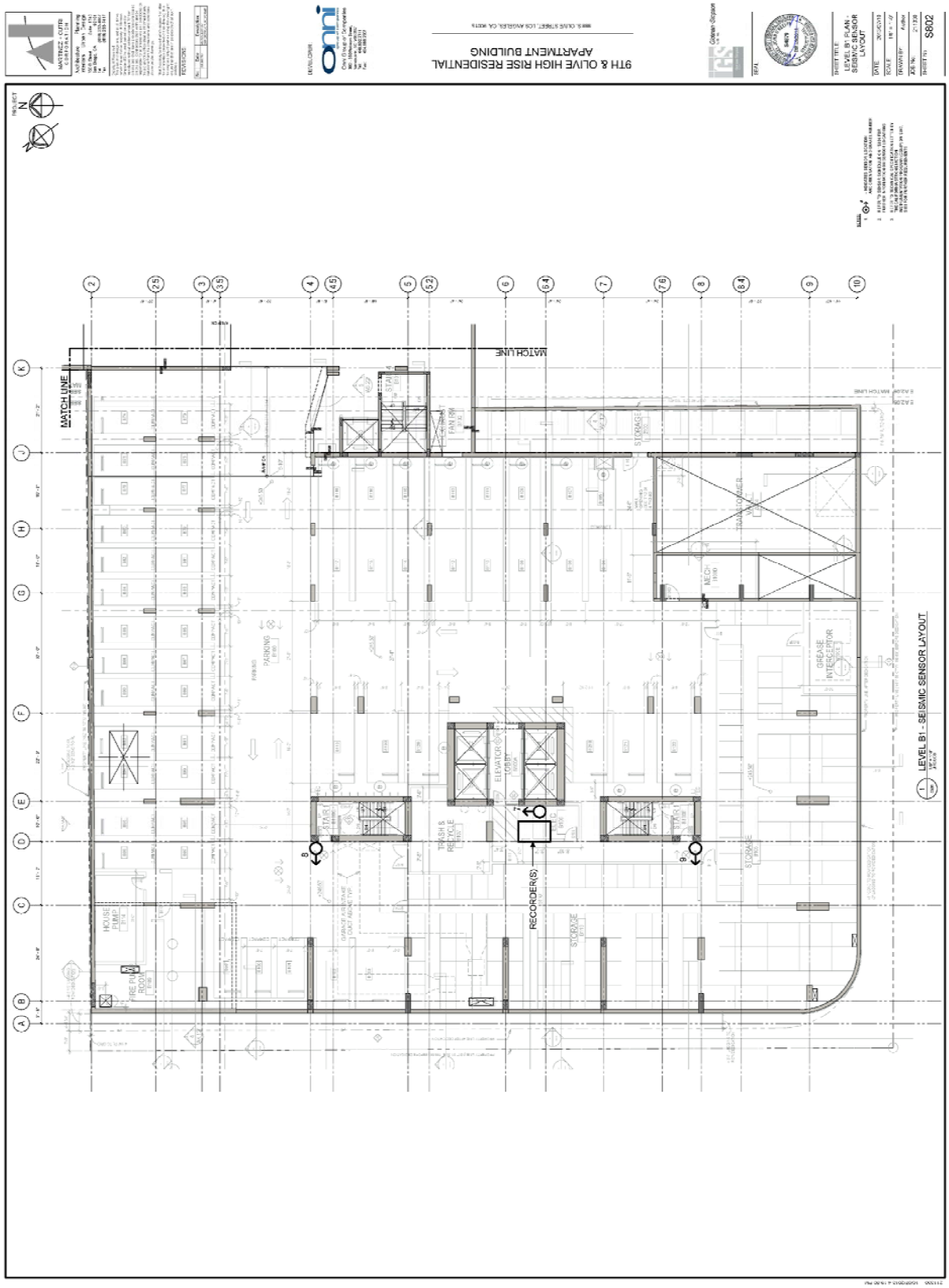
9TH & OLIVE HIGH RISE RESIDENTIAL
APARTMENT BUILDING
LEVEL B1 PLAN - SEISMIC SENSOR LAYOUT
S802
MATCH LINE
RECORDER(S)
LEVEL B1 - SEISMIC SENSOR LAYOUT

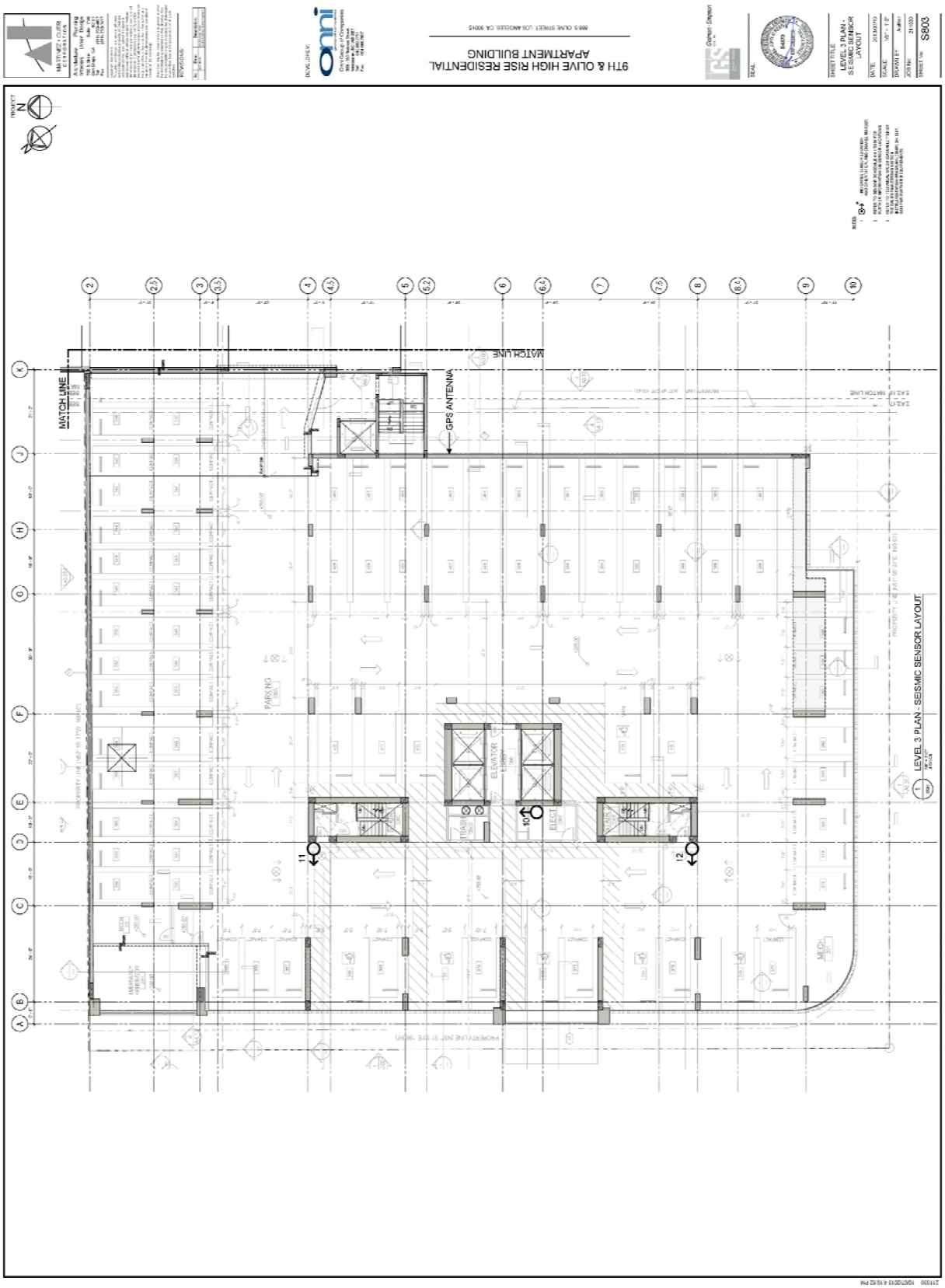
9TH & OLIVE HIGH RISE RESIDENTIAL
APARTMENT BUILDING
LEVEL 3 PLAN - SEISMIC SENSOR LAYOUT
S803
MATCH LINE
GPS ANTENNA
ELEVATOR
PARKING
LEVEL 3 PLAN - SEISMIC SENSOR LAYOUT

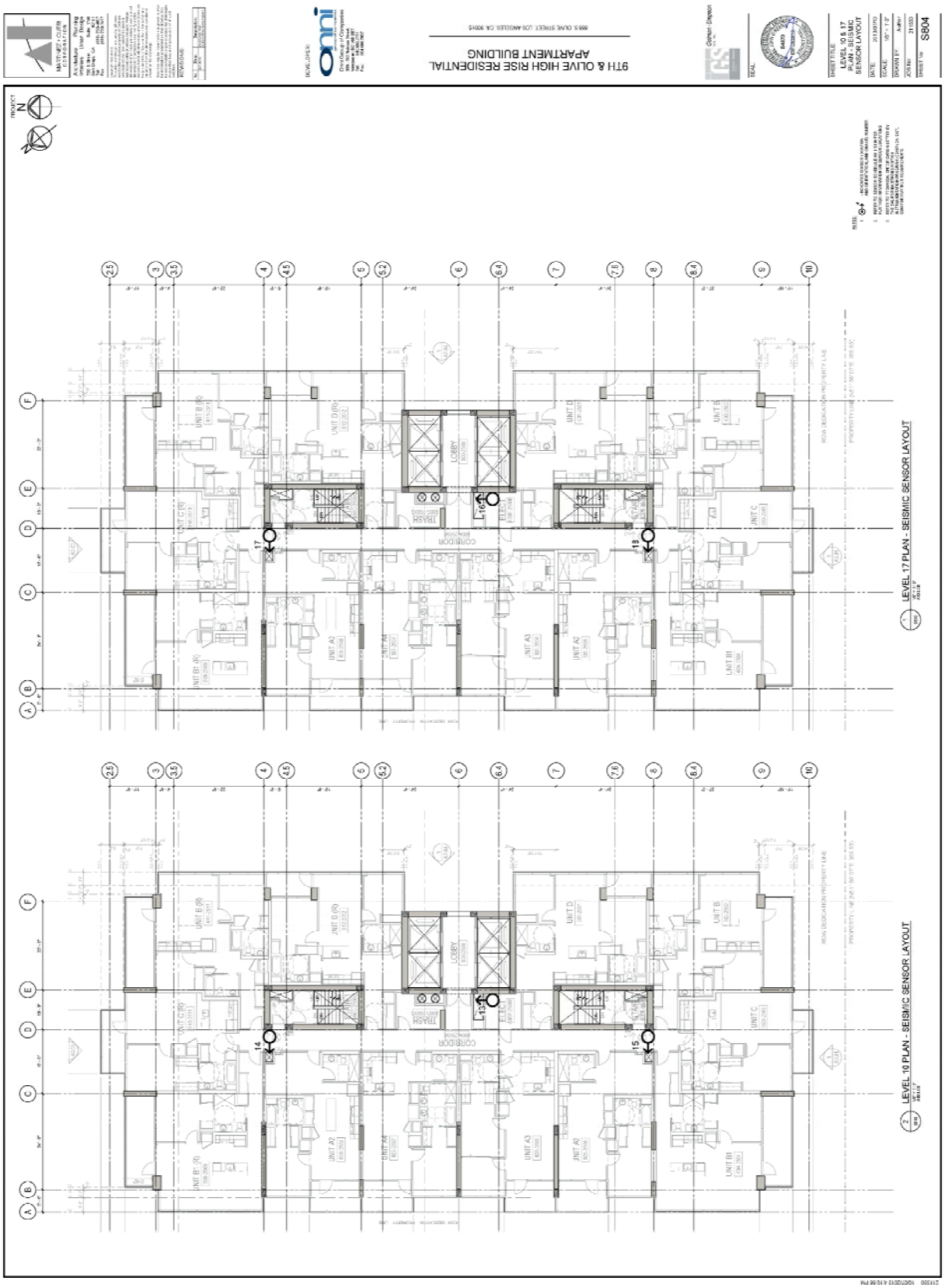
9TH & OLIVE HIGH RISE RESIDENTIAL
APARTMENT BUILDING
LEVEL 17 PLAN - SEISMIC SENSOR LAYOUT
LEVEL 10 PLAN - SEISMIC SENSOR LAYOUT
S804

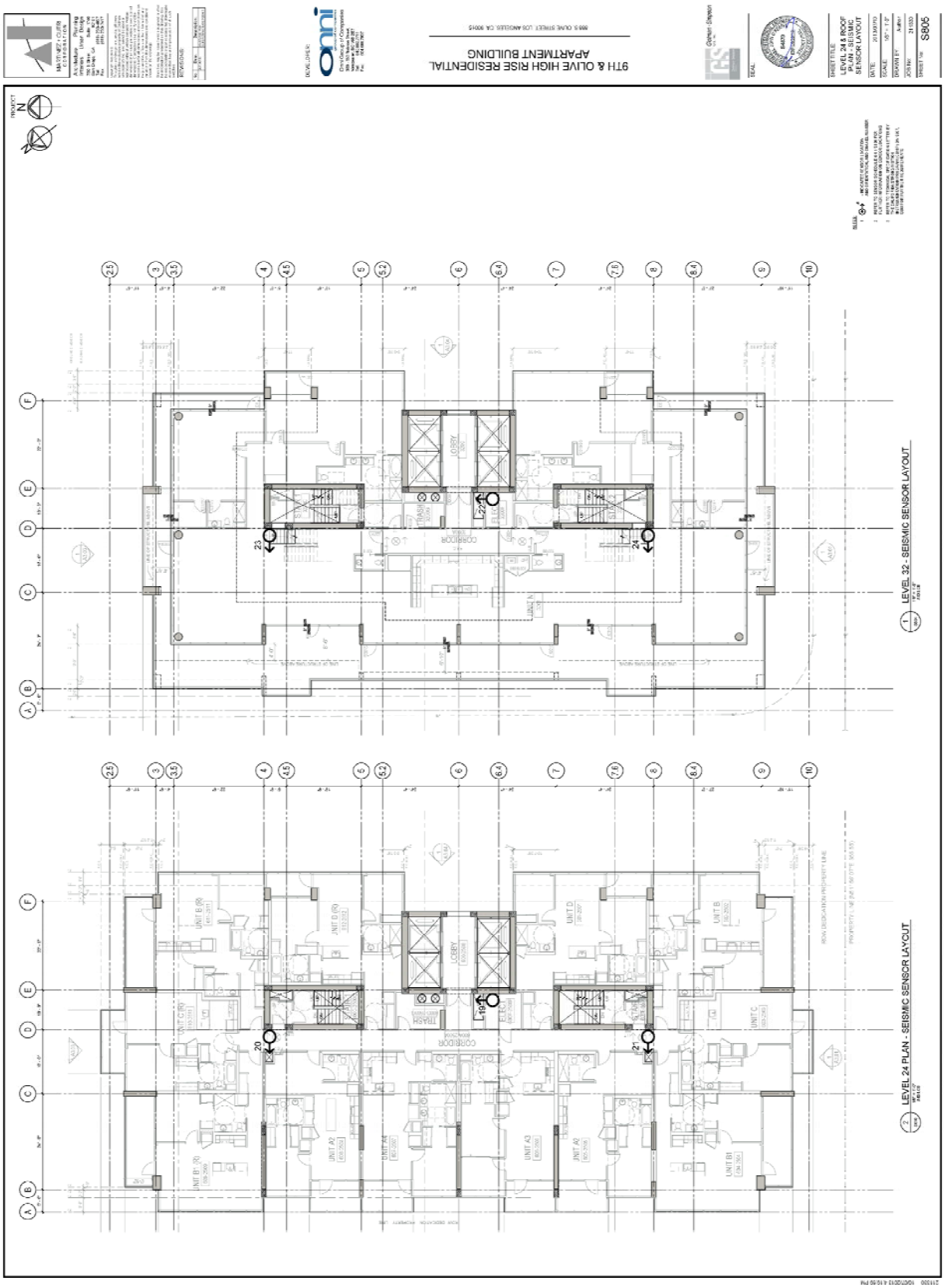
9TH & OLIVE HIGH RISE RESIDENTIAL
APARTMENT BUILDING
LEVEL 24 & ROOF PLAN - SEISMIC SENSOR LAYOUT
S805
LEVEL 32 - SEISMIC SENSOR LAYOUT
LEVEL 24 PLAN - SEISMIC SENSOR LAYOUT

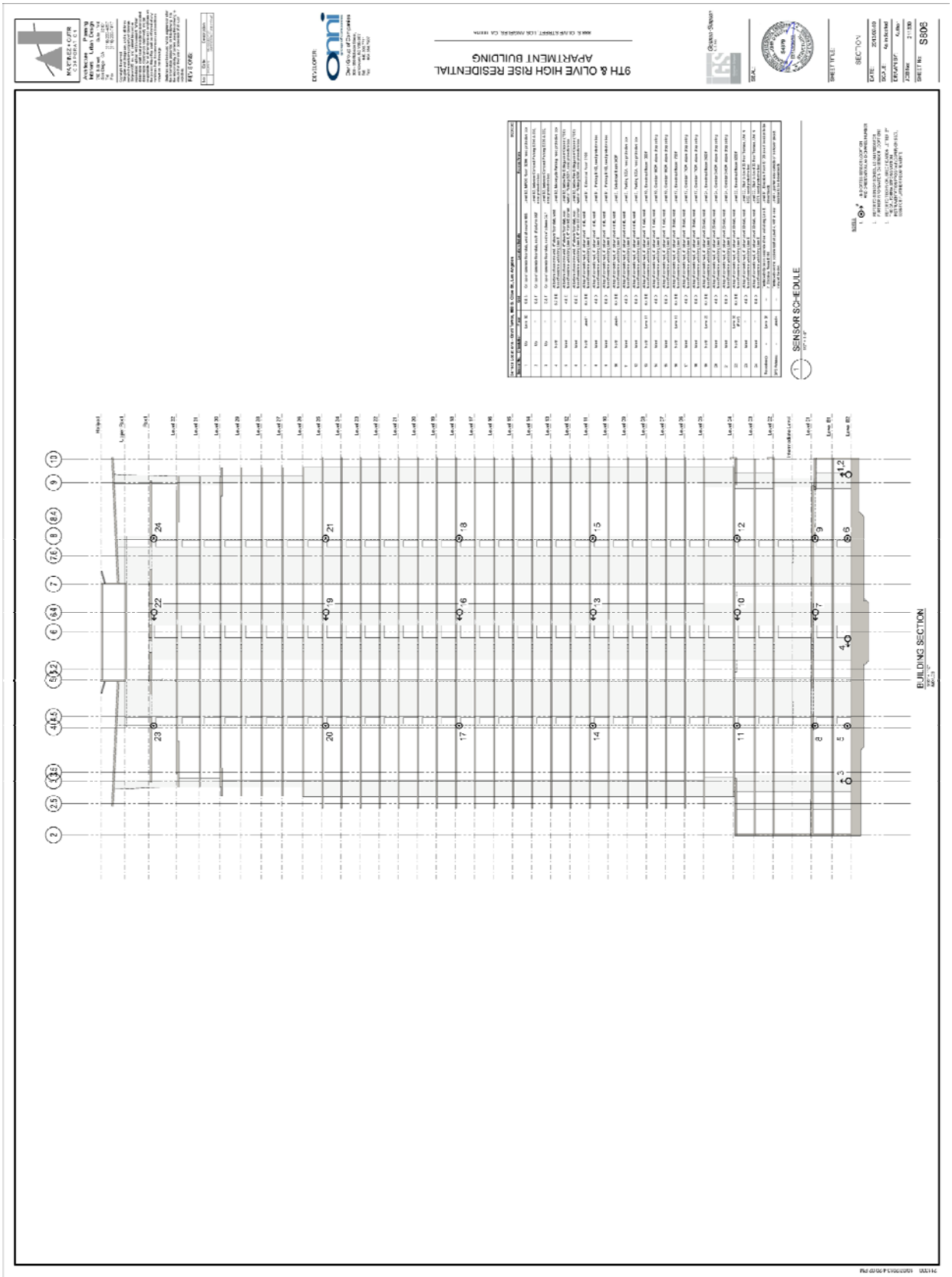
9TH & OLIVE HIGH RISE RESIDENTIAL
APARTMENT BUILDING
SENSOR SCHEDULE
BUILDING SECTION

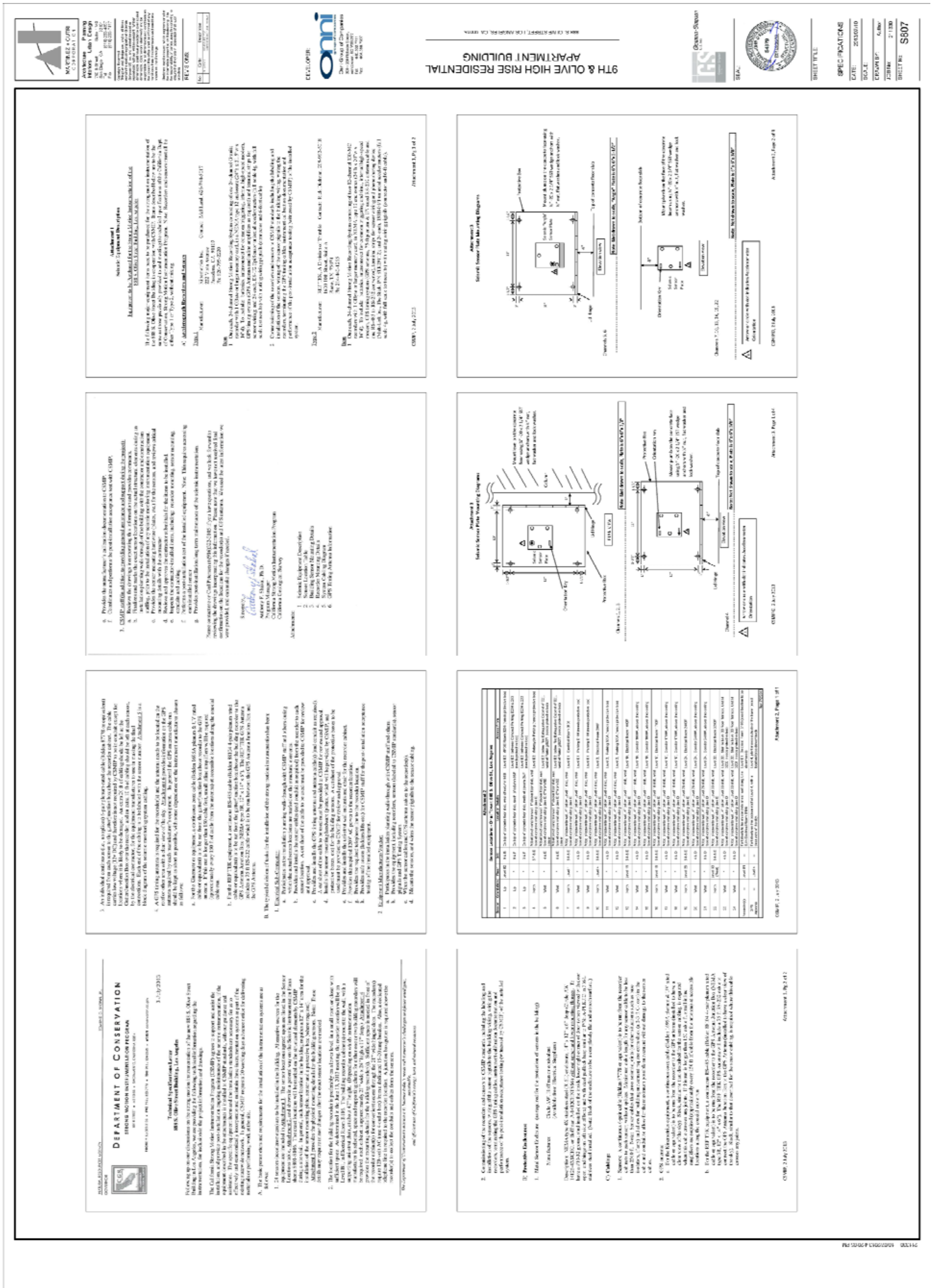
9TH & OLIVE HIGH RISE RESIDENTIAL
APARTMENT BUILDING
SPECIFICATIONS
S807

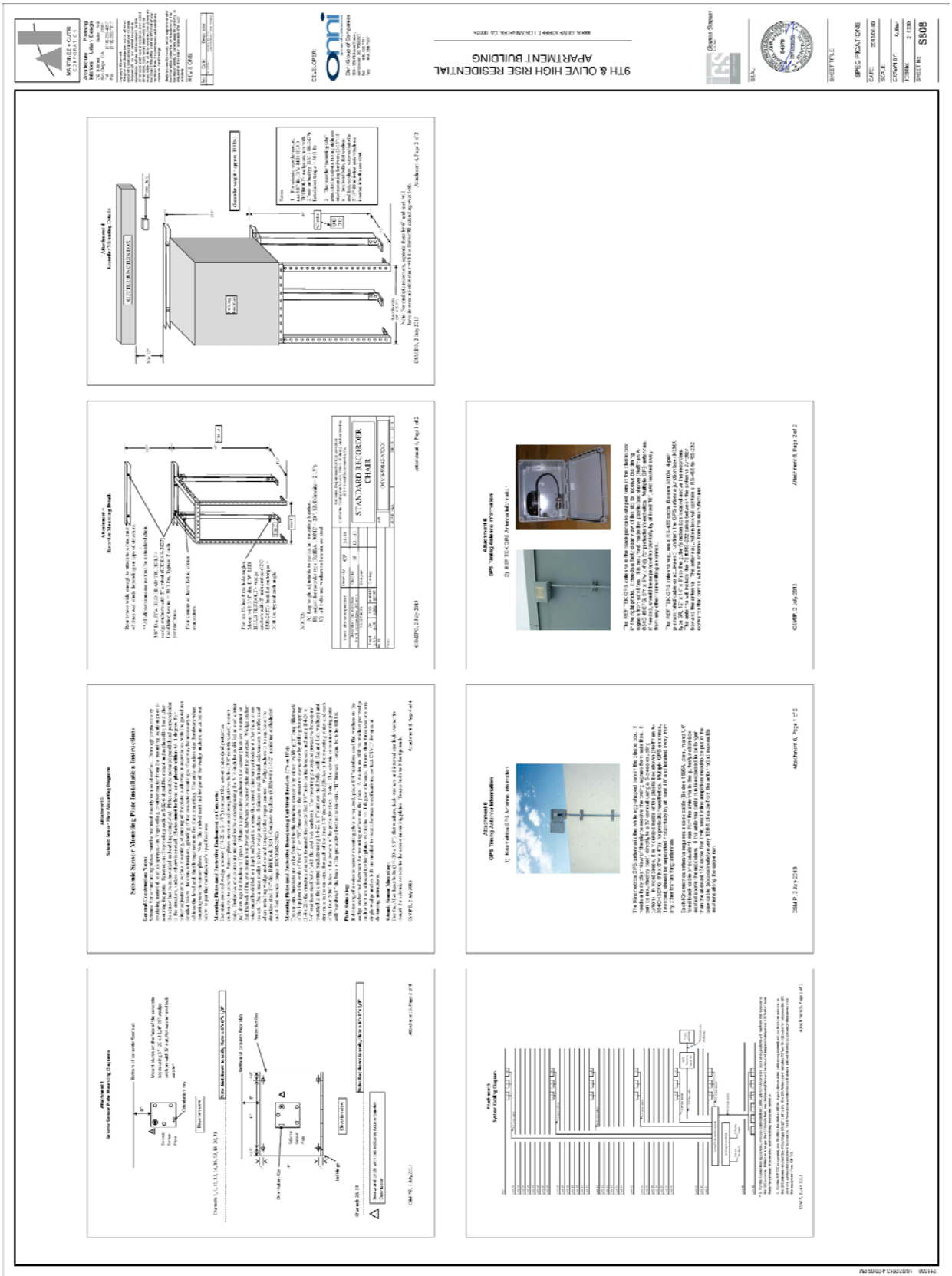

RECENT DEVELOPMENTS AND STATUS OF THE CALIFORNIA STRONG MOTION INSTRUMENTATION PROGRAM

Anthony Shakal and Moh Huang

California Strong Motion Instrumentation Program
California Geological Survey, Sacramento, California

Abstract

This paper reviews the recent accomplishments and current status of the California Strong Motion Instrumental Program. With the completion of the instrumentation of the new San Francisco Oakland Bay Bridge, all major bridges in California will have been instrumented, as well as the BART tube, two tunnels and a new series of hospitals and new geotechnical arrays. New approaches to instrumentation in recent years are discussed. The current state of instrumentation accomplished by the program is summarized.

Introduction

The California Strong Motion Instrumentation Program was started after the 1971 San Fernando earthquake, in which there was significant amount of structural damage and relatively few recordings of strong shaking. In the 40 years since, CSMIP has instrumented many sites and structures and important strong motion records have been obtained. Accelerographic instruments have significantly improved during this period, and the last of the original instruments installed are now being replaced. The Strong Motion Instrumentation Advisory Committee (SMIAC) has provided important ongoing input and advice to the program. This paper summarizes CSMIP status and recent developments in the instrumentation of bridges, buildings, geotechnical arrays and free field sites.

Instrumentation of Transportation Structures

Many bridges have been instrumented since CSMIP began to instrument bridges with Caltrans support after the 1989 Loma Prieta earthquake. There are currently 65 regular bridges instrumented, and all 10 of the major/toll bridges in California have been instrumented with extensive instrumentation. Fig. 1 shows the location of the eight toll bridges in the San Francisco Bay area, most being Caltrans structures (Golden Gate Bridge the exception).

Fig. 1. The eight major / toll bridges in the San Francisco Bay area. With the completion of the East Span of the San Francisco - Oakland Bay Bridge, all will have extensive strong motion instrumentation (map from http://bata.mtc.ca.gov/bridges/)

San-Francisco-Oakland Bay Bridge

A bridge with high current interest, opened to traffic on September 3, 2013, is the San Francisco – Oakland Bay Bridge (SFOBB), the east span of the San Francisco to Oakland bridge system of Interstate 80. Chief Bridge Engineer Brian Maroney of Caltrans described the construction challenges at the SMIP12 Seminar (Maroney, 2012). The bridge includes a self-anchored suspension section (SAS), an unusual structure and the signature architectural element of the bridge. The bridge can be considered as four separate structures, including the SAS, the Yerba Buena Island and Oakland landfall sections, and the Skyway, a long concrete structure over the Bay. Fig. 2 shows the sensor locations on the SAS section, which has 83 sensors, including 75 accelerometers, 6 tiltmeters and 2 relative displacement sensors. Since CSMIP worked with Caltrans early in the design process, sensor emplacements were included in the design plans. This allowed casings for the downhole sensors to be placed in several of the concrete piles when they were being poured during construction. Sensors are installed at the pile tip and key locations extending all the way to the tower top. (Since construction of the bridge is still being completed, some sensors are not yet installed, but should be by

early 2014.) The SAS also includes accelerometers on the main suspension cable to record its response. There will be a total of about 200 sensors on the new East Span.

In a project like this, a significant amount of the effort occurs in the detailed planning and blueprint development stage. This approach allows the sensor cabling and other components to be installed by electrical contractors along with the other systems, for lighting, corrosion control and communication, providing a more economical approach to achieve extensive instrumentation of a large structure.

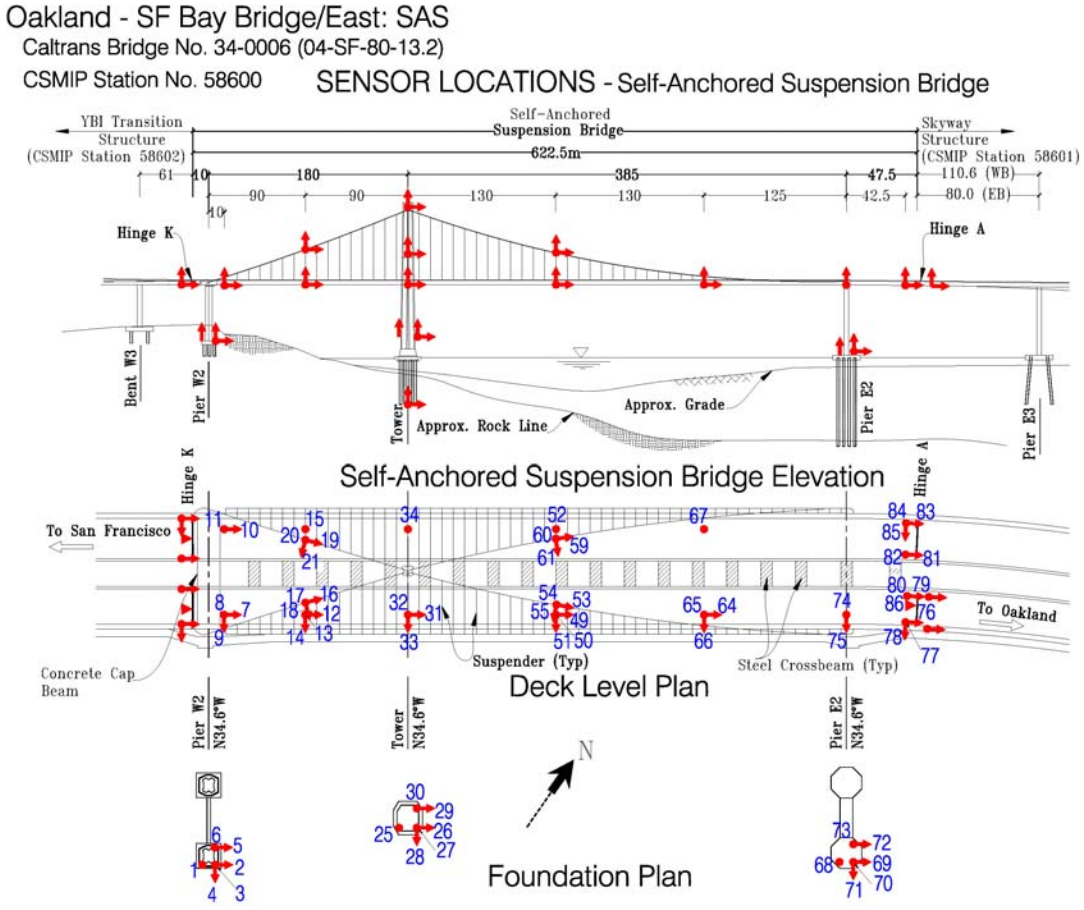

Fig 2. Sensor layout for the Self Anchored Suspension (SAS) section of the new San Francisco - Oakland Bay Bridge. The instrumentation system was designed to capture important motions of the structure and includes sensors from the pile tip to the top of the tower, on the cables, the deck and other locations.

Bay Area Rapid Transit (BART) Transbay Tube

The BART Transbay tube, which carries subway traffic between Oakland and San Francisco, was completed in the early 1970s. It is an important transportation lifeline, carrying as many people during rush hour as the Bay Bridge.

A few accelerographs were installed when it was built, but in the end they were not maintained and were not operational, for example, during the 1989 Loma Prieta earthquake, the largest earthquake shaking at the structure since it was completed. The lack of what would have been critical information was noted in the Governors Board of Inquiry Report (Housner et al., 1990). In November 2004 a local bond measure was passed to fund the seismic upgrade of the tube, and strong motion instrumentation was included in the upgrade project. A special panel was convened by BART to plan a strong motion instrumentation system.

The BART tube is 3.6 miles (5.8 km) long, and is constructed of a series of 57 segments that were laid in a trench on the floor of the bay. The strong motion instrumentation was installed in the lower of the two rectangular passageways, or galleries, between the eastbound and westbound tubes. The strong motion system includes triaxial sensor sets at a series of locations along the length of the tube. A total of 40 sensors are installed, including 33 accelerometers, 4 extensometers and 3 relative displacement sensors. This system has the greatest linear extent of any system CSMIP has installed. To economize on cable lengths, and limit the maximum length, recorders were located at several locations along the length of the tube. They are linked together over the full length to achieve common triggering. Also, a GPS timing signal is provided to each recorder to synchronize the timing of the digital sampling in all recorders. The system came on line in late 2012, and no strong motion records have yet been obtained, although ambient motion records have been taken for analysis.

Instrumentation of Buildings

Understanding the response of a building requires that sensors be located near the perimeter of each of a series of floors along the building height, with all sensors recorded with a single time basis. This is in contrast with the three instruments required by some building codes, which provide very limited information. CSMIP began intensive instrumentation of buildings in the late 1970s, with central recording of accelerometers deployed on a number of floors. One of the first buildings instrumented, in 1978, was the Imperial County Services Building in El Centro. The M6.5 Imperial Valley earthquake occurred the following year, and the instrumentation system successfully measured the motion as the earthquake shaking damaged the building. This was a successful start to the building instrumentation effort. Since instrumentation of a building may cost as much as 10 freefield stations, there were reservations to commit to the expenditure. The success of the El Centro building recording reassured SMIP and the SMIAC advisory committee of the effectiveness of the overall plan. A long-term plan for the instrumentation of 400 buildings was laid out. A total of 235 buildings, including 60 hospitals with OSHPD support, have been instrumented to date.

San Francisco - 62-story Concrete Core Building

An unusual project completed last year was the instrumentation of a new 62-story residential building in San Francisco. It is of a new design, with a concrete central core. The interest in the building was such that after CGS developed an initial plan with 36 sensors distributed over the height of the building, the largest number to date, the USGS also became interested and proposed adding an additional 36 sensors. After a lengthy process to obtain permission from the condominium owners, and working out the details between CGS and the USGS for a joint instrumentation project, instrumentation was completed in late 2012, becoming the first building instrumented cooperatively by CGS and USGS (Huang et al., 2012). Sets of ambient motion data were recorded soon after the system was online, and Celebi et al. (2013) recently completed an effort analyzing the modes and modal periods of the building.

Hospital Instrumentation

Soon after the 1989 Loma Prieta earthquake, SMIP began instrumenting hospitals with support of the Office of Statewide Planning and Development (OSHPD). Tokas and Lobo (2012) summarized key aspects of the OSHPD hospital seismic safety program and hospital instrumentation. During the OSHPD – CSMIP partnership, 60 hospital buildings have been instrumented. The instrumentation of hospital buildings according to a long term plan is being augmented by OSHPD with the instrumentation of existing hospital buildings being seismically strengthened and new hospitals incorporating specialized seismic provisions such as base isolation, dampers and the like.

CSMIP experience is that hospitals are generally difficult buildings to instrument well, because instrumentation work at key structural locations is often not compatible with the ongoing functions and patient services at the hospital. The ideal time to do effective instrumentation of a hospital is during construction, if possible, or at least before it opens to take patients.

Location

Since the purpose of structural instrumentation is to record the motion of a structure during strong shaking, it is important that the structure be located where there is a reasonable likelihood that strong motion recordings will be obtained. The locations of the currently instrumented hospitals in California are shown on the map in Fig. 3. The map indicates a good correspondence between the locations of instrumented hospitals and the areas of higher likelihood of ground shaking over 20%g, according to current seismic hazard estimates (Petersen et al., 1996). This correspondence can only be accomplished if there is a step in the planning process to carefully consider shaking likelihood before the instrumentation decision is made, even if the structure is of a new type with receptive ownership.

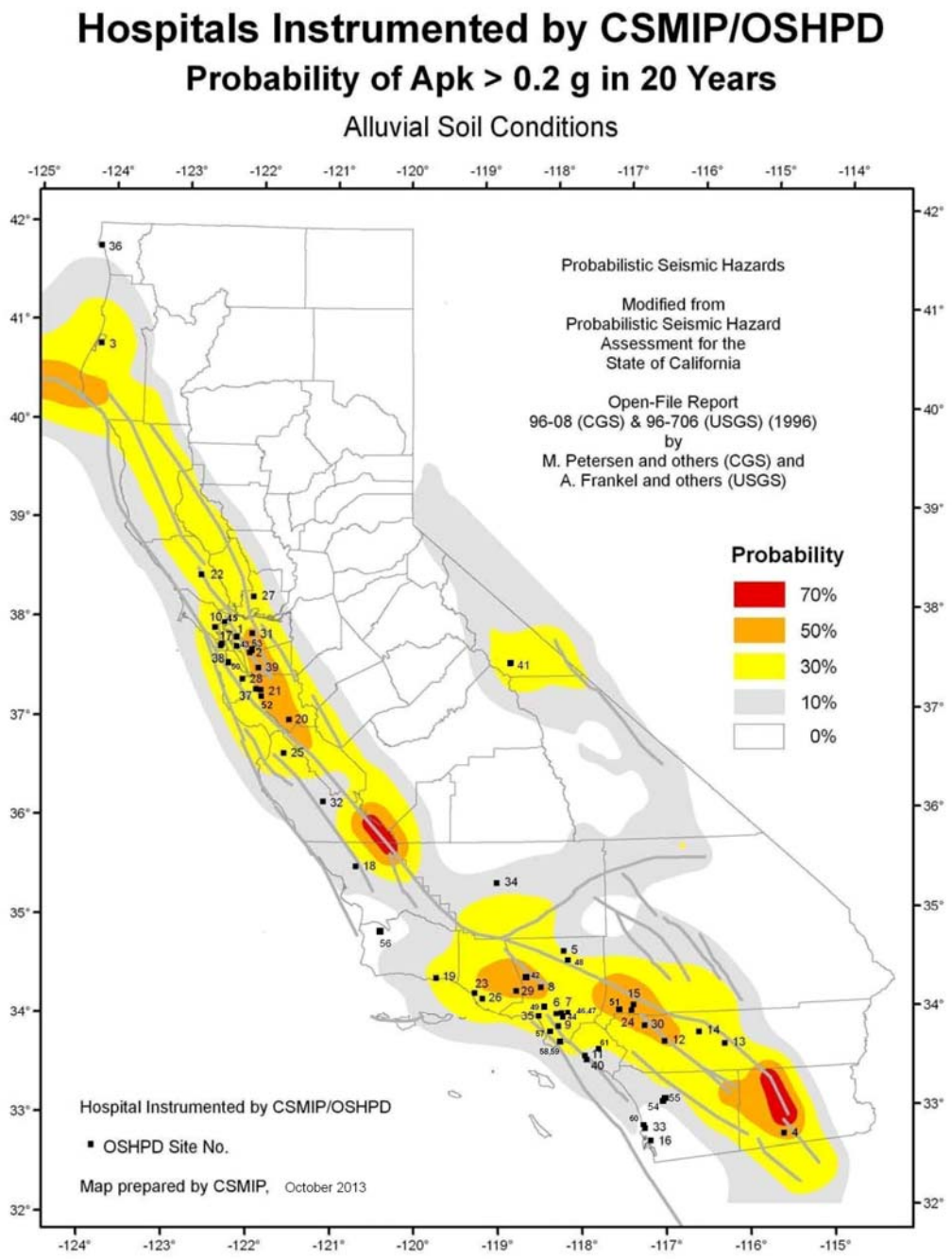

Fig. 3. Map showing the locations of the hospital buildings instrumented under the CSMIP-OSHPD project and the probability of ground acceleration exceeding 20%g in 20 years.

Below-Building Instrumentation

A unique situation developed with a hospital now under construction in Ventura County. Soil-structure-interaction has been extensively studied in the past, but always with data from the free surface or basement. Measuring the motion in the third dimension, underneath the building, has been a longstanding goal. An

opportunity arose with a new building at the Port of Long Beach in 2010, and the necessary detailed planning was completed, but the construction of the building was unfortunately suspended as an economy measure.

The Ventura Memorial Hospital is being constructed in an area with liquefiable sediments. As a result, OSHPD required soil improvement by cement deep soil mixing (CDSM). As part of the overall project, it was decided to include downhole accelerometers in the deep soil improvement region beneath the building, complimented by measurement at depth in the unimproved parking lot area, away from the building. Work is now underway, and downhole instrument casings are in place under the building being built. The downhole casing for the subsurface instrument in the parking lot area is also completed. The downhole accelerometers will be installed during construction of the building, when the building itself will also be instrumented.

Instrumentation of Other Structures

Dams

A significant number of dams were instrumented by CSMIP until the law was changed as discussed below. Recently the Division of Safety of Dam in the Department of Water Resources reinstituted support for the maintenance of instrumented dams. SMIP has 27 dams in the network at this time. All were initially instrumented with film instruments. Though the instrumentation at many dams has been upgraded, it has not been possible to upgrade some dams that have no available power on site, especially high in the Sierras. The interconnection cable meant to provide common starting often receives lightning damage, and some of the dams may be covered with 5 to 8 feet of snow in the winter. Work continues to address these challenges to upgrade the few remaining dams.

Tunnels and Wharfs

The first tunnel instrumented in California was the Caldecott Tunnel Bore 3 near Oakland, in 1978. After 35 years, two more tunnels are being instrumented. The new Devils Slide Tunnels, constructed for the realignment of Highway 1 near Pacifica to avoid repeated landslides, were recently instrumented. Another tunnel still under construction is the Caldecott Bore 4, which will be instrumented prior to opening.

Other structures instrumented in recent years include wharf structures at the Ports of Oakland, Long Beach and Los Angeles. A second oil off-loading wharf is currently being instrumented near Richmond. Petroleum loading wharfs involve special challenges because of fire safety requirements, but their response is important to measure since they represent a critical lifeline.

Instrumentation of Geotechnical Arrays

Predicting the effects of the near surface geologic conditions on the motion occurring at the surface is an important problem. A key to progress is obtaining more data at a variety of site conditions. Toward that goal, SMIP has installed and maintains a significant number of geotechnical arrays. Each array consists of a vertically stacked series of triaxial accelerometer packages installed at depths chosen in consideration of the geologic conditions and soil profile. These downhole instruments are complemented by a triaxial package at the surface. The downhole instruments are locked in place in special casings surrounded by special grout targeted to be similar in seismic properties to the surrounding medium.

Array depth, the depth of the deepest accelerometer package, ranges from 77 feet to 825 feet (24 to 252 m). Fig. 4 shows typical array geometry. The example is

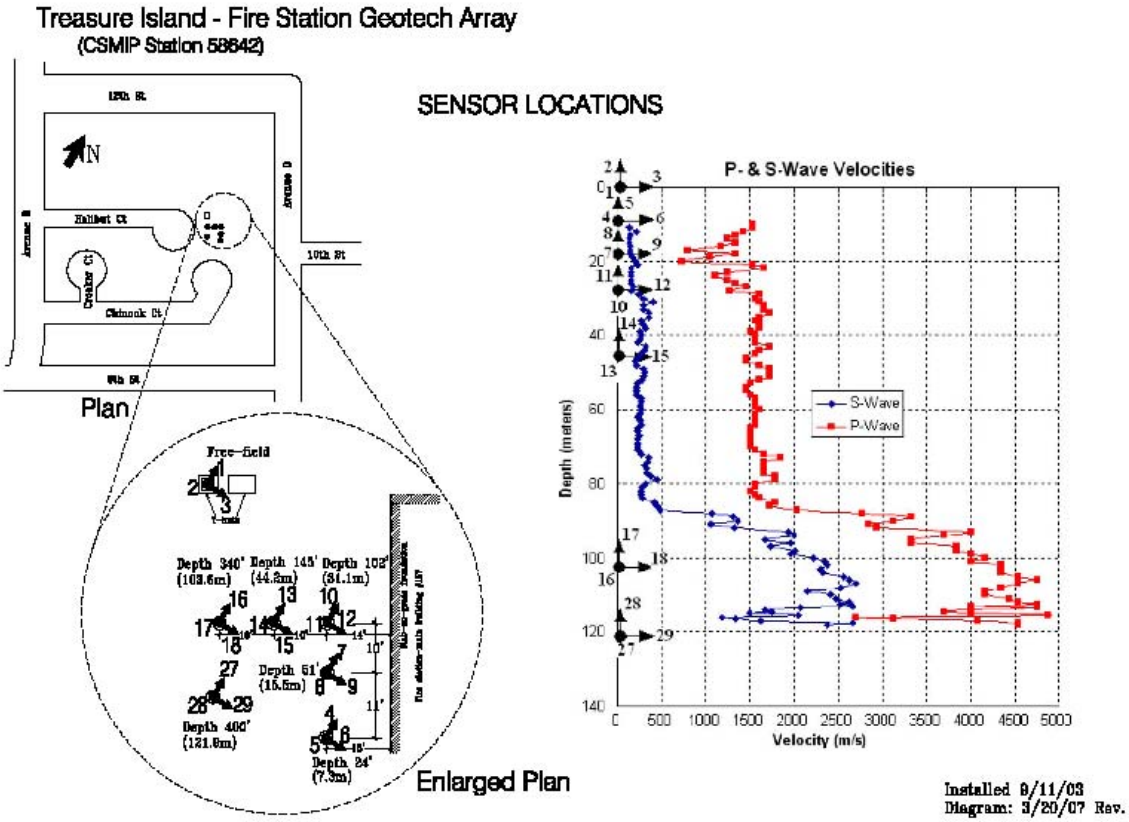

Fig 4. Layout of the Treasure Island Geotechnical Array sensors, from 400 ft (122 m) to the surface freefield. The P and S velocity profiles are also shown.

the Treasure Island array, near San Francisco, one of the first and deepest arrays, extending to 400 ft (122 m) depth. This array, like nearly all SMIP geotechnical

arrays, is a cooperative effort with another agency or agencies, in this case with NSF, EPRI and the USGS.

Table 1 lists the 38 geotechnical arrays installed and maintained by CSMIP as of fall 2013; four more are underway. The most frequent partner in the array projects is Caltrans, and many of the geotechnical arrays are on Caltrans rights-of-way near major bridges or transportation corridors.

Though not all arrays have recorded strong motion data yet, very interesting results have been obtained. Perhaps the most interesting set of data is from the Turkey Flat array near Parkfield, California for the 2004 Parkfield earthquake. A blind prediction experiment was conducted and unexpected results were obtained (e.g., Real et al., 2006; Shakal et al., 2006). The motion at the surface at the center of the alluvial valley, given the motion at an outcrop at the valley edge, was not successfully predicted, though many competent investigators, using the most modern methods, made predictions. Kramer (2009) and Kramer et al. (2011) summarized the lessons learned and implications for practice.

In general, it is well known that the amplitude of ground motion increases near the surface. An example of the change of amplitude with depth is shown in Fig. 5. The motion with peak amplitude of 11%g at the 330 ft depth increased to 22% g at the surface. For recordings like this, from small magnitude simple events, the input and reflected motions, separated by travel time, can often be seen in the record. For larger, more complex events with more complex source time functions, this simple signature is not present, but the surface motion is still larger than at depth.

In contrast, the amplitude of the motion does not always increase near the surface, as shown in the records from a distant large earthquake (Fig. 6). In this case the dominant arriving waves are longer period surface waves, propagating horizontally, rather than body waves propagating vertically. For these long-period waves, there is no net increase near the surface. The near surface geology has little effect on the motion amplitude in this case.

Table 1. CSMIP Geotechnical Arrays

No.	Station No.	Station Name	N. Lat. W. Long.	No. Depths (Sensors)	Partner	Geology	Installation Date
1	58137	Alameda - Posey and Webster Geotech Array	37.7897 122.2766	4 (12)	Caltrans	Deep alluvium	03/24/05
2	67265	Antioch - San Joaquin Rvr Nth Geo. Array	38.0377 121.7515	6 (18)	Caltrans	Deep alluvium	06/26/12
3	67266	Antioch - San Joaquin Rvr Sth Geo. Array	38.0179 121.7516	5 (15)	Caltrans	Deep Alluvium	01/18/07
4	47750	Aptos - Seacliff Bluff Array	36.9715 121.9103	3 (9)	NSF	Alluvium	11/02/00
5	68321	Benicia - Martinez Br Nth Geotech Array	38.0508 122.1277	3 (9)	Caltrans	Shallow fill over bay mud	06/29/07
6	68323	Benicia - Martinez Br Sth Geotech Array	38.0334 122.1170	3 (9)	Caltrans	Thin alluvium over soft rock	06/29/07
7	13186	Corona - I15/Hwy 91 Geotech Array	33.8817 117.5491	4 (12)	Caltrans	Shallow alluvium over rock	12/12/01
8	68206	Crockett - Carquinez Br Geotech Array #1	38.0540 122.2250	3 (9)	Caltrans	Shallow alluvium over soft rock	05/01/03
9	68259	Crockett - Carquinez Br Geotech Array #2	38.0548 122.2264	3 (9)	Caltrans	Shallow alluvium over soft rock	09/25/08
10	01794	El Centro - Meloland Geotechnical Array	32.7738 115.4486	4 (12)	Caltrans	Deep alluvium	02/10/99
11	89734	Eureka - Geotechnical Array	40.8187 124.1656	5 (15)	Caltrans	Deep soft alluvium	08/30/95
12	58968	Foster City - San Mateo Br Geotech Array	37.5727 122.2639	4 (12)	Caltrans	Shallow alluvium over rock	05/22/03
13	58964	Half Moon Bay - Tunitas Geotech Array	37.3584 122.3975	4 (12)	Caltrans	Alluvium over soft rock	06/28/01
14	58486	Hayward - I580/238 East Geotech Array	37.6896 122.0962	4 (12)	Caltrans	Deep alluvium	06/23/11
15	58487	Hayward - I580/238 West Geotech Array	37.6887 122.1074	6 (18)	Caltrans	Deep alluvium	06/06/11
16	58798	Hayward - San Mateo Br Geotech Array	37.6169 122.1541	5 (15)	Caltrans	Deep alluvium	07/16/99
17	24703	Los Angeles - La Cienega Geotech Array	34.0362 118.3784	4 (12)	Caltrans	Deep soft alluvium	12/15/94
18	24400	Los Angeles - Obregon Park	34.0370 118.1783	2 (6)	UCSB	Deep alluvium over soft rock	06/25/97
19	14785	Los Angeles - Vincent Thom Geo Array East	33.7489 118.2678	4 (12)	Caltrans	Deep soft alluvium	09/10/98
20	14783	Los Angeles - Vincent Thom Geo Array W1	33.7500 118.2751	4 (12)	Caltrans	Deep soft alluvium	09/11/98
21	14784	Los Angeles - Vincent Thom Geo Array W2	33.7502 118.2777	3 (9)	Caltrans	Deep soft alluvium	09/11/98
22	68285	Novato - Petaluma River Geotech Array	38.1184 122.5015	5 (15)	Caltrans	Shallow alluvium over rock	10/24/08
23	58204	Oakland - Bay Bridge Geotech Array	37.8212 122.3272	5 (15)	Caltrans	Alluvium	09/09/10
24	25325	Oxnard - Hwy 101 Bridge Geotech Array	34.2434 119.1936	3 (9)	Caltrans	Deep alluvium	04/17/08
25	24206	Palmdale - Hwy 14 Bridge Geotech Array	34.5473 118.1300	3 (9)	Caltrans	Shallow alluvium over hard rock	02/11/10

Table 1. CSMIP Geotechnical Arrays (Cont'd)

No.	Station No.	Station Name	N. Lat. W. Long.	No. Depths (Sensors)	Partner	Geology	Installation Date
26	36529	Parkfield - Turkey Flat #1	35.8780 120.3587	2 (6)	CGS	Soft rock	03/03/87
27	36520	Parkfield - Turkey Flat #2	35.8822 120.3510	3 (9)	CGS	Shallow alluvium over soft rock	12/17/86
28	68797	Rohnert Park - Hwy 101 Geotech Array	38.3472 122.7134	3 (9)	Caltrans	Alluvium	05/20/03
29	23792	San Bernardino - I10/215 West Geotech Array	34.0637 117.2979	4 (12)	Caltrans	Deep alluvium	05/16/08
30	03192	San Diego - Coronado East Geotech Array	32.6983 117.1449	4 (12)	Caltrans	Deep alluvium	06/27/02
31	03193	San Diego - Coronado West Geotech Array	32.6881 117.1640	5 (15)	Caltrans	Deep alluvium	06/28/02
32	58961	San Francisco - Bay Bridge Geotech Array	37.7867 122.3892	3 (9)	Caltrans	Fill and alluvium over soft rock	08/05/03
33	58700	San Francisco - Golden Gate Bridge Nth Geo Array	37.83 122.48	2 (6)	GGB	Rock	01/28/94
34	58700b	San Francisco - Golden Gate Bridge Sth Geo Array	37.8198 122.4788	2 (6)	GGB	Rock	
35	58267	San Rafael - Richmond Bridge Geotech Array	37.9427 122.4808	2 (6)	Caltrans	Alluvium	08/18/05
36	24764	Tarzana - Cedar Hill B	34.1605 118.5353	2 (6)	NSF	Thin alluvium over soft rock	06/05/97
37	58642	Treasure Island - Geotechnical Array	37.8252 122.3741	7 (21)	NSF	Shallow fill over deep alluvium	10/30/92
38	68310	Vallejo - Hwy 37/Napa Rvr East Geotech. Array	38.1217 122.2751	3 (9)	Caltrans	Bay mud	01/24/06
Underway							
39	23793	San Bernardino - I10/215 East Geotech Array	34.064 117.288	4 (12)	Caltrans	Deep alluvium	n/a
40	24185	Moorpark - Hwy118/Arroyo Simi Geo. Array	34.2876 118.8646	3 (9)	Caltrans	Shallow alluvium over soft rock	n/a
41	58525	Newark - Dumbarton Br East Geotech Array	37.5127 122.1091	6 (18)	Caltrans	Deep alluvium	n/a
42	58526	Palo Alto - Dumbarton Br West Geotech Array	37.4986 122.1289	6 (18)	Caltrans	Deep alluvium	n/a

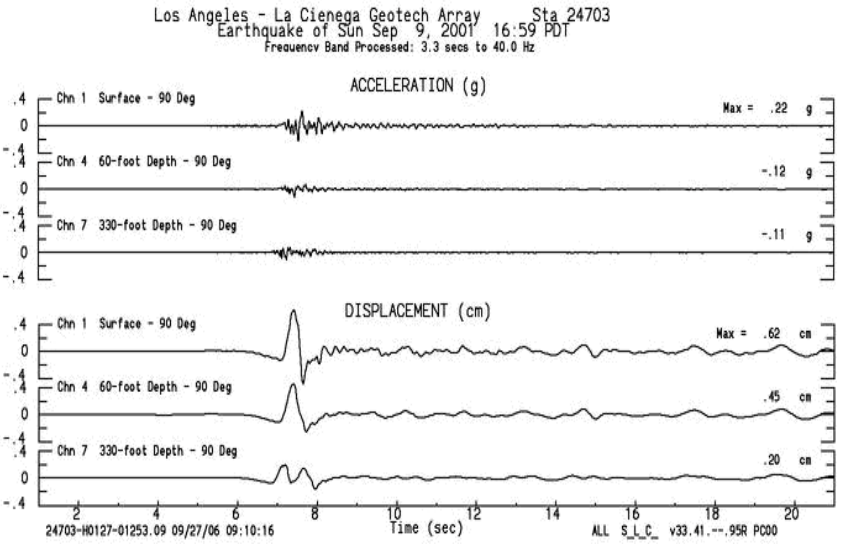

Fig. 5. Data from a small earthquake (M4.2, on 9/9/01) recorded at the La Cienega array. The data shows the increase of the amplitude near the surface, and the incoming and the reflected phases separated by the travel time in the near surface layers.

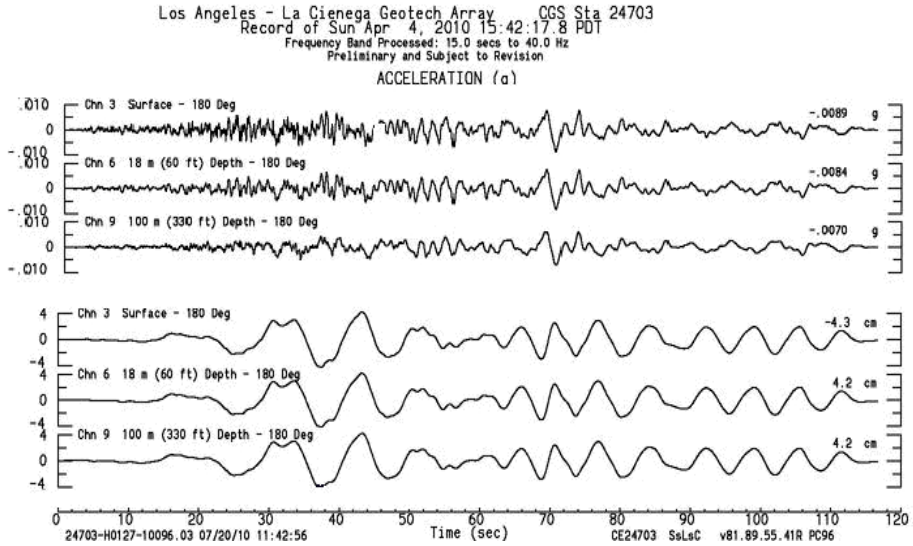

Fig. 6. Downhole data recorded at the La Cienega geotechnical array for a large distant event (M7.2 Calexico earthquake of 4/4/10) showing little amplification of the motion near the surface.

Overall Progress

It is useful to review the instrumentation accomplished in the 40+ years since CSMIP began strong motion instrumentation. The first stations, installed in the early 1970s, were all free field stations, because of their relatively low cost and rapidness of installation, important during a time the new program was under close scrutiny by the Legislature. The instrument state of the art at the time was film-recording, analog instruments, and the SMA-1 was the most reliable. Interestingly, CSMIP is just now replacing the last of these instruments, after 40 years of service, with QuakeRock instruments, discussed below. Very few instruments can meet the long-term reliability and low power requirement of the SMA.

The number of installations over time is shown in Fig. 7. The number of accelerometers in the network is plotted for a common base, since some structures may have many sensors, while freefield stations have three. The plot of the freefield instruments installed shows the initial effort in the 1970s. It also shows a small increase in the mid 1980s, when the Parkfield Array was completed. Finally, it shows a large increase associated with the TriNet Project in southern California after the 1994 Northridge earthquake, a joint effort with USGS and Caltech funded by FEMA. Nearly all the 400 stations installed in that effort are still online, and the TriNet project is still the basis for the more advanced state of seismic instrumentation in Southern California. The installation rate after TriNet is greater than that before partly because of the OES-funded CISN project which, while not as large as the TriNet project in the short term, continues year to year.

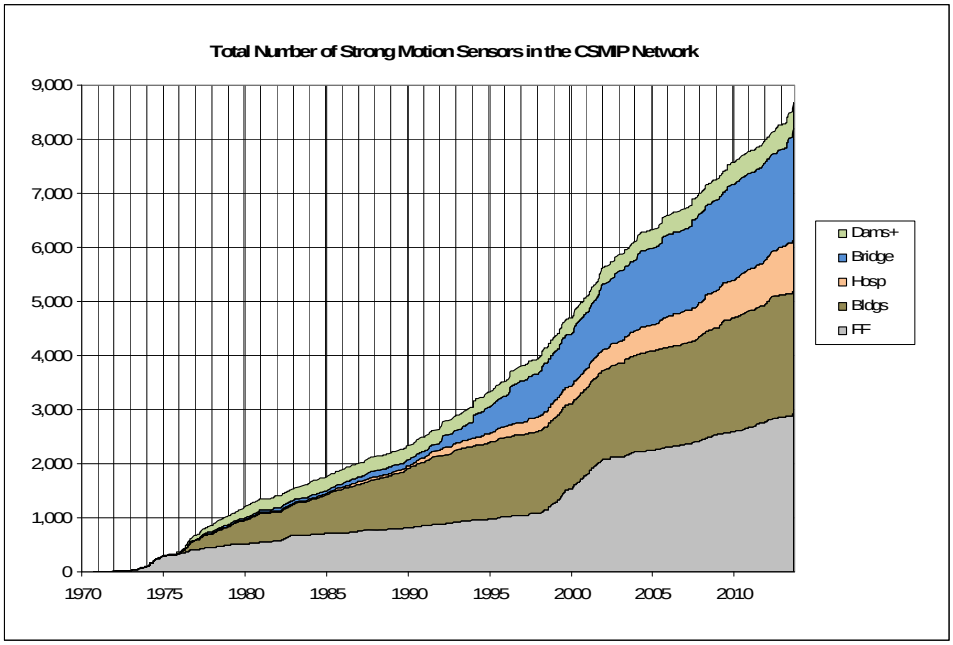

Fig 7. Total number of strong motion sensor installed in the CSMIP network from the early 1970s to the present, in structural (dams, bridges and hospitals) and freefield categories. The geotechnical array sensors are included in the free field count.

Building instrumentation shows instrumentation starting at low level in the late 1970s, than increasing at a nearly steady rate. The 175 regular buildings instrumented have about 2300 channels.

There were few bridges or hospitals instrumented until the early 1990s, when two things happened. First, the law mandating the CSMIP program was changed to bar it from instrumenting structures for which building permit fees were not paid in the local jurisdiction. At that point SMIP could no longer instrument bridges, hospitals or dams using its permit-fee funding. Second, in view of the damage that occurred to bridges in the 1989 Loma Prieta earthquake, and the little recorded data to guide future design, the Governor's Board of Inquiry report (Housner et al., 1990) called for Caltrans to actively support bridge instrumentation. An active partnership with CSMIP began at that time, and the resulting instrumentation accomplishments are clear in Fig. 7. Caltrans also began, especially after the 1994 Northridge earthquake, to call for a free field station at each instrumented structure, not routinely done at that point. In addition, in certain cases they called for downhole arrays to be installed in the vicinity of instrumented bridges. These arrays are expensive to prepare; Caltrans drillers were used to perform the drilling and logging to manage costs. The instrumentation of downhole arrays supported by Caltrans will benefit geotechnical engineering in general, leading to increased understanding of near surface motions.

Hospital instrumentation saw similar significant changes in the early 1990s. OSHPD developed an ongoing project with CSMIP after the Loma Prieta earthquake, as discussed above, supporting hospital instrumentation as well as establishing a formal basis for hospital selection. The subsequent, ongoing instrumentation work supported by OSHPD, including the special categories discussed above, has led to a significant increase in the rate of instrumentation in recent years

QuakeRock

As a result of the efforts of CGS and USGS, and the recordings obtained in other countries, a large number of strong motion records have been obtained in the last 20 years. As would be expected from a likelihood perspective, most are at intermediate distance from moderate events. There are relative few records from large earthquakes, and particularly few at close in distances, within 10-20 km from the fault. To address this paucity, since the location of future earthquakes is not known, would require a large number of instruments placed along many faults in areas where large earthquakes may occur. To address this need SMIP has begun a project to put out a significant number of economical, low-power, autonomous accelerographs along major faults in southern California. A normal stand-alone station, with the supporting infrastructure, usually costs $10,000 to $15,000 to install. The approach here uses an economical instrument with low power

requirements and a simple installation method so the total installation can be accomplished at perhaps a quarter of the regular cost. Fig. 8 shows a pilot installation, in which the installed, anchored instrument is covered by a faux, fiberglass rock to blend in with surroundings, dispensing with the usual instrument housing and the pouring of a concrete pad. This approach requires visiting the site to recover data, and yields data with the ~.003g resolution of the classic SMA, instead of the micro-g resolution of more expensive, high powered conventional instruments. Since addressing the near field paucity of data for improving design does not require immediate data, and much of the building code is currently based on records with SMA-type resolution, neither of these factors interferes with the goal.

Replacement for SMA

The QuakeRock instrument is a good replacement for the classic SMA instrument, in general. Its low power requirement allows it to be a direct, economical replacement in cases where funding or adequate power are not available to allow installation of a conventional digital accelerograph. SMIP has installed over 50 of the QuakeRock instruments as direct SMA replacements, where AC power is not available, with good results. Considering the number of privately owned SMAs still located at lifeline structures and in code-type building instrumentation, this could be an effective approach to replace them. The cost of digitizing film accelerograms will continue to go up, while the expertise to do accurate digitization will continue to become more rare, meaning that obtaining the spectrum of the motion after a significant earthquake could be significantly delayed, and may have quality problems. The QuakeRock type of instrument would already have digitized the record, and the spectrum can be quickly calculated.

Fig. 8. Illustration of the installation of a QuakeRock accelerograph in a roadside environment. The instrument is shown at upper left (RefTek's 148-01 accelerograph), attached to the mounting plate (upper right), which is attached to an anchoring rod driven into the ground. The finished deployment at bottom shows the faux rock cover over the instrument. The instrument operates autonomously on the included D-cell lithium batteries for up to two years.

Convenient Access to Data

A major evolution of the last several years is the increasingly convenient access to data, whether raw, processed or spectral, at the Center for Engineering Strong Motion Data (CESMD), at www.strongmotioncenter.org. The Center is a cooperative effort of the CGS and USGS, and strong motion records from many earthquakes and stations are now available there. The Virtual Data Center (VDC) developed at UC Santa Barbara is being integrated into the CESMD. Haddadi and Stephens (2013, this volume) describe the recent advances at the Center.

Summary

The California Strong Motion Instrumentation Program, started after the 1971 San Fernando earthquake, in which there was significant structural damage and few strong motion records, has instrumented many sites and structures and recorded important strong motion records. Instrumented structures include 235 buildings, including 60 hospitals, strategically chosen. Bridge instrumentation includes 65 regular bridges and all 10 toll/major bridges in the State. Ground response instrumentation includes 38 geotechnical arrays with downhole sensors and 800 regular freefield stations.

Acknowledgements

The work of the California Strong Motion Instrumentation Program has benefited significantly from the input received from the Strong Motion Instrumentation Advisory Committee over the years. The careful work of the CSMIP technical staff, lead by Carl Petersen, is critical to successful instrumentation and to the recording of quality strong motion data; Stephen Fife led field staff instrumenting and maintaining many of the stations. Hamid Haddadi and his staff carefully review, quality control and post incoming data on the CESMD web site.

References

Celebi, M., M. Huang, A. Shakal, J. Hooper and R. Klemencic (2013). Ambient response of a unique performance-based design tall building with dynamic response modification features, Structural Design of Tall and Special Buildings, doi: 10.1002/tal.1093.

Haddadi, H. and C. Stephens (2013). Update on data and features of the Center for Engineering Strong Motion Data, *Proceedings of SMIP13 Seminar on Utilization of Strong-Motion Data*.

Housner, G., J. Penzien, N. Agbabian, C. Arnold, L. Dickenson, E. Elsesser, I. Idriss, P. Jennings, W. Podolny, A. Scordelis and R. Wallace (1990). "Competing Against Time", Report to Governor George Deukmejian from the Governor's Board of Inquiry on the Loma Prieta Earthquake, Governors Office of Planning and Research, Sacramento, California.

Huang, M., P. Hipley and A. Shakal (2013). Seismic instrumentation of toll bridges in California, Sevnetgh National Seismic Conference on Brdiges and Highways, Oakland, Californa, Paper P10.

Huang, M., A. Shakal, C. Petersen, M. Celebi, J. Hooper and R. Klemencic (2012). Strong motion instrumentation of a 62-story concrete core residential building in San Francisco, *Proceedings of SMIP12 Seminar on Utilization of Strong-Motion Data,* p. 81-96.

Kramer, S. (2009). Analysis of Turkey Flat ground motion prediction experiment – lessons learned and implications for practice, *Proceedings of SMIP09 Seminar on Utilization of Strong-Motion Data,* p. 1 -22.

Kramer, S., A. Shakal, H. Haddadi, and C. Real (2011). Near surface geology and the Turkey Flat ground motion prediction experiment – lessons learned and implications for practice, 4th International Symposium on the Effects of Surface Geology on Seismic Motion, IASPEI / IAEE International Symposium, Santa Barbara, U.S.

Maroney, B. (2012). San Francisco - Oakland Bay Bridge New East Span: Construction Progress and Challenges, *Proceedings of SMIP12 Seminar on Utilization of Strong Motion Data*, p. 125.

Petersen, M. and others (CGS) and Frankel, A. and others (USGS) (1996). Probabilistic Seismic Hazard Assessment for the State of California, Open-File Report 96-08 (CGS) and 96-706 (USGS).

Real, C., A. Shakal and B. Tucker (2006). Overview of the Turkey Flat ground motion prediction experiment, *Proceedings of SMIP06 Seminar on Utilization of Strong-Motion Data,* p. 117 - 136.

Shakal, A., H. Haddadi and C. Real (2006). Recorded data and preliminary review of predictions in the Turkey Flat Blind Prediction Experiment for the September 28, 2004 Parkfield earthquake, *Proceedings of SMIP06 Seminar on Utilization of Strong-Motion Data,* p. 137 - 152.

Tokas, C. and R. Lobo (2012). Hospital Seismic Safety Program and strong motion instrumentation, *Proceedings of SMIP12 Seminar on Utilization of Strong-Motion Data,* p. 111 - 124.

UPDATE ON DATA AND FEATURES OF THE CENTER FOR ENGINEERING STRONG MOTION DATA (CESMD)

Hamid Haddadi

California Strong-Motion Instrumentation Program, California Geological Survey, Sacramento

And

Christopher Stephens

National Strong-Motion Project, US Geological Survey, Menlo Park

Introduction

Strong-motion data from the United States and other seismically active countries are served to engineers, seismologists, and public safety authorities through the Center for Engineering Strong Motion Data (CESMD) at www.strongmotioncenter.org. The CESMD is a joint effort between the US Geological Survey and the California Geological Survey, in cooperation with US and international strong-motion seismic networks and data centers. The transfer of operational and maintenance responsibilities for the COSMOS Virtual Data Center from its original home at UC Santa Barbara to the CESMD have been completed, along with software upgrades and improvements in the virtual links to worldwide data providers. Two search options are now available at the CESMD: US structural and ground response data at the Engineering Data Center (EDC), and worldwide ground response data at the Virtual Data Center (VDC), shown in Figure 1.

Figure 1. Two search options available at the EDC and VDC pages of the CESMD

New and Improved Search, Select, and Display Features of the CESMD

Automated Internet Quick Report

The CESMD now automatically posts strong-motion data from the California Integrated Seismic Networks (CSMIP, NSMP, SCSN, NCSN, BDSN) within minutes following an earthquake as an Internet Quick Report (IQR). In addition to related products such as ShakeMap, these reports are used by public safety authorities and engineers for rapid response to earthquakes. The IQR pages are reviewed and archived at the CESMD as Internet Data Reports (IDR). The IDR Page for the M4.8 Isla Vista earthquake of 29 May 2013 is shown in Figure 2 as an example.

Figure 2. CESMD Internet Data Report for the M4.8 Isla Vista earthquake of 29 May 2013

Small Records FTP Site

In response to engineering seismology needs in the US, the CESMD now also provides strong-motion records at the Small Records FTP site from lower magnitude (<M3.5) and smaller amplitude (<0.5%g) records from California for use in studies such as developing ground-motion prediction equations in regions of the country with infrequent strong earthquakes.

The EDC web pages for earthquakes now show links (e.g., at the bottom of Figure 2) to the Small Records FTP site when low magnitude and small amplitude records are available. Figure 3 shows the Small Records FTP page for the M4.8 Isla Vista earthquake of 29 May 2013.

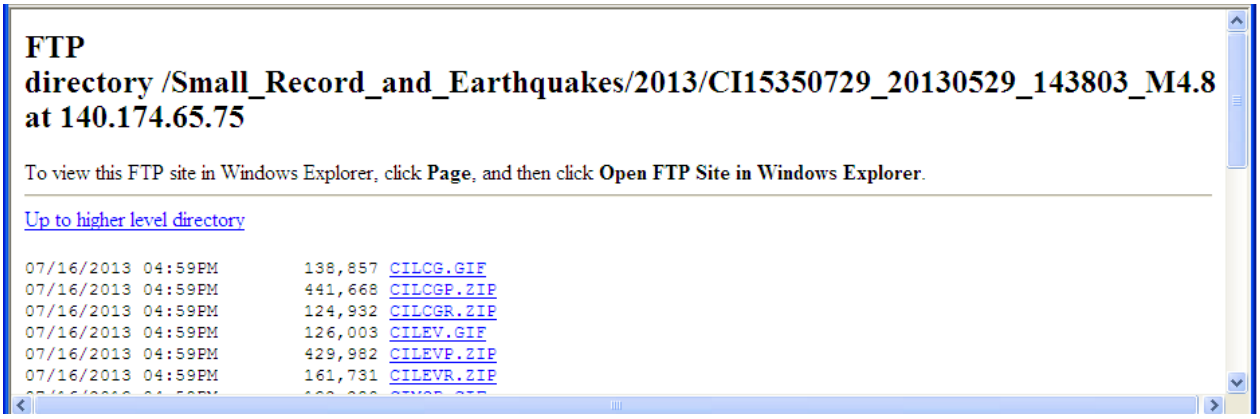

Figure 3. Small Records FTP page for the M4.8 Isla Vista earthquake of 29 May 2013

IQR Station Map

The EDC provides earthquake-specific interactive station maps on which seismic stations are displayed with links to station information pages, plots of record waveforms, and data download pages. Recently, the capability has been added to the interactive station maps to show the list of all stations that are displayed on the map for the selected earthquake (Figure 4). The list is sorted alphabetically and helps the user find stations by name and then locate stations easily on the interactive map by clicking on the station entry on the list. The interactive maps for larger earthquakes also display a finite fault model when it becomes available.

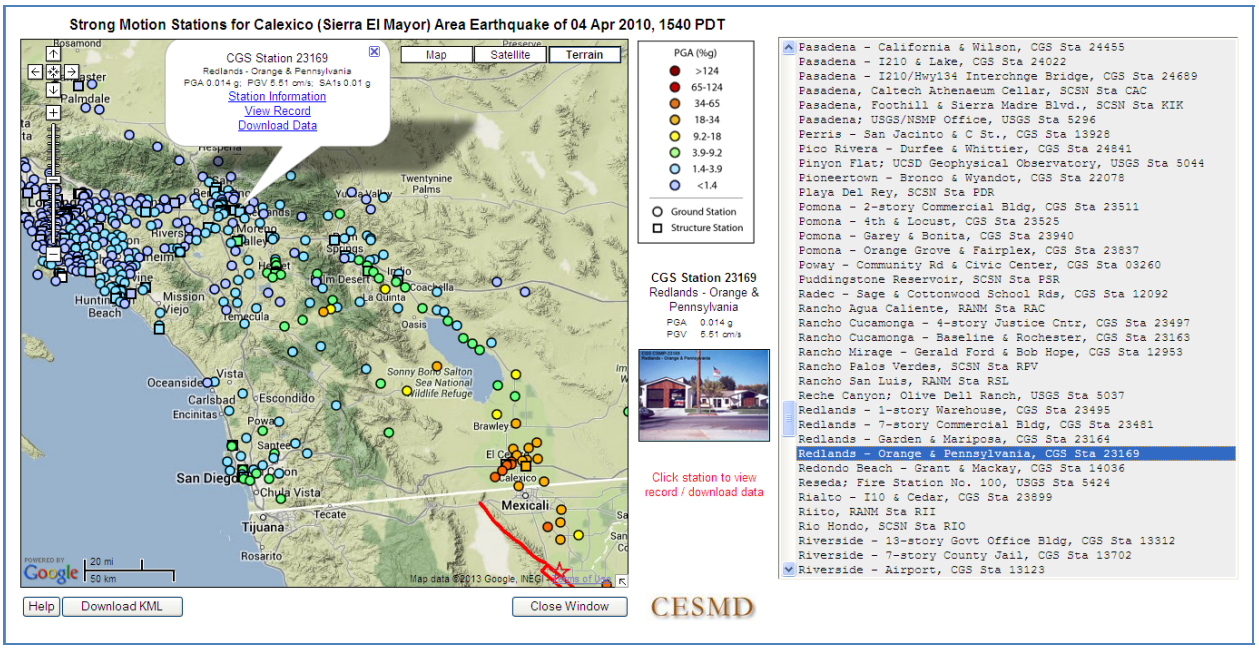

Figure 4. CESMD Interactive station map and list for the M7.2 Calexico (Sierra El Mayor) earthquake of 4 April 2010

Regional Stations Maps

Two interactive maps are served at CESMD to display all stations in Northern California and Southern California with links on the maps to the station information pages and all strong-motion data recorded at the stations. Because of the number of stations, it takes some time to download and display all stations. To reduce the delay, the stations have been divided into two groups. The Northern California Station Map shows all CISN strong-motion stations north of latitude 35°. This is complemented by the Southern California Station Map, which shows all stations south of latitude 36°. There is a one-degree overlap (35°N to 36°N latitude) in the maps. The user can switch back and forth between the maps by clicking on the “See...more stations” link provided. Also list of all stations that are shown on the maps are provided. Stations listed on the right side of the maps are sorted alphabetically. By clicking on a station’s name, the location of the station is shown on the map, with links to the station information page and to a table that shows all the strong motion records (if any) obtained at that station. Figure 5 shows the new features using the Northern California stations map as an example.

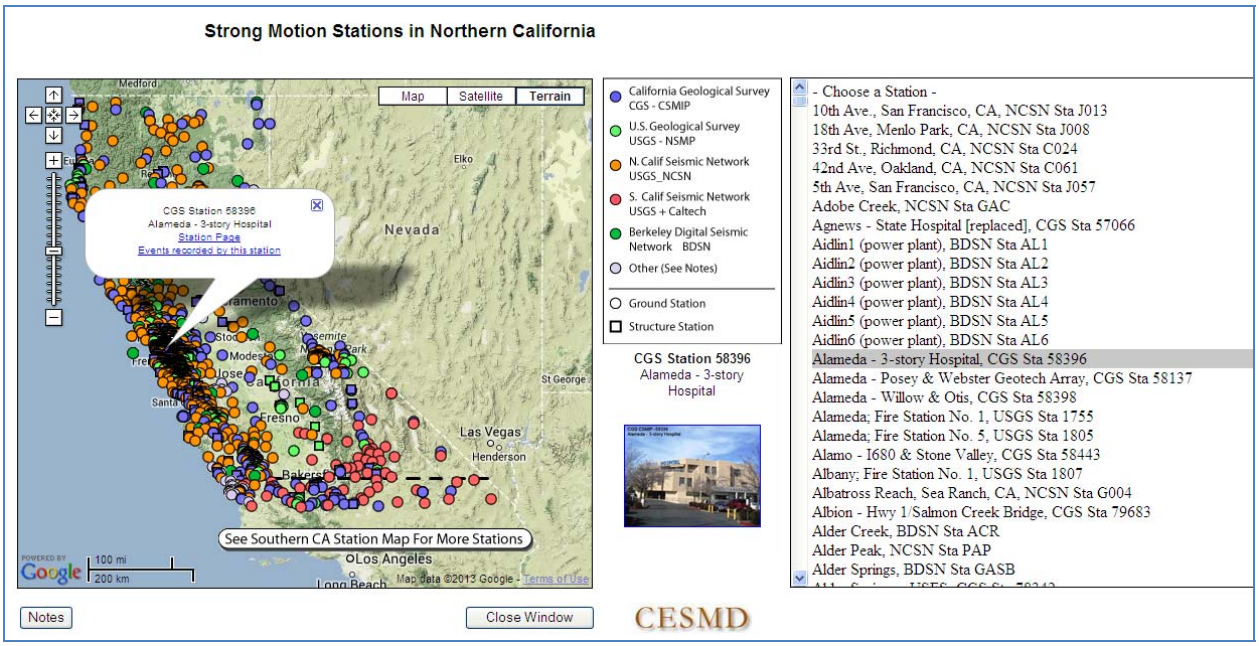

Figure 5. Regional stations map for Northern California that displays stations from different seismic networks in that region

Earthquake map

Similar to the interactive regional stations maps, the interactive earthquake map now provides a list of all earthquakes shown on the map in alphabetical order. Also, recently a new tool was added to the earthquake map to select, display and list all earthquakes within an area of interest by drawing a polygon on the map. Figure 6 shows the earthquake map with a polygon drawn to select earthquakes within the user-drawn area of interest. The result of the selection is shown in Figure 7 on the map as well as on the earthquake list.

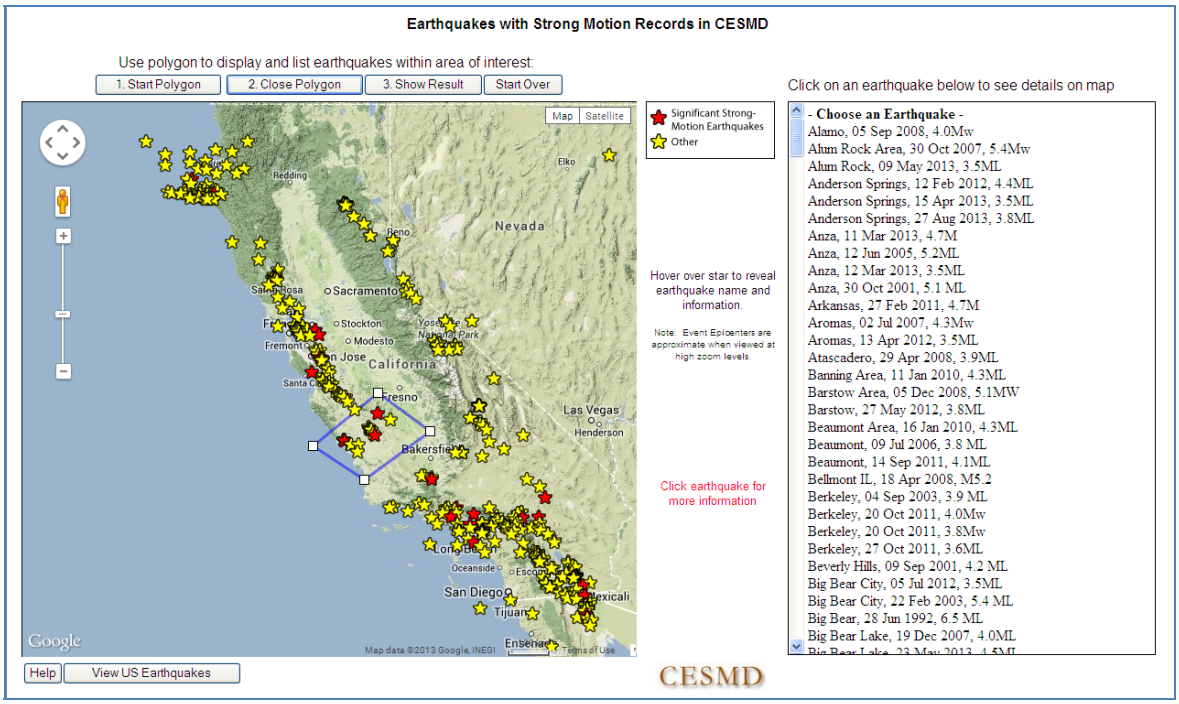

Figure 6. Selection of earthquakes on the earthquake interactive map using a polygon

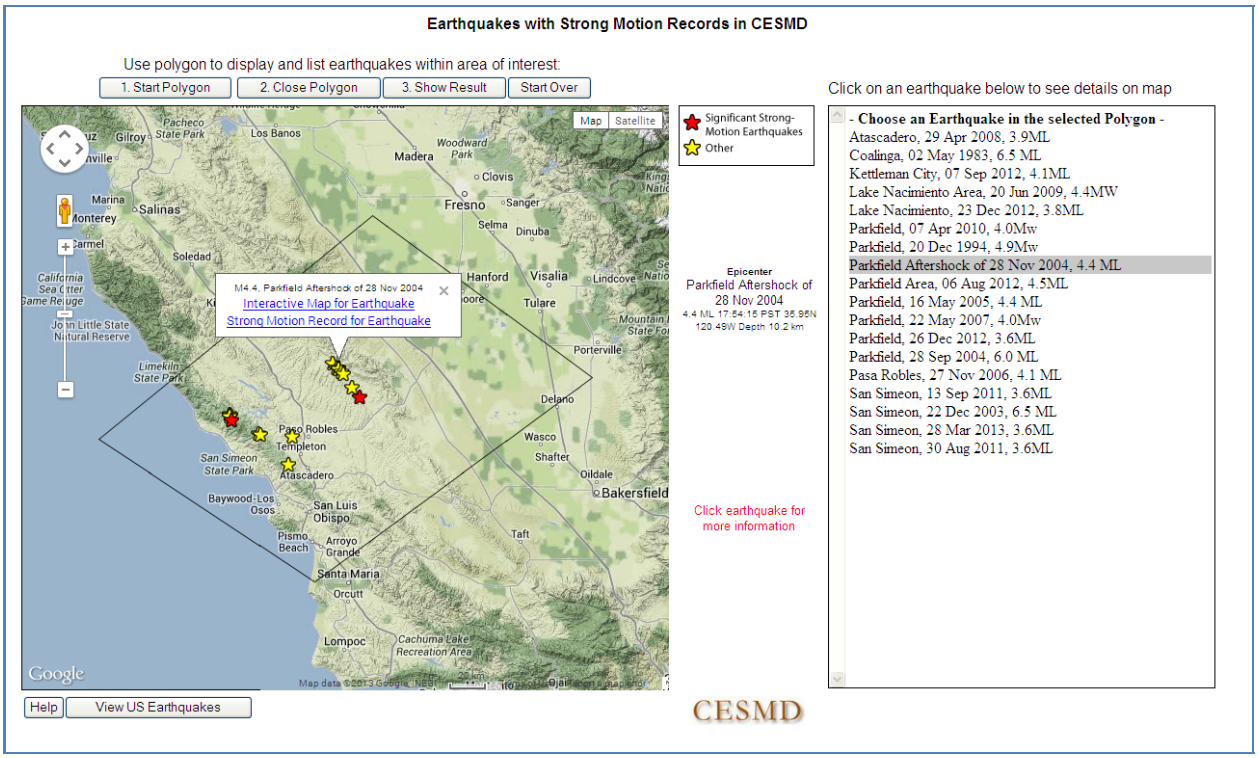

Figure 7. The results of using a polygon to display and list earthquakes in an area of interest

Virtual Data Center

Transfer and upgrade of operational and maintenance responsibilities for the COSMOS Virtual Data Center (VDC) from its original home at UC Santa Barbara to the CESMD have been completed. The VDC Tagged Format (VTF) was adopted as the standard at the CESMD for converting strong-motion data from each originating network's format to facilitate incorporating data into the VDC. The revised process of uploading metadata to the database and generating display images for groups of records automatically without detailed human interaction is a major improvement in the VDC operation. Figure 8 shows the new face of the VDC.

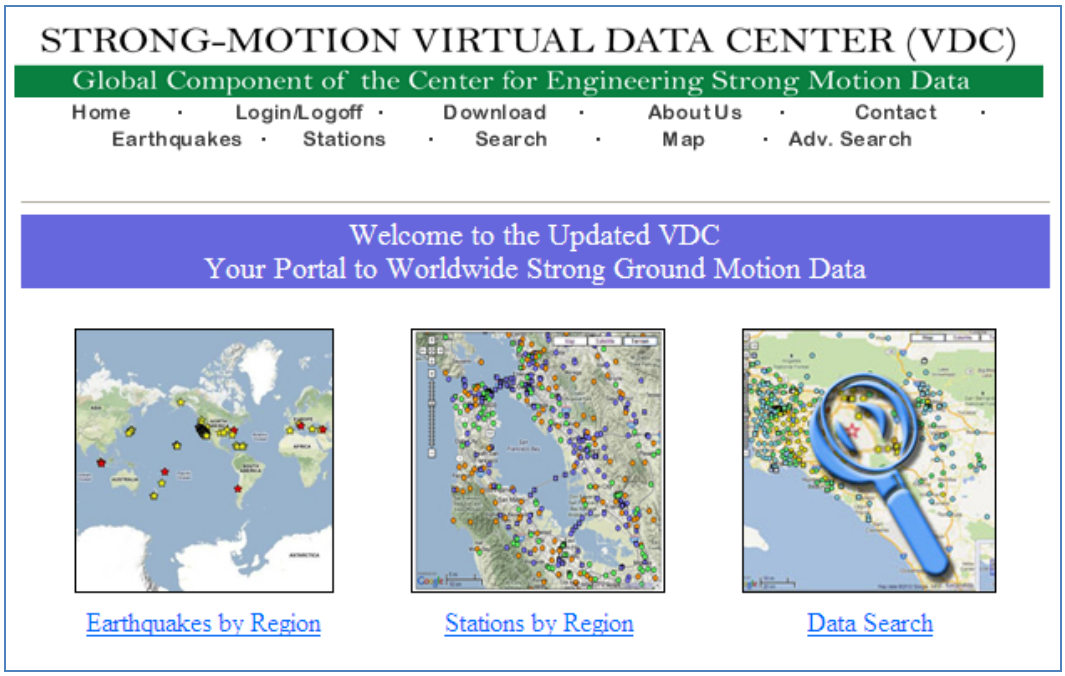

Figure 8. The new face of the CESMD Virtual Data Center

Data Available at CESMD

As of early October 2013, the EDC has posted over 9300 station records, each including three or more accelerogram component, from a total of about 310 earthquakes mostly in the United States. The VDC has posted parametric information and plots of time histories for over 11500 accelerogram component from about 700 national and international earthquakes, and has provided virtual access to the seismic networks data servers to to download records.

The CESMD benefits from ongoing cooperation with COSMOS, which assists in facilitating access to strong-motion data from other countries, and also provides advice on the development of user applications.

More information about the Center for Engineering Strong Motion Data (CESMD), its objective, operation and the web portal, can be found at the proceedings of the 15th World Conference on Earthquake Engineering held in September 2012 in Lisbon, Portugal (Haddadi et al, 2012).

Reference

Haddadi H., A. Shakal, M. Huang, J. Parrish, C. Stephens, W. Savage and W. Leith (2012). Report on Progress at the Center for Engineering Strong Motion Data (CESMD), Proceedings of the 15th World Conference on Earthquake Engineering, Lisbon, Portugal.